INHIBITION OF INFLUENZA REPLICATION USING PROTEIN MIMETICS

INHIBITION OF INFLUENZA A REPLICATION USING CELL PENETRATING PROTEIN MIMETICS

By KENNETH A. MWAWASI B.SC

A Thesis Submitted to the School of Graduate Studies in Partial Fulfillment of the Requirements for the Degree Master of Science

McMaster University, MASTER OF SCIENCE (2014) Hamilton, Ontario (Medical Sciences)

TITLE:	Inhibition of Influenza A Replication Using Cell-Penetrating Protein Mimetics
AUTHOR:	Kenneth A. Mwawasi, B.Sc (Biochemistry - McMaster University)
SUPERVISOR:	Dr. James Mahony
NUMBER OF PAGES:	xvii, 99

ABSTRACT

The *Influenza* virus is a major human respiratory pathogen responsible for seasonal 'flu' outbreaks and sporadic global pandemics. The *Influenza* polymerase complex is necessary for viral RNA synthesis and full virulence and requires the assembly of three conserved subunits: PA, PB1 and PB2. A recombinant chimeric protein mimetic consisting of the N-terminus (20 amino acids) of PB1 fused to Maltose Binding Protein (MBP) and Tat Nuclear Localization Signal (NLS) was designed and purified with the aim of inhibiting the assembly of the polymerase by mimicking PB1. The cell-penetrating protein mimetic was shown to efficiently enter the cell nucleus and prevent assembly of the Influenza polymerase, thus inhibiting viral replication. When MDCK cells were incubated with the mimetic and subsequently challenged with *Influenza A* virus, viral replication decreased up to 98% at 50 µM. Using a nuclear extraction assay, the mimetic was shown to efficiently penetrate the plasma membrane and enter the host nucleus. GST pull-down assays showed that the mimetic interacts with PA. Molecular modeling was then employed to predict the improved hypothetical free energy of binding between PB1 and PA and determined two significant substitutions for PB1 threonine at position six: glutamic acid (T6E) and arginine (T6R). These mutations increased potency of the mimetic at 25 µM (71% for T6E and 77% for T6R compared to 36% for the native construct) and 12.5 µM (27% for T6E and 70% for T6R compared to 16% for the native construct), suggesting a more stable interaction with PA consistent with molecular modeling. Using various *in vitro* assays, the mimetic was shown to be non-toxic to host cells. Targeting critical protein-protein interactions using a peptide fused to

a cell-penetrating carrier protein presents a novel and intriguing approach in designing anti-viral therapeutics.

ACKNOWLEDGEMENTS

I would first and foremost like to thank my supervisor Dr. James Mahony for giving me the opportunity to conduct exciting and impactful research in his laboratory, originally as an undergraduate co-op student and again as a graduate student for my Masters. I have learned a great deal under his supervision, and I appreciate his insight, enthusiasm and patience with regards to the scientific process that drives medical research. I would also like to thank the members of my supervisory committee: Dr. Dawn Bowdish, Dr. Marie Elliot and Dr. Murray Junop. Their knowledge and diverse academic backgrounds undoubtedly allowed to them to provide me with valuable insight and challenged me to improve my own craft as a scientist, and I am truly grateful and honoured to have them on my committee.

I feel privileged to have worked with the many intelligent, fun and unique individuals in the Mahony lab over the years. I think everyone positively impacted me in some fashion, and I would like to thank the past and present members of the lab for an enjoyable experience: David Bulir, Dr. Christopher Stone, Sylvia Chong, Rob Clayden, Tiffany Leighton, Jordan Nelson, Steven Liang, Matthew Lee, Christopher Chiang, Daniel Waltho, Alexandra Ruyter, Andrea Granados, Jerry Wang and Lieqi Liu.

I owe my deepest and heartfelt gratitude to my family who have supported me as I pursued my goals and ambitions. Their encouragement and support have been a continuous source of inspiration and I cannot imagine completing this chapter of my life without them. Thank you Mom and Dad for always believing in me.

This thesis is dedicated to my mother and father, Grace and Basil Mwawasi.

TABLE OF CONTENTS

List of Abbreviations……..…xii
List of Figures……xiv
List of Tables……...xvi
Declaration of Academic Achievement……...xvii

Chapter 1 – Introduction……...1
1.1 Overview of Influenza……...2
1.2 Influenza History……3
1.3 Taxonomy and Nomenclature……4
1.4 Clinical Manifestations and Epidemiology……..6
1.5 Influenza Viral Life Cycle……..9
1.6 Antigenic Drift and Shift……..16
1.7 Influenza Therapies: Vaccines and Antivirals……17
1.8 Influenza Polymerase: a possible drug target……19
1.9 Peptide Mimetics……..22
1.10 Thesis Objectives……..23

Chapter 2 – Materials and Methods……26
2.1 Genetic cloning and construct design for the Gateway system……27
2.2 Recombinant protein expression and purification……..28
2.2.1 *E. coli* chemical competent cell preparation……28
2.2.2 *E. coli* transformation……..…28
2.2.3 Recombinant protein expression and purification……...29
2.2.4 Protein quantification……30
2.3 MDCK cell culturing……30
2.4 Influenza culturing……31
2.4.1 Propagation……...31
2.4.2 Plaque assay titering……32
2.4.3 Hemagglutination tittering……...32

2.5 cDNA creation from HepG2 cells……..33
2.5.1 RNA extraction from HepG2 cells……..33
2.5.2 RT-PCR for the preparation of cDNA……34
2.6 Viral inhibition assay to determine mimetic activity……34
2.6.1 Fluorescence microscopy……34
2.6.2 Quantitative polymerase chain reaction……35
2.7 Toxicity assays……36
2.7.1 RBC lysis assay……36
2.7.2 MDCK growth assay……37
2.7.3 ATP bioluminescence assay……37
2.8 Protein analysis……38
2.8.1 Polyacrylamide gel electrophoresis of proteins……38
2.8.2 Western Blot analysis……39
2.9 Cellular uptake of peptide mimetics assay……39
2.10 Nuclear isolation method……40
2.11 GST pull down assay……41
2.12 HSA expression……41
2.12.1 HSA construct expression optimization in *E. coli*……41
2.12.2 HSA construct expression in a cell-free expression system……42
2.13 *P. pastoris* yeast expression system……43
2.13.1 Genetic cloning of His-HSA-NLS-PB1$_{1-20}$ into pPicz9ssamp……43
2.13.2 Electrocompetent P. pastoris preparation and transformation……44
2.13.3 *P. pastoris* miniexpression……45
2.14 *L. lactis* secretion system……45
2.14.1 Genetic cloning of HisMBP-NLS-PB1$_{1-20}$ into *pUB1000*……45
2.14.2 Electrocompetent *L. lactis* MG1363 preparation and transformation……46
2.14.3 *L. lactis* anaerobic secretion assay……47

Chapter 3 – Results……48
3.1 Inhibition of Influenza A replication using a non-toxic cell penetrating PB1$_{1-20}$ mimetic *in vitro*……49

3.1.1 The HisMBP-NLS-PB1$_{1-20}$ mimetic inhibits Influenza replication……..49
3.1.2 The HisMBP-NLS-PB1$_{1-20}$ mimetic is non toxic *in vitro*……..51
3.2 Molecular Modeling of the PB1-PA Interaction Increases the Anti-Viral Activity of the PB1 Mimetic……54
3.2.1 The T6E and T6R mutations increase the anti-Influenza potency of the PB1 mimetic……54
3.2.2 The T6E and T6R mimetics increase anti-viral potency of the PB1 mimetic by decreasing total *in vitro* viral transcript……..56
3.2.3 The native PB1, T6E, and T6R mimetics are non toxic *in vitro*……57
3.3 Mimetic mechanism of action……60
3.3.1 The NLS is sufficient for recombinant protein mimetic entry into the cell…60
3.3.2 The NLS targets mimetics to the cell nucleus……..61
3.3.3 The HisMBP-NLS-PB1$_{1-20}$ mimetic binds to GST-PA$_{257-716}$ *in vitro*……62
3.4 Evaluating the efficacy of the 7mer mimetic……63

Chapter 4 – Discussion……..67
4.1 Inhibition of Influenza with using a non-toxic 20-mer PB1 mimetic……67
4.2 Using molecular modeling to increase potency of the PB1 mimetic……68
4.3 Mimetic mechanism of action……70
4.4 Evaluating the efficacy of the 7-mer mimetic……..73
4.5 The global burden of Influenza and need for effective therapies……75
4.6 Future directions……..78
4.6.1 Carrier molecule……78
4.6.2 Delivery of therapeutic mimetics……79
4.6.3 Biochemical investigation of the binding relationship between native/ T6E/ T6R PB1$_{1-20}$ and PA……...80
4.7 Closing remarks……..……81

References……82

Appendix……93
5.1 Supplementary Figures……..93
5.2 Supplementary Tables……98

List of Abbreviations

APS - Ammonium persulfate

ATP - Adenosine triphosphate

BMM – Buffered Minimal Media

BSA – Bovine Serum Albumin

CBC – Complete Blood Count

CCD – Coiled Coil Domain

CPP - Cell Penetrating Protein

CPSF - Cleavage and Polyadenylation Specificity Factor

Ctrl – control mimetic

DFA – Direct Fluorescent Antibody

DTT - Dithiothreitol

EDTA – Ethylenediaminetetraacetic acid

FITC - Fluorescein isothiocyanate

FBS – Fetal Bovine Serum

FOV – Field of view

FPLC – Fast Protein Liquid Chromatography

GST – Glutathione S-Transferase

HA – Hemagglutinin

HEPES - 4-(2-hydroxyethyl)-1-piperazineethanesulfonic acid

HIV – Human immunodeficiency virus

HRP – Horse Radish Peroxidase

HSA – Human Serum Albumin

IPTG – Isopropyl β-D-1-thiogalactopyranoside

ITC – Isothermal Titration Calorimetry

LAIV - live attenuated Influenza vaccine

LDAO - N,N-Dimethyldodecylamine N-oxide

LB – Luria Bertani

M1/M2 – Matrix Protein 1/2

m^7GTP – 7-Methylguanosine 5'-triphosphate

MBP – Maltose Binding Protein

MDCK – Madin-Darby Canine Kidney

MEM – Minimum Essential Medium

NA – Neuraminidase

NAI - Neuraminidase inhibitor

NES – Nuclear Export Signal

NLS – Nuclear Localization Signal

NP - Nucleoprotein

NP-40 - nonyl phenoxypolyethoxylethanol

NS1/NS2 – Nonstructural Protein 1/2

NTA - Nitrilotriacetic acid

OD_{600} – Optical Density at 600nm

PA – Acidic Polymerase Protein

PI3K - phosphoinositide 3-kinase

PB1/PB2 – Basic Polymerase Protein 1/2

PBS – Phosphate Buffered Saline

PCR – Polymerase Chain Reaction

qPCR – quantitative polymerase chain reaction

RBC – Red Blood Cell

RIG-1 - retinoic acid inducible gene 1

SDS-PAGE – Sodium Dodecyl Sulfate Polyacrylamide Gel Electrophoresis

SH3 – Src Homology 3

SPR – Surface Plasmon Resonance

TCA - Tetrachloroacetic acid

TEMED - Tetramethylethylenediamine

TIV – trivalent inactivated virus

TRIM25 - Tripartite motif-containing protein 25

TPCK - Tosyl phenylalanyl chloromethyl ketone

RPM – Revolutions per Minute

vRNP – Viral Ribonucleoprotein

YPD(S) – Yeast Peptone Dextrose (Sucrose)

ZMM – Zhorov Molecular Modeling

LIST OF FIGURES

Figure 1.1 The Influenza A virion

Figure 1.2 The Influenza A virus life cycle

Figure 1.3 Topology of the $PB1_{1-25}$ and $PA_{257-716}$ interaction

Figure 1.4 ClustalW alignment of $PB1_{1-50}$ of different Influenza A strains display sequence similarity

Figure 3.1.1 The HisMBP-NLS-$PB1_{1-20}$ mimetic inhibits Influenza A replication and growth

Figure 3.1.2 The PB1 mimetic is non toxic *in vitro*

Figure 3.2.1 The T6E and T6R mutations increase the *in vitro* anti-Influenza potency of the PB1 mimetic

Figure 3.2.2 The T6R and T6E mutations increase the anti-viral potency of the PB1 mimetic by decreasing total viral transcript

Figure 3.2.3 The native, T6E, and T6R PB1 mimetics are non toxic *in vitro*

Figure 3.3.1 The NLS is necessary and sufficient for recombinant protein cell entry

Figure 3.3.2 The NLS is sufficient to target recombinant proteins to the nucleus

Figure 3.3.3 The HisMBP-NLS-$PB1_{1-20}$ mimetic binds to GST-$PA_{257-716}$ *in vitro*

Figure 3.4 The HisMBP-NLS-$PB1_{1-20}$ mimetic inhibits Influenza A replication more effectively than the 7mer constructs

Figure 4.1 Space-filling representation of $PB1_N$ in complex with PA_C

Figure 4.2 Schematic diagram of hydrogen bonding between $PB1_{1-15}$ and PA_C

Supplementary Figure S1 *In silico* ZMM molecular modeling predicts low energy mutants at the PB1 position 6

Supplementary Figure S2. NLS-$PB1_{1-7}$ inhibits Influenza A replication and growth

Supplementary Figure S3. Purified recombinant proteins used in this thesis

Supplementary Figure S4. A $PB2_N$ mimetic inhibits Influenza A replication

Supplementary Figure S5. Overexpression of HisHSA-NLS-$PB1_{1-20}$ in *E. coli* leads to C-terminal degradation

LIST OF TABLES

Table 5.1 – List of expression strains

Table 5.2 – List of cloning primers used in this thesis

DECLARATION OF ACADEMIC ACHIEVEMENT

Kenneth A. Mwawasi performed all experiments described in this thesis with the exception of the following:

- The SuperScript ® III Platinum ® One-Step qRT-PCR described in Chapter 2 section 2.6.2 and presented in Figure 3.2.2 was performed by Sylvia Chong.
- The ZMM analysis described in Supplementary Figure S1 on the McMaster SHARCNET servers was performed by Dr. Seiji Sugiman-Marangos
- The viral inhibition assay shown in Supplementary Figure S2 was performed by Lieqi Liu
- The viral inhibition assay shown in Supplementary Figure S4 was performed by Steven Liang

CHAPTER ONE

INTRODUCTION

1.1 Overview of Influenza

The Influenza virus is a major human respiratory pathogen, with infection characterized by the sudden onset of high fever, malaise, muscle soreness, rhinorrhea and headache (Monto et al 2000). A member of the *Orthomyxoviridae* family (which include Thogoto, Lake Chad and infectious salmon anemia viruses), it is a negative-sense, single-stranded RNA virus encapsulated in a lipid envelop (Cheng et al 2012; Presti et al 2009). There are three genera of the Influenza virus based on the antigenic differences of their Matrix and Nucleoproteins, all of which infect humans: Influenza A, Influenza B and Influenza C. Although Influenza B and C have been isolated from seals and swine (respectively), there is generally no established animal reservoir for these viruses to cause global epidemics (Osterhaus et al 2000; Zambon 2009). Influenza A has been isolated from several other animals, including aquatic birds (its natural reservoir), horses and canines, and is generally associated with more severe disease in humans. Due to its propensity to infect a wide variety of avian and mammalian species as well as its easy transmission to the upper human respiratory tract via aerosols, Influenza A is the causative agent of seasonal flu outbreaks, which according to the World Health Organization, is responsible for tens of millions of cases of severe respiratory illness and 250,000-500,000 deaths worldwide every year (Cheng et al 2012; Zambon 2009). Two major surface proteins, Hemagglutinin and Neuraminidase, are further used to classify Influenza A strains (H#N#) according to their antigenic properties. There are currently 16 H and 9 N known Influenza subtypes worldwide

(Cheng et al 2012; Fouchier et al 2005). Additionally, Influenza A is responsible for abrupt and sporadic pandemics, as with the 1918 pandemic that caused 40 million deaths worldwide, and the most recent 2009 pandemic with confirmed cases in more than 200 countries (Cheng et al 2012; Das et al 2010).

1.2 Influenza History

The term 'influenza' is of Italian origins meaning influence of the stars, as it was believed that diseases manifesting as coughs and fever were influenced by the stars and heavenly bodies (Fleming et al 2003). Descriptions of Influenza-like illness began in the 16th century, although epidemics of disease similar to Influenza have been recorded as far back as 500 BC (Shahab et al 1994). Prior to the late 19th century microbiology era, little was known about the causes of infectious disease such as colds, measles and smallpox. It was not until 1892 that Richard Pfeiffer reported the discovery of a new bacterium, *Bacillus influenza* (currently known as *Haemophilus influenzae*), as the causative agent of pandemic influenza (Taubenberger et al 2007). While the scientific world generally accepted the bacterium as the etiological agent of influenza, Olitsky and Gates provided strong evidence against it in 1922, as they showed that the infective agent survived passage through filters that excluded *B. influenza* (Oltisky and Gates 1922). Influenza A was first isolated from diseased chicken in 1901; however it was not recognized as the Influenza virus until 1955 (Shahab et al 1994). In 1933, Smith et al extracted the Influenza A virus from a human patient and established it as the causative agent of influenza (Smith et al 1933).

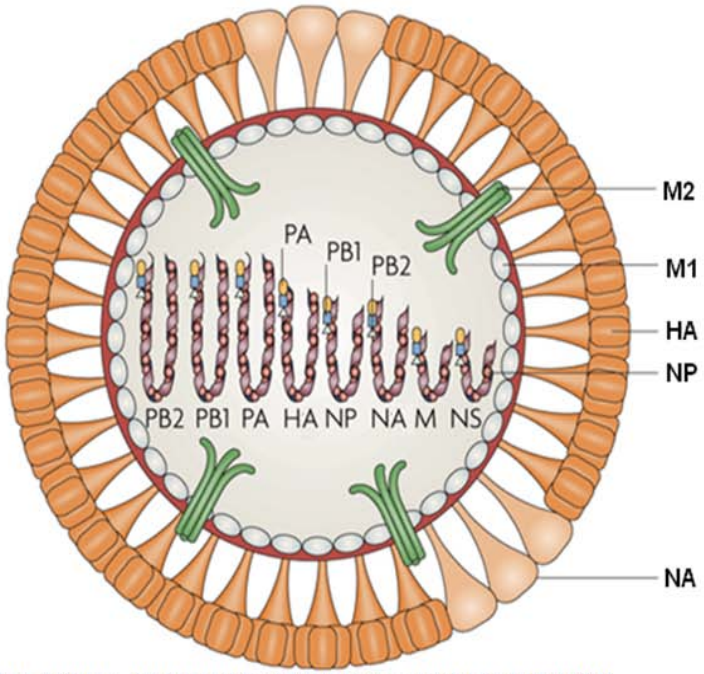

Figure 1.1 The Influenza A virion (adapted from Subbarao and Joseph 2007)
The Influenza A viral particle is shown. The virus contains an eight segmented negative sense RNA genome encoding 11-12 proteins (depending on the reading frame) encapsulated in a lipid envelope.

1.3 Taxonomy and Nomenclature

Common to all members of the single-stranded RNA *Orthomyxoviridae* family, the Influenza virus has a lipid-containing envelope (**Fig 1.1**) and a genome that is divided into eight gene segments that encode 11-12 proteins depending on the reading frame (Das et al 2010, Chen et al 2001). The influenza genus is further divided into types A, B, and C depending on the antigenicity of their Matrix and Nucleocapsid proteins, which is determined by complement fixation assays (Henle et al 1958). Influenza A, which is associated with more severe disease and pandemics in humans, is further subtyped by two surface proteins, Hemagglutinin (H) and Neuraminidase (N), which facilitate the binding and release of viral particles, respectively. There are currently 16 H and 9 N genes, making all of the Influenza A strains by various

combinations of H and N (Cheng et al 2012; Fouchier et al 2005). The Influenza nomenclature is determined by the type (A, B, C), place of isolation, strain number, year of isolation and subtype (H#N#) in sequential order. Using one of the recent 2009 pandemic 'swine flu' viruses as an example, the nomenclature is A/California/04/2009(H1N1) (Cheng et al 2012). All of the 16 H and 9 N subtypes are found in aquatic birds (Influenza A's natural reservoir), while only the H1, H2 or H3 and N1 or N2 subtypes are routinely found in humans with influenza (Alexander 2007). Due to its segmented genome, two different subtypes of Influenza A can infect the same cell, leading to the genetic reassortment of Hemagglutinin and Neuraminidase genes (**see Section 1.6**). A pandemic can occur if the new virus has preserved replicative and transmissibility efficacy between humans while presenting new H and N antigens in which the population lacks effective neutralizing antibodies (Cheng et al 2012).

A phylogenetic analysis of the A/2009/H1N1 strain revealed that the virus could be traced to avian, human and swine origins (Smith et al 2009). This is quite different from the previous two pandemic Influenza A viruses, where H1 shifted to H2 in 1957, and H2 to H3 in 1963, but both sources of antigenic shift came strictly from avian species (Kawaoka et al 1989). The A/2009/H1N1 strain contained a triple reassortment of Hemagglutinin and Neuraminidase genes from avian, swine and human sources prior to becoming endemic in swine herds, making it more distinct and genetically divergent than the seasonal circulating human H1N1 strains (Cheng et al 2012; Shinde et al 2009).

1.4 Clinical Manifestations and Epidemiology

Influenza is spread from person to person primarily by large droplet aerosol transmission from coughs, sneezes, and even regular speech (Lidwell 1974). This generally requires close contact since the droplets travel a short distance (less than a meter) in air, although contact with contaminated surfaces is another mechanism of transmission (Brankston et al 2007). The virus infects the columnar epithelia of both the upper and lower respiratory tracts and has an average incubation time of 2 days (with a range of 1-4 days) in adults. Although influenza infections are usually symptomatic (see below) especially in young children and the immunocompromised, approximately 50% of total human Influenza infections may be asymptomatic (Bridges et al 2003). Nevertheless, an asymptomatic infected person may still shed the virus and therefore still be contagious even before symptoms appear.

The clinical symptoms of seasonal influenza include fever, cough, sore throat, rhinorrhea, headache, fatigue, malaise, nausea or vomiting, diarrhea and myalgia. In addition to these symptoms, Influenza infections can lead to more severe and life threatening complications such as viral pneumonia, bronchitis, ear infections and bacterial secondary pneumonia (from pathogens such as *Streptococcus pneumoniae*, *Haemophilus influenzae*, and *Staphylococcus aureus*) with acute respiratory disease syndrome (ARDS), requiring increased intensive care (Cheng et al 2012).

The infectious prevalence of seasonal influenza (colloquially known as the flu season) typically begins in the late autumn and lasts until mid spring. In the Northern

hemisphere, this corresponds to late November to March; in the Southern hemisphere, this corresponds to April through September (Cox and Subbarao 2000). Because the primary mechanism of transmission is through aerosol droplets, the crowding of individuals during winter months has been suggested as a key contributing factor to the spread of the influenza virus during 'flu' season (Lagacé-Wiens et al 2010). Epidemiological evidence suggests that transmission is strongly associated with the rainy season, although animal model studies suggest that transmission is increased in a dry environment, albeit through an unknown mechanism (Monto 2008). The intensity of seasonal influenza in individual communities varies from year to year and depends on the size of the susceptible population. Previous exposure to influenza and vaccination can dramatically reduce the host susceptibility size due to the presence of neutralizing antibodies to the virus (Lagacé-Wiens et al 2010; LaForce et al 1994).

Four major Influenza pandemics have occurred in the past century, each containing its own unique epidemiological pattern and origin: the 1918 H1N1 'Spanish flu', 1957 H2N2 'Asian flu', 1968 H3N2 'Hong Kong flu' and the 2009 H1N1 'swine flu'. Despite its name, the geographic origins of the 1918 Influenza virus remain unclear, although it is believed that it may have initiated in China or military camps in the United States after the First World War (Cox and Subbarao 2000; Taubenberger 2006). The pandemic was characterized by three epidemiological waves: the first had a very low incidence of clinical disease and a relatively limited spread. The second wave was the global outbreak and peaked in October 1918, while a smaller third wave followed in February 1919. A hallmark of the 1918 pandemic was the high rate of morbidity and

mortality, especially in otherwise healthy young adults in addition to young children and the immunocompromised (Frost 2006). Genetic reconstruction of the 1918 virus showed that it was more virulent by coding for more effective anti-inflammatory proteins and possessing a higher propensity to cause viral pneumonia, although controversy remains whether the virus itself was the major cause of mortality (Lagacé-Wiens et al 2010; Pappas et al 2008; Taubenberger 2006).

The 1957 H2N2 ‘Asian flu’ pandemic was somewhat better characterized than the 1918 pandemic due to better intercontinental communications between countries and the ability for independent laboratories to isolate the virus in cell culture (Lagacé-Wiens et al 2010). The virus originated in Guizhou, China in February 1957 and spread globally by November of the same year. The 1957 virus primarily infected young children, the elderly and the immunocompromised similar to seasonal Influenza; however this virus was unique in that the Hemagglutinin and Neuraminidase antigens (H2N2) were different than the major circulating strains, which were descendents of the 1918 H1N1 strain (Lagacé-Wiens et al 2010). Genetic evidence suggests that the virus was the result of a single reassortment event between avian H2N2 and human H1N1 (Cox and Subbarao 2000).

Perhaps the most docile of the influenza pandemics, the 1968 H3N2 ‘Hong Kong’ virus was first described in Hong Kong in July of 1968 and spread relatively slowly to the rest of the world, reaching North America in late 1968 and Europe one year later (Lagacé-Wiens et al 2010). The pandemic had the lowest mortality of the Influenza

pandemics, possibly because of the acquired partial immunity against the N2 antigen from the 1957 virus. It is believed that the H3N2 virus occurred from a single reassortment event between an H3-containing avian Influenza strain and the human H2N2 virus (Cox and Subbarao 2005).

The most recent 2009 H1N1 'swine flu' pandemic was first described in Mexico in April 2009, and reached nearly every country by July of the same year (Dawood et al 2009; Lopez et al 2009). Interestingly, despite its ubiquitous spread and high incidence of disease (leading to a high number of hospitalizations), mortality rates from this pandemic were much lower than past influenza pandemics and seasonal influenza mortality rates (Lagacé-Wiens et al 2010). The 2009 virus was unique not only in its spread but also its genetics: it was a triple reassortment of avian, swine and human viruses. Because the avian and human components were already present in separate ancestor swine viruses, the pandemic 2009 strain likely originated in pigs and emerged as a result of genetic reassortment of swine adapted viruses containing these components (Smith et al 2009).

1.5 Influenza Viral Life Cycle

Common to all members of the *Orthomyxoviridae* family, the Influenza genome is divided into eight single stranded negative sense gene segments, which encode 11-12 proteins depending on the reading frame (Das et al 2010; Chen et al 2001). Each single stranded RNA segment is associated with the trimeric polymerase (consisting of the PB1, PB2 and PA subunits) as well as Nucleoproteins (NP) to form viral

Ribonucleoproteins (vRNP) inside the virion. The structural protein M1 surrounds the vRNP core, forming a critical interaction that affects the replication efficiency of the virus (Liu et al 2002).

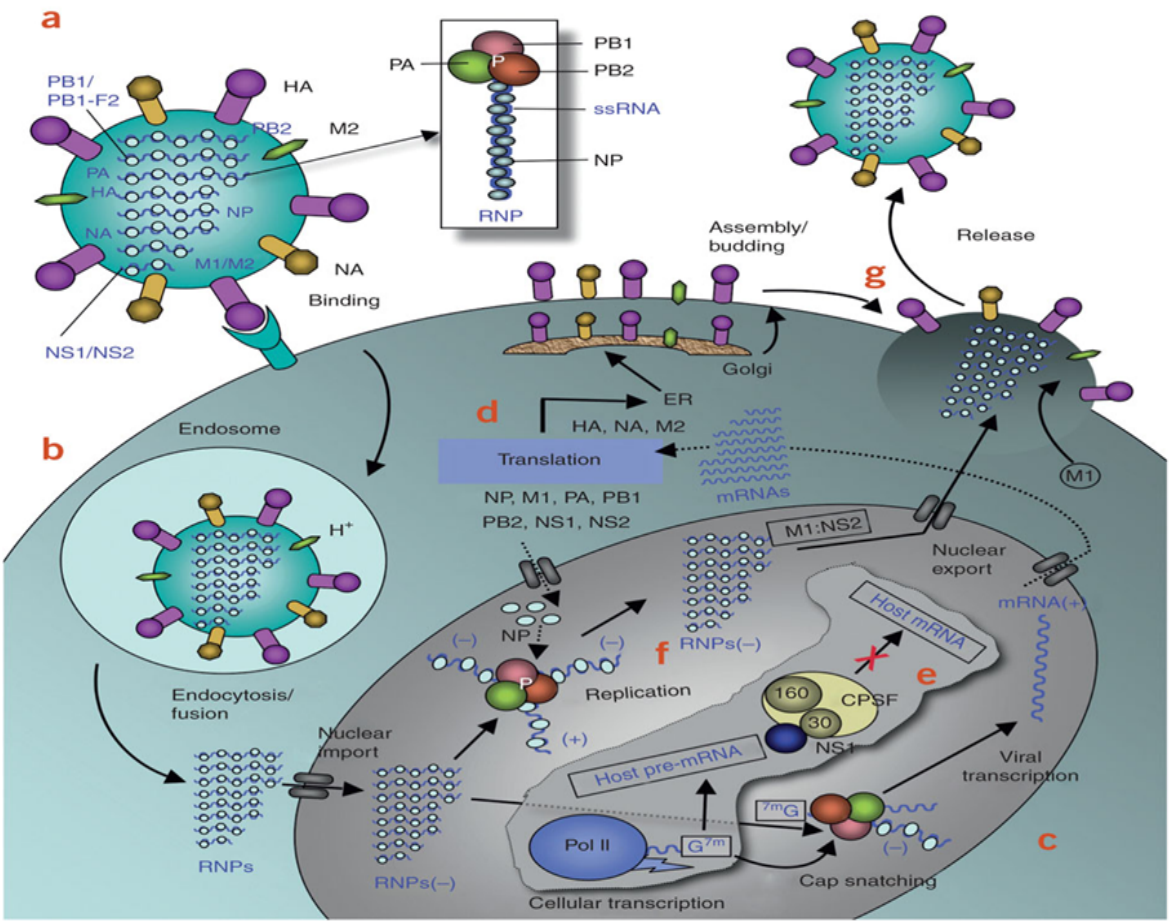

Figure 1.2 The Influenza A virus Life Cycle

The entire Influenza A life cycle from viral entry to progeny release is shown (see text for full details) **(A)** The Influenza life cycle begins when mature HA on the outside of the viral envelope binds to sialic acid on the cell surface **(B)** The drop in pH in the endosome causes a conformational change in HA that fuses the viral and host membranes. This also leads to the influx of protons through the M2 ion channel which ultimately leads to the disassembly of the lipid envelope. **(C)** vRNPs containing viral RNA are escorted into the nucleus where the Influenza polymerase transcribes the segmented viral genome through a cap-snatching mechanism **(D)** Transcripts of the surface exposed proteins (HA, NA, M2) are translated in the ER, targeted to the Golgi apparatus where they are glycosylated and brought to the lipid rafts on the surface of the host cell **(E)** NS1 inhibits the post transcriptional modification of several host pre-mRNAs , ensuring that host machinery remains dedicated to translating viral transcripts **(F)** The Influenza polymerase is also responsible for replicating viral RNA in a two-step process to create vRNA for viral progeny **(G)** The cycle ends when the replicated vRNPs bind to M1 (which binds to the NES-containing NS2), get exported out of the nucleus and are packaged with the surface exposed proteins at the host membrane. Viral progeny are released when NA cleaves sialic acid. Figure taken from Das et al 2010.

Two major viral surface proteins, Hemagglutinin (HA) and Neuraminidase (NA) are involved in cell entry and viral progeny release, respectively. The viral life cycle begins when HA binds to the sialic acid receptors present on the surface of the host cell membrane (**Fig 1.2A**). Human viruses preferentially bind to N-acetylneuraminic containing α-2,6 linkages to galactose that are abundantly present in the upper respiratory tract, whereas avian viruses preferentially bind to sialic acid containing α-2,3 linkages (von Itzsen 2007; Glaser et al 2005; Shinya et al 2006). The specificity lies within the structural topology of the glycans: because of the unique shape of α-2,6 glycans, HA undergoes an umbrella-like formation when binding to it, while it undergoes a cone-like formation when binding to α-2,3 glycans due their smaller space-filling structure (Chandrasekaran et al 2008; Wilks et al 2012). Prior to this occurring, the precursor Hemagglutinin protein (HA0) must undergo proteolytic cleavage of its conserved Q/E-X-R motif into two functional disulfide-linked subunits: HA1 and HA2 (Chen et al 1998). The HA1 subunit has an active role in the biochemical binding of sialic acid, while the HA2 subunit is involved in membrane fusion (Chen et al 2012). Conserved amino acids Tyr 98, Ser 136, His 183, and Glu 190 of HA1 all form hydrogen bonds with hydrophilic carboxylate and hydroxyl groups of sialic acid (Skehel and Wiley 2000).

Once bound to the host cell receptors, the virus is internalized into the cytoplasm through clathrin-mediated endocytosis (**Fig 1.2B**), although the virus may also be internalized in clathrin-deficient cells through macropinocytosis (Edinger et al 2014). Although poorly understood, the clathrin-dependent process was recently shown to be

regulated by Ras-phosphoinositide 3-kinase (PI3K) signaling and intracellular Ca^{2+} levels (Fujioka et al 2011, Fujioka et al 2013). Acidification of the endosome triggers the irreversible conformational change of Hemagglutinin, causing HA1 to separate from HA2 (Das et al 2010). The N-terminal fusion peptide of HA2 (containing two conserved ionizable residues, aspartate and histidine) attaches to the endosomal membrane and promotes its fusion with the viral envelope (Harrison 2008). The pH drop subsequently activates M2, an ion-gated channel protein on the viral membrane necessary for the unpacking of viral particles inside the cell. M2 is a homotetrameric single-pass membrane protein containing a His 37 residue that acts as a pH sensor and detects the acidic environment of the endosome, and a Trp 41 residue that acts as an ion gate. Interaction of His 37 with the Asp 44 residue keeps the gate locked at high pH. At low pH, protonation of the His 37 residue destabilizes the interaction with Asp 44 and the transmembrane helix, thereby allowing an influx of protons into the virus (Schenll and Chou 2008). The influx of protons leads to the uncoating of the viral lipid envelope, as well as the release of viral ribonucleoprotein particles (Helenius 1992). Once the M1 structural protein dissociates from the vRNP, the RNA gene segments are escorted into the host nucleus due to their association with NP, which contain an NLS (Cheng et al 2012; Das et al 2010).

Inside the host nucleus, negative-sense viral RNA (imported by NP containing a NLS) is replicated and transcribed to positive-sense mRNA by the Influenza polymerase (**Fig 1.2C**). The polymerase is a heterotrimer consisting of the basic subunits PB1 and PB2, and the acidic subunit PA (Cheng et al 2012). Viral transcription is initiated when

the PB2 subunit binds the 10-15 nucleotide cap (m^7GTP) of host precursor messenger RNA (pre-mRNA) in the nucleus. The cap is then cleaved off by the PA subunit and used to prime transcription of viral RNA to messenger RNA. This mechanism is termed 'cap-snatching' and has been observed in other RNA viruses (Fujimura and Esteban 2011; Dias et al 2009). Viral mRNA is then exported out of the nucleus and into the host cytoplasm, where it is translated to produce viral proteins.

The surface exposed proteins HA, NA and M2 are processed in the endoplasmic reticulum and then glycosylated in the Golgi apparatus (**Fig 1.2D**) before being transported to the cell membrane (Das et al 2010). The nonstructural NS1 protein of Influenza A is a primarily nucleus-localized effector responsible for binding the 30 kDa subunit of Cleavage and Polyadenylation Specificity Factor (CPSF), an essential component of the 3' end processing machinery of cellular pre-mRNAs (**Fig 1.2E**). This interaction plays a critical role in preventing the poly(A) 3'-end processing of host pre-mRNA, thereby preventing the ultimate translation of host mRNA (Gack et al 2009; Nemeroff et al 1998). Since viral mRNA does not require 3' processing, this ensures that the host cellular machinery remains primarily dedicated to the translation of viral mRNA and not host mRNA (Zambon 2001). NS1 also antagonizes the host innate immune response by specifically binding to and inhibiting TRIM25, an ubiquitin ligase necessary for the activation of RIG-I, a protein that recognizes viral RNA and initiates an anti-viral signaling cascade (Hale et al 2008).

In the nucleus, the polymerase is also responsible for the replication of viral RNA (**Fig 1.2F**), which occurs in two steps: a full length copy of the viral RNA is first made (termed complementary RNA, or cRNA), and then copied to create more vRNA (Nemeroff et al 1998). Although the mechanism is poorly understood, it is well established that viral RNA replication (unlike transcription) does not require a primer, but does require the Nucleoprotein (NP), which likely binds to the polymerase, resulting in its modification and propensity to initiate replication (Cheng et al 2010; Newcomb et al 2009).

After efficient replication and transcription of the viral genome, newly packaged vRNPs associate with M1, which in turns binds to the C-terminal domain of NS2. The vRNP-M1-NS2 complex is thought to be escorted out of the nucleus due to the presence of a leucine-rich nuclear export signal (NES) in NS2 (Shimizu et al 2011). However, NS2 is also involved in the regulation of viral transcription and replication in the absence of M1, implying that NS2 may also interact with vRNP (Robb et al 2009). The final stage of the viral life cycle involves the association of the vRNP and M1 with the HA and NA proteins clustered within lipid rafts on the cell membrane to form progeny virions (Takeda et al 2003). NA is a tetrameric sialidase and cleaves N-acetylneuraminic acid (the predominant sialic acid found in mammals), therefore allowing release of viral progeny and the start of a new infection cycle (**Fig 1.2G**) (Air 2012; von Itzstein 2007).

The functional NA sialidase is a homotetramer, and individual monomers do not have enzymatic activity (Buchner and Kilbourne 1972; Paterson and Lamb 1990). The monomers each contain 470 amino acids and are arranged in four domains: a globular 'head' domain that carries the enzymatic active site, followed by a thin stalk of variable length, a hydrophobic membrane-anchoring transmembrane domain and a cytoplasmic N-terminus (Air 2012). The globular head domain is characterized by a hexameric bladed propeller structure, with each blade composed of four antiparallel beta sheets connected to variable loops by disulfide bonds (Bossart-Whitaker et al 1993; Tulip et al 1991). The biochemically active site of the globular head is a conserved and rigid domain consisting of eleven amino acids that interact with the ligand (sialic acid) and another six amino acids that form a secondary shell that hold the eleven amino acids in place (Burmeister et al 1992). NA groups fall into two distinct categories: Group 1 (N1, N4, N5 and N8) and Group 2 (N2, N3, N6, N7 and N9). Group 1 Neuraminidases contain an additional cavity in the active site (which is not present in Group 2) created by the movement of an exposed NGTVKDR loop that has been proposed as a possible drug target (Li et al 2010; Thompson et al 1994).

Following the globular head domain is a thin stalk domain of variable length and unknown structure. The stalks are usually around 50 amino acids in length, however deletions of up to 18 amino acids have been observed in some N1 and N2 strains (Blok and Air 1982; Els et al 1985). Interestingly, despite the presence of Cys-containing sites of predicted glycosylation, no post-translational modification of NA has been observed. The transmembrane domain follows the stalk, and contains 7-29 hydrophobic amino acids with alpha helical secondary structure (Air 2012). The cytoplasmic N-terminal

domain is a short conserved polypeptide (MNPNQK) of unknown function, although viruses with mutations in this tail display reduced budding and abnormal morphology phenotypes (Barman et al 2004; Jin et al 1997).

1.6 Antigenic Drift and Shift

One of the evolutionary strategies employed by the Influenza virus is its propensity to mutate and change, thus evading the host immune system and allowing the virus to propagate in nature. There are two main mechanisms by which it achieves this: antigenic drift and antigenic shift (Cheng et al 2012). Antigenic drift is the gradual evolutionary change of surface and effector proteins, due to the high rate of mutations in Influenza, which is estimated to be one mutation per genome per life cycle (Carrat and Flauhault 2007). This is a fairly high rate of mutation, considering that the Influenza genome is only approximately 14,000 bases (Drake 1993). The change involves point mutations, usually within the antibody-binding site of surface-exposed proteins (M2, HA, NA) consequently leading to the inability of host antibodies to neutralize the virus and thus allowing it to propagate more rapidly in the population (Webby and Webster 2001). Interestingly, the rate of antigenic drift appears to vary from strain to strain, with rates being the highest for the H3 strains (Fitch et al 1997; Lindstrom et al 1999). Because the rate of drift occurs more rapidly in H3 strains, new variants tend to replace old ones, and the H3 evolution appears to be more linear than other Hemagglutinin types (Treanor 2004). Additionally, there appears to be a bias towards certain regions of H3 *HA* gene, since as many as 35% of all known mutations in H3 occur in 18 of the 329 codons this gene (Carrat and Flauhault 2007).

Antigenic shift is only observed in Influenza A, and occurs when two different virus strains infect the same cell, leading to reassortment of different Hemagglutinin (and less frequently Neuraminidase) subtypes in a virus. This can result in a new Influenza A strain that has never circulated in the population before and has been the cause of previous Influenza pandemics (Cox and Subbarao 2000). Major antigenic shifts are estimated to occur every 10 to 50 years (or three times every century), which correspond to the three pandemics experienced in the 20th century (1918, 1957, 1968) (Potter 2001). Once a shifted virus enters the population, it still remains susceptible to antigenic drift as with any other Influenza virus: all current circulating Influenza viruses are antigenic drift variants of previous Influenza pandemic viruses (Carrat and Flauhault 2007).

1.7 Influenza Therapies: Vaccines and Antivirals

The main strategy in preventing and controlling Influenza disease for the past 60 years has been vaccination (Osterholm et al 2012). Two types of Influenza vaccines are primarily used in North America: trivalent inactivated Influenza vaccine (TIV) and live attenuated Influenza vaccine (LAIV). Each vaccine contains the three dominant Influenza subtypes currently circulating in the population (two of which are usually A/H1N1 and A/H3N2) which are propagated in chicken eggs; however TIV strains are inactivated and therefore cannot cause disease. LAIV contain live (attenuated) Influenza viruses and therefore may cause mild symptoms as stated in **Section 1.4**. TIV is an intramuscular injection vaccine and can be administered to any individual over 6 months

old while LAIV is an intranasal spray that can only be administered to nonpregnant individuals 2-49 years old (Fiore et al 2010). Despite the best available medical treatments, the greatest setback of the 2009 pandemic was the lack of effective vaccine until late 2009, contributing to the increased hospitalization rates (Cheng et al 2012). A 2011 study estimated that pandemic H1N1 vaccine effectiveness (the risk of laboratory-confirmed infection between vaccinated and non-vaccinated individuals) in Europe was approximately 70% (Hardelid et al 2011). Had an earlier vaccine been available during the pandemic, hospitalization rates might have decreased significantly not only because of Influenza-immune individuals in the population, but also because the vaccine benefits would have been extended to non-protected individuals through herd immunity (Kim et al 2011). While vaccinations continue to be a seemingly viable option against seasonal Influenza infections, they only protect against less than 7% of the population, mainly because they are not available in countries that do not have the capacity to produce the vaccine domestically or do not have cost-effective purchase agreements in place (Stohr et al 2006).

Antivirals are important Influenza therapies, especially during the initial outbreak of a pandemic where an effective vaccine is not yet available (Hayden and Pavia 2006). The two most routinely used classes of drugs with anti-Influenza activity are the M2 ion channel inhibitor adamantanes such as amantadine and rimantadine, and the Neuraminidase inhibitors (NAIs) such as oseltamivir and zanamivir (Hurt 2014). However, due to antigenic drift, antiviral resistance has become a persistent problem in combating Influenza disease. Since 2007, all circulating Influenza strains have

developed adamantane resistance due to a S13N mutation on the M2 protein (Hay et al 1988). Interestingly, resistance to adamantanes appears to be non-specific, possibly due to the similar binding mechanisms among these classes of drugs (Cheng et al 2012). NAIs are sialic acid analogues that function by blocking the enzymatic activity of NA, therefore preventing viral progeny release. Because the NA active site is critical for viral replication, it was hypothesized that any mutation conferring resistance to NAIs would also compromise viral fitness (Hurt 2014). Nevertheless, an oseltamivir resistant H275Y mutation on NA that also retains viral fitness has been observed in approximately 2% of Influenza strains tested (Cheng et al 2012). Unlike adamantane resistance however, this mutation only confers resistance to oseltamivir and not other NAIs such as zanamivir, due to the difference in NA binding mechanisms between the two drugs: the binding of oseltamivir to the active site of NA requires a conformational change, while this is not required for zanamivir (Moscona 2009). The efficacy and safety of newer antivirals such as the NP inhibitor nucleozin and the polymerase inhibitors such as viramidine and T-705 still need to be investigated before they are used as viable therapeutics (Amorim et al 2013; Cheng et al 2012; Sidwell et al 2005).

1.8 Influenza Polymerase: a possible drug target

The heterotrimeric 250 kDa RNA-dependent RNA polymerase (also referred to as the replicase) is absolutely necessary for full virulence (Resa-Infante et al 2011; Guu et al 2008; Tsai et al 2006). The PB1 domain is the catalytic component responsible for transcribing and replicating viral RNA, while PB2 and PA are involved in cap-snatching. Since the N-terminus of PB1 interacts with the C-terminus of PA, the C-terminus

interacts with the N-terminus of PB2, and the middle domain is the catalytic polymerase domain, PB1 is considered the core of the viral replicase (Tsai et al 2006; Gonzalez et al 1996; Toyoda et al 1996).

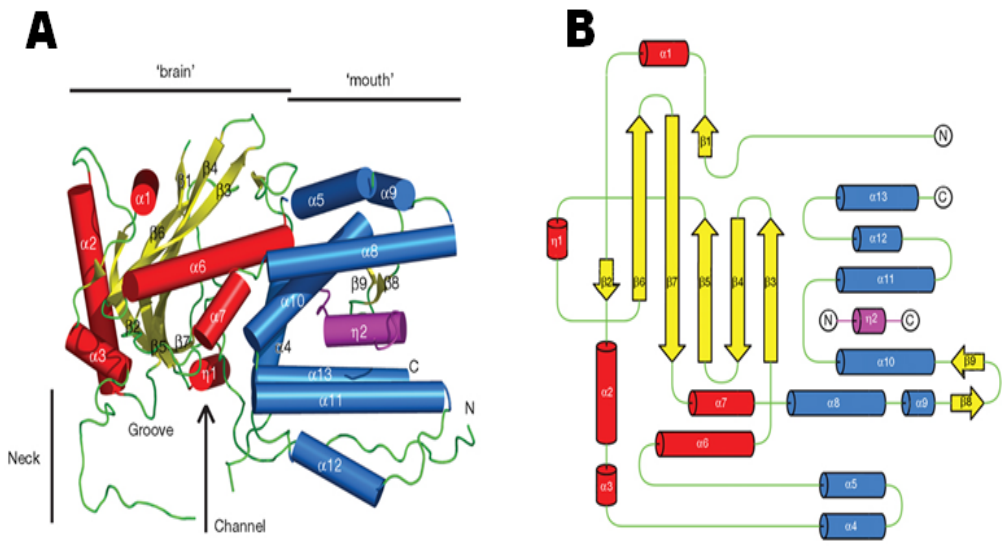

Figure 1.3 Topology of the $PA_{257-716}$ and $PB1_{1-25}$ interaction (He et al 2008)
The complex formed between the C-terminus of PA (PB1-interacting helical domain in blue, strands in yellow, and extended loops in red) and the N-terminus of PB1 (purple) is shown through a topological diagram. Figure taken from He et al (2008).

The biochemical interactions between the polymerase components have been well studied in the literature. The published crystal structure of $PB1_{1-25}$ in complex with $PA_{257-716}$ shows that PB1 interacts in a conserved cleft of the C-terminus of PA with an array of hydrogen bonds and hydrophobic interactions that resemble the "jaws of a dragon's head" (**Fig 1.3**) (Boivin et al 2010; He et al 2008). Residues 1-3 of PB1 (aspartic acid, valine and asparagine, respectively) form anti-parallel beta-sheet like interactions with Ile 621 to Glu 623 of PA. Asn 412, Ile 621, Pro 620 and Gln 670 of PA all form hydrogen bonds with the carbonyl oxygen atoms of Asp 2, Val 3, Phe 9, Leu 10

and Val 12 of PB1, respectively. Hydrophobic interactions also contribute greatly to the PB1-PA binding complex, as Pro 5 of PB1 packs between Phe 411 and Trp 706 of PA, while Leu 8 interacts with Met 595, Trp 619, Val 636 and Leu 640 (Obayashi et al 2008).

The N-terminus of PB2 (amino acids 1-37) was also crystallized in complex with the C-terminus of PB1 (amino acids 678-757), providing even greater insight into the structural biochemistry of the polymerase complex. The PB1-PB2 interaction is supported by four main salt bridges: Glu 2 and Lys 698, Arg 3 and Asp 725, Arg 3 and Lys 698, and Glu 6 and Lys 698. Additional hydrogen bonding between main chain atoms and buried hydrophobic interactions further contribute to the interaction (Sugiyama et al 2009). Interestingly, although PB2 and PA do not directly interact together, a 2013 study has shown that co-incorporation of PB2 and PA from the same Influenza strain into progeny viruses might be a requirement for genetic reassortment (Hara et al 2013).

The polymerase has no proofreading ability, resulting in approximately one mutation per genome per replication cycle, which is fairly substantial considering that the Influenza genome is only 14,000 bases (Drake 1993). Comparatively, *H. sapiens* have an estimated mutation rate of only one mutation every 2.5×10^{8} bases, and the four orders of magnitude higher rate of mutation in Influenza due to the low fidelity of the polymerase contributes greatly to antigenic drift (Nachman and Crowell 2000).

The polymerase is an intriguing target for drug discovery. Despite antigenic drift, there is a lower probability of obtaining a mutation in any of the polymerase subunits since the virus expresses their mRNA levels at a much lower amount compared to other viral transcripts. Furthermore, a mutation in PB1, PB2 or PA might compromise viral fitness, since a functioning polymerase is absolutely necessary for full virulence (Cheng et al 2012). Of the three current anti-virals targeting polymerase function, ribavirin (nucleoside inhibitor) is not considered a drug of choice because of its toxicity and lack of community benefit, and viramidine (another nucleoside inhibitor) and favipiravir (nucleotide analogue) are both in clinical trials and not yet FDA or Health Canada approved (Cheng et al 2012; Kiso et al 2010; Sidwell et al 2005).

1.9 Peptide Mimetics

Peptide mimetics are small (generally 1-40 amino acids in length) dominant negatives that contain the binding domain of a certain protein, but lack a catalytic or effector domain (Mason 2010). The peptide binds to a protein of interest, but because it lacks a catalytic domain it does not contribute in downstream signaling. Therefore, peptide mimetics essentially mimic the protein of interest's binding partner and can be employed to inhibit signal pathways and other molecular processes. The use of peptide mimetics to target specific proteins and disrupt critical protein-protein interactions has been previously used *in vitro* to reasonable success in bacterial and viral pathogenesis. For instance, the Mahony laboratory has used a peptide mimetic targeting the *Chlamydia pneumonia* Type III Secretion (T3SS) tethering protein CdsL by mimicking the T3SS ATPase to inhibit growth and replication of the bacteria (Stone et al 2011).

Similarly, a peptide mimetic targeting the HIV-1 glycoprotein gp120 by mimicking the host cell receptors CCR5 and CD4 was shown to inhibit HIV-1 entry into GHOST cells expressing the CCR5 and CD4 receptors (Kwong et al 2011).

Unlike small molecules that bind to a specific amino acid or site on a protein, mimetics can have several interacting amino acids, thereby making abrogation by a single amino acid mutation unlikely. Nevertheless, peptide mimetics are not without their limitations: their large >900 Dalton size does not allow them to passively cross the plasma membrane, therefore requiring modification to obtain cellular entry if the target is not surface exposed. Furthermore, peptides and proteins are prone to proteolytic degradation, making their bioavailability an issue (Mason 2010). Nevertheless, peptide mimetic therapy is an intriguing and innovative strategy in combating bacterial pathogens, especially Influenza that mutates quite rapidly.

1.10 Thesis Objectives: Targeting the Polymerase with PB1 mimetics

In 2007, Ghanem et al employed peptide mimetics *in vitro* by transfecting HEK293T cells with plasmids expressing the N-terminus (first 25 amino acids) of the PB1 protein, and showing a decrease in viral titer after infection with the 1933 Influenza strain compared to cells transfected with an empty plasmid (Ghanem et al 2007). The purpose of this thesis is to extend the above research in a more clinically relevant setting by designing a stable and effective chimeric cell-penetrating peptide containing the N-terminus of PB1 that would bind to the C-terminus of PA and prevent assembly of the Influenza A polymerase, therefore inhibiting replication. We chose the N-terminus of

PB1 as a mimetic since the PB1-PA interaction is absolutely necessary for the viral polymerase to assemble and the first 50 amino acids of this protein are very well conserved among different Influenza A strains (**Fig 1.4**), making this therapeutic applicable to all Influenza A strains. In this thesis, a small 20 amino acid PB1 peptide mimetic ($PB_{1\text{-}20}$) was designed using overlapping PCR and attached to the HIV-1 Tat Nuclear Localization Signal (NLS) and affinity tagged *E. coli* Maltose Binding Protein (HisMBP) to create a chimeric HisMBP-NLS-$PB1_{1\text{-}20}$ protein. We show that this mimetic inhibits Influenza A replication and growth *in vitro*, and that the protein is also non-toxic *in vitro*.

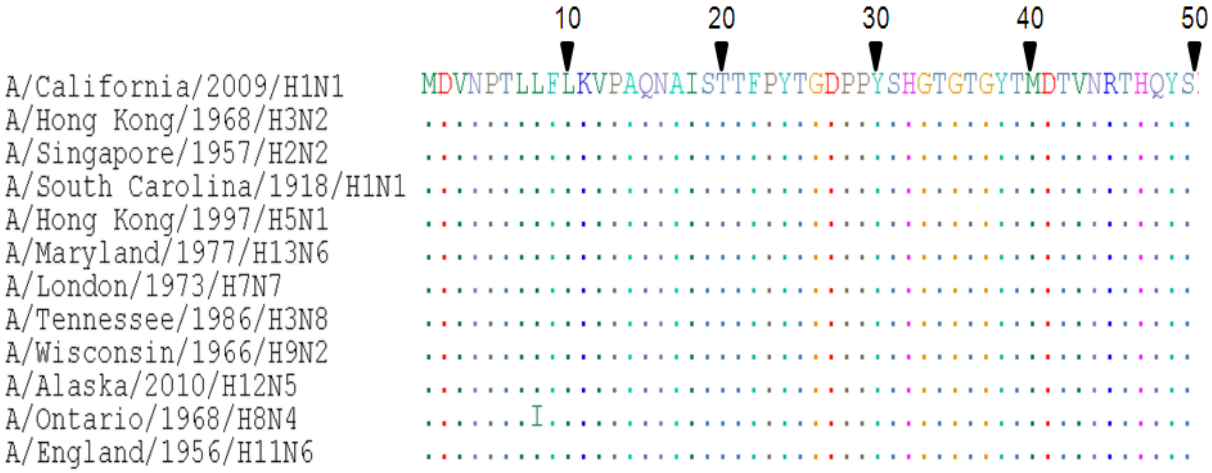

Figure 1.4 ClustalW alignment of $PB1_{1\text{-}50}$ of different Influenza A strains display sequence similarity
The first 50 amino acids of PB1 from 12 different Influenza A strains were aligned using the ClustalW algorithm. Sequences display 100% identity (as shown by dots) with the exception of the conserved A/Ontario/1968/H8N4 L8I mutation, which still retains the same charge and similarity. The first four strains from the top are the most recent Influenza A pandemics in reverse chronological order (swine, Hong Kong, Asia, Spanish).

We then employed *in silico* ZMM molecular modeling to analyze the binding domains of the PB1-PA interaction in order to determine the hypothetical free energy of binding between different amino acids at different N-terminal PB1 positions. We

identified two significant substitutions for threonine at position 6 as having a much lower free energy of binding (see **Supplementary Figure S1**): T6R and T6E. Using an *in vitro* inhibition assay and qPCR, both mutations were shown to increase the potency of the HisMBP-NLS-PB1$_{1-20}$ mimetic. The mutant mimetics were also shown to be non-toxic *in vitro*.

The mechanism of inhibition was also investigated: we hypothesized that the mimetic would enter the cells and be targeted to the nucleus via the NLS, and bind to the C-terminus of PA, thereby preventing the polymerase from assembling and inhibiting Influenza replication. Using a cell uptake assay, NLS-tagged proteins were shown to enter the cell cytoplasm within an hour of incubation. By biochemically extracting cell nuclei, NLS-tagged proteins were also shown to be targeted to the nucleus. A GST pull down was used to show that the HisMBP-NLS-PB1$_{1-20}$ mimetic interacts with the C-terminus of PA.

Previous unpublished work in the Mahony laboratory suggested that a peptide mimetic containing just the first seven amino acids of the PB1 N-terminus attached to a nuclear localization signal (NLS-PB1$_{1-7}$) was sufficient to inhibit Influenza A replication and growth at a working concentration of at least 200 µM (see **Supplementary Figure S2**). This experiment was repeated to see if the 7-mer attached to maltose binding protein (HisMBP-NLS-PB1$_{1-7}$) could also inhibit Influenza A at a similar concentration to the 20-mer mimetic.

CHAPTER TWO

MATERIALS AND METHODS

2.1 Genetic cloning and construct design for the Gateway® system

Chimeric amplicons of the HIV-1 Tat NLS (YGRKKRRQRRR) and first 20 amino acids of the PB1 polymerase subunit ($PB1_{1-20}$) were amplified using overlapping PCR primers (listed in the Appendix) as previously described (Heckman and Pease, 2007). The amplicons contained *attB* recombination overhang sites at each end and were cloned into the Invitrogen Gateway® Cloning System. Purified PCR products were incubated with the Gateway® *pDONR201* entry vector and Gateway® BP Clonase enzyme mix in TE Buffer (10 mM Tris-HCl pH 8.0, 1 mM EDTA) for 1 hour at room temperature to generate *pENT* vectors (BP Reaction). The reactions were stopped by incubating with 0.2 µg/mL Proteinase K for 10 minutes at 37°C. The *pENT* vectors were transformed into *Escherichia. coli* Turbo (New England Biolabs, Ipswich MA) chemically competent cells by 42°C heat shock and subsequently plasmid purified and used in a Gateway® LR reaction with the *pDEST-HisMBP* (N-terminal HisMBP fusion tag) or *pDEST15* (N-terminal GST fusion tag) vectors and Gateway® LR Clonase enzyme mix to generate the desired expression plasmids.

The C-terminus of pandemic 2009 H1N1 Influenza A PA gene ($PA_{257-716}$) was PCR amplified from the *pCAGGS-ACal04PA* vector (graciously donated to us by Dr. Toru Takimoto) with primers containing the 5' *attB* Gateway® recombination sites. The gene was ultimately cloned into the desired expression plasmid. All constructs were sequenced in the *pENT* vectors by the MOBIX facility.

2.2.1 *E. coli* chemical competent cell preparation

E. coli BL21 (DE3), Rosetta (DE3) (Life Technologies, Burlington ON) or Turbo were cultivated in aerobic conditions at 37°C in LB broth (1% w/v bacto-tryptone, 0.5% w/v bacto-yeast extract, 1% w/v NaCl) shaking at 250 RPM overnight. Cells were inoculated in a 1:50 ratio into new LB broth and incubated at 37°C and 250 RPM until an OD_{600} of 0.5 was obtained. Cells were then incubated on ice for 15 minutes and harvested at 1,500 x g for 10 minutes at 4°C. The cells were resuspended in ice cold 10 mM $MgSO_4$ and incubated on ice for 30 minutes. The cells were harvested as previously described, and incubated on ice with 50 mM $CaCl_2$ for 30 minutes. The cells were harvested and resuspended in ice cold 50 mM $CaCl_2$ supplemented with 15% (v/v) glycerol. The cells were aliquoted in 55 µL fractions and stored at -80°C.

2.2.2 *E. coli* transformation

Chemically competent *E. coli* cells were thawed on ice and incubated with 50-150 ng of plasmid DNA on ice for 20 minutes. Cells were then heat shocked for 42 seconds at 42°C and incubated on ice for another 2 minutes. After the addition of 700 µL SOC media (2% w/v bio tryptone, 0.5% w/v yeast extract, 0.05% w/v NaCl, 5 mM KCl, 10 mM $MgCl_2$, 4 mM glucose), cells were incubated at 37°C for one hour. Cells were then plated on LB 1.5% (w/v) agar supplemented with either 100 µg/mL ampicillin or 30 µg/mL kanamycin overnight at 37°C. Individual colonies were selected for screening and glycerol stocks were created for long term -80°C storage by mixing stationary phase bacteria in LB broth with glycerol to a final concentration of 10%.

2.2.3 Recombinant protein expression and affinity purification

E. coli BL21 (DE3) or Rosetta (DE3) *pLysS* cells containing expression plasmids under control of the *tac* or *lacUV5* promoters were incubated overnight at 37°C and 250 RPM in LB broth. Stationary phase cells were inoculated at a 1:50 ratio in 6 L of LB broth supplemented with 100 µg/mL of ampicillin. Cells were incubated at 37°C and 250 RPM until the cultures reached an OD_{600} of 0.6, at which the expression of recombinant proteins was induced with the addition of 0.5 mM IPTG. The cultures were then incubated for an additional two hours at ambient room temperature and 250 RPM. Cells were harvested at 8, 000 x g for 2 minutes at 4°C and resuspended in either Nickel A Buffer for 6xHis-tagged proteins (20 mM Tris-HCl pH 7.0, 0.03% LDAO, 0.02% β-mercaptoethanol, 500 mM KCl, 10% glycerol, 10 mM imidazole) or PBS for GST-tagged proteins containing one EDTA-free Protease Inhibitor mini tablet (Roche, Laval QC). The cells were then lysed by sonication six times at 25 Watt for 20 seconds with 30 second rests on ice in between each pulse. The soluble supernatant fraction was separated from the insoluble pellet fraction by centrifugation at 42, 000 x g for 45 minutes at 4°C and filtered through a 0.22 µm bottle filter (Fischer Scientific, Whitby ON).

Hexa-histidine tagged recombinant proteins were purified by Fast Protein Liquid Chromatography (FPLC) using the Akta FPLC (GE Healthcare). Lysates were run through a 1 ml His-Trap™ FF column (charged with 15 ml of 100 mM $NiCl_2$) and washed with Nickel A Buffer. GST-tagged proteins were purified on a 1 ml GSTrap™ FF column and washed with PBS. Proteins were eluted off the column with either Nickel B

Buffer (Nickel A with 300 mM imidazole) or 1.5 mg/mL reduced glutathione in 20 mM Tris pH 9.0, and then dialyzed into PBS containing 10% glycerol using the HiPrep 26/10 Desalting Column (GE Healthcare). Purified proteins were concentrated at 1,500 x g for 60 minutes (4°C) in an Amicon Ultra-15 Centrifugal Filter (Millipore, Billerica MA).

2.2.4 Protein quantification

Purified protein was quantified using a modified version of the Lowry assay (Lowry et al, 1951). Protein was treated with 127.5 µL of a copper sulfate containing buffer (Reagent A), followed by 1 mL of dilute Folin reagent (Reagent B) according to the manufacturer's instructions (Biorad, Mississauga ON). Absorbance was read at 750 nm and the protein concentration was determined based on a BSA standard curve in the same buffer that the protein of interest was dialyzed into in **Section 2.2.3**.

2.3 MDCK cell culturing

Madin-Darby Canine Kidney cells (Cederlane, Burlington ON) were used as a host cell line for Influenza propagation, tittering, infection, and toxicity experiments. Cells were cultured in MEM (Invitrogen, Mississauga ON) supplemented with 10% heat-inactivated FBS (Invitrogen) at 37°C and 5% CO_2 in a sterile T75 or T125 culture flask. Cells were split every 2-4 days by removing the media, washing the monolayer with 1 mL of sterile 5 µg/mL Trypsin-EDTA (Invitrogen), and incubating cells with 5 mL of Trypsin-EDTA at 37°C and 5% CO_2 for 5-10 minutes. Trypsin-treated cells were then added to a new T75 or T125 flasks containing MEM+10%FBS in a 1:6 ratio.

For long term storage, confluent MDCK cells were treated with Trypsin and harvested at 500 x g for 5 minutes. The cells were then resuspended in 10 mL of MEM+10% FBS, and 900 µL of cells were added to 100 µL of sterile DMSO in a 1.5 mL cryoprotective vial. Cells were incubated at -20°C for one hour, -80°C overnight (16-20 hours) and then stored in liquid nitrogen.

To quantify cell concentration for seeding, Trypsin-treated cells were harvested at 500 x g for 5 minutes, resuspended in 10 ml of MEM+10% FBS and 0.4% Trypan Blue was added in a 1:1 ratio. A 10 µL aliquot of this solution was added to a single chamber of a Bright-Line Hemacytometer (Hausser Scientific, Horsham PA) and the number of cells in each corner square were added and averaged to determine the concentration of MDCK cells according to the manufacturer's guidelines.

2.4.1 Influenza culturing: propagation

Unquantified pandemic H1N1 Influenza A virus (A/California/04/2009(H1N1)) was obtained from a clinical swab from the St. Joseph's Hospital virology laboratory, and 20 µL was added to 10 mL of R-Mix Refeed Media (Diagnostic Hybrids, Athens OH). The diluted virus was then added to a Rhesus Monkey Kidney round bottom glass tube (Diagnostic Hybrids) and incubated at 37°C and 5% CO_2 for six days (tubes were gently shaken every 24 hours). The infected cells were scraped with a sterile cell scraper, vortexed for 10 seconds with sterile glass beads and centrifuged at 500 x g for 5 minutes. The supernatant (containing propagated H1N1 virus) was run through a 0.2 µm filter and stored in aliquots at -80°C.

2.4.2 Influenza culturing: plaque assay titering

Confluent MDCK cells were seeded into separate wells of a 9.5 cm^2 6-well plate and incubated at 37°C and 5% CO_2 until 100% confluency (approximately $9.5x10^5$ cells per well). The cells were washed twice with sterile PBS, and H1N1 virus from **Section 2.4.1** was serially diluted into PBS supplemented with 20 µg/mL TPCK-treated Trypsin (Sigma-Aldrich, Oakville ON). Duplicate 100 µL aliquots of each dilution were added to each well and incubated at 37°C and 5% CO_2 for 30 minutes (plates were gently swirled every 5 minutes). The infected cells were washed twice with sterile PBS, overlaid with 2 mL of MEM supplemented with 0.2% (w/v) agarose (no FBS) per well and the plates were incubated at 34°C and 4% CO_2 for 72 hours. After the incubation period, the agar was gently removed and 1 mL of 0.5% (w/v) crystal violet solution was added to each well. After a 30 minute incubation at room temperature, the plates were washed with sterile ddH_2O to remove excess stain. The number of plaques was counted at the appropriate dilution and the original virus stock was quantified as plaque forming units per mL (pfu/mL).

2.4.3 Influenza culturing: hemagglutination assay tittering

Human red blood cells described were harvested at 1, 000 x g for 5 minutes at room temperature. A packed cell volume of 2 mL was diluted with sterile PBS supplemented with 20 µg/mL TPCK-treated Trypsin to get a 2.5% RBC solution. Fifty microliters of this solution was added into separated wells of a clear, round bottom 96 well plate. Fifty microliters of unquantified virus from 2.4.1 was added to the first well,

and two-fold serial dilutions were performed on each subsequent well (50 µL of RBC-virus solution into 50 µL RBC). The plate was incubated from 1 hour at 37°C and 5% CO_2. Titer was determined by the highest dilution of virus that agglutinated red blood cells.

2.5.1 RNA extraction from HepG2 cells

HepG2 cells (donated to us from Dr. Shirya Rashid) were cultured in DMEM (Invitrogen) supplemented with 10% heat-inactivated FBS (Invitrogen) at 37°C and 5% CO_2 in a sterile T75 culture flask and split every 2-4 days. Confluent cells were treated with 5 µg/mL of Trypsin-EDTA and incubated at 37°C and 5% CO_2 for 5 minutes. Trypsin-treated cells were harvested at 500 x g for 5 minutes and the cell pellet was then resuspended with 600 µL of Buffer RLT (QIAGEN, Toronto ON) supplemented with 0.1% β-mercaptoethanol. Cells were vortexed for 1 minute and 600 µL of 70% ethanol was added to the lysate after homogenization. The lysate was then centrifuged in an RNeasy spin column (QIAGEN) for 2 minutes at 16,000 x g. The column (containing bound RNA) was washed with 700 µL of Buffer RWI (QIAGEN) and centrifuged for 15 seconds at 8,000 x g. The column was then washed twice with 500 µL Buffer RPE (QIAGEN) and centrifuged for 2 minutes at 16, 000 x g. RNA was eluted with sterile water and centrifugation at 16, 000 x g for 1 minute. RNA was quantified using the Nanodrop Spectrophotometer (Fisher Scientific).

2.5.2 RT-PCR for the preparation of cDNA

RNA extracted from 2.5.1 was incubated with 1.4 volumes of dNTP buffer (1.4 mM dNTP, 250 ng non-specific primers) for 5 minutes at 70°C. The reaction was chilled on ice and subsequently incubated with 1.7 volumes of 1^{st} strand buffer (200 mM NaCl, 50 mM Tris-HCl pH 8.9, 25 mM MgSO4, 0.05% (w/v) gelatin, 40 units RNaseOUT (Invitrogen), 0.02 M DTT) for two minutes at 37°C. 200 units of M-MLV (Invitrogen) was then added to the reaction and incubated at room temperature for 10 minutes and 37°C for 50 minutes. Once completed, the reaction was stopped with a 10 minute 70°C incubation. Samples (now containing cDNA) were stored at -20°C until needed.

2.6.1 Viral inhibition assay to determine mimetic activity: fluorescence microscopy

MDCK cells were seeded into shell vials containing microscopic cover slips at a concentration of 2.5 x 10^5 cells per vial (as described in 2.3) in MEM+10% FBS and incubated 16-24 hours at 37°C and 5% CO_2 to allow cells to adhere. The media was removed, cells were washed with sterile PBS and incubated with the appropriate constructs from **Section 2.2.3** in MEM without FBS for one hour at 37°C and 5% CO_2.The media was removed and the cells were challenged with pandemic 2009 H1N1 Influenza A in MEM at an MOI of 0.1. Shell vials were centrifuged at 1, 500 x g for 30 minutes and incubated 37°C and 5% CO_2 for another 30 minutes. The viral media was removed and the cells were treated with another round of purified recombinant protein in MEM for 24 hours at 37°C and 5% CO_2.

After 24 hours, the media was removed and the cells were fixed to the cover slips with the addition of 1 mL of ice cold acetone and incubated at room temperature for 30 minutes. The fixed cells were washed with sterile PBS and then incubated with D-Ultra Respiratory Virus Screening DFA Reagent (Diagnostic Hybrids) for 30 minutes at room temperature in the dark. Vials were washed with sterile PBS and cover slips were mounted face down on glass slides with mounting media (sterile PBS and 50% glycerol). Cover slips of fixed cells were visualized by fluorescence microscopy using the Olympus BX51 Fluorescence Microscope at 10X Magnification. Percent inhibition was calculated as follows: (V-Y)/Vx100%, where 'V' is the average number of viruses per field of view (FOV) of the virus only control and 'Y' is the average number of viruses/FOV of the peptide variable. Statistical significance was calculated using Student's t-test.

2.6.2 Viral inhibition assay to determine mimetic activity: quantitative polymerase chain reaction

MDCK cells were seeded into separate wells of a 6 well plate and incubated at 37°C and 5% CO_2 until confluency as described in 2.4.2. The cells were washed with 1 mL of sterile PBS and treated with 50 µM of purified recombinant protein mimetics in MEM for 1 hour at 37°C and 5% CO_2. The cells were then infected with pandemic H1N1 Influenza A in MEM (MOI = 0.1) for 2 hours at 37°C and 5% CO_2. After the incubation time, the viral media was removed, 2 mL of 50 µM mimetic was added per well, and the plate was incubated at 37°C and 5% CO_2 for 24 hours. Total nucleic acids (both host and viral) were then extracted from infected cells using the NucliSENS miniMAG

extraction protocol (Biomémireux, Laval QC) according to the manufacturer's guidelines.

The SuperScript ® III Platinum ® One-Step qRT-PCR kit (Invitrogen) was used in a qPCR assay according to the manufacturer's guidelines. Decrease in fold change was calculated by dividing the average Matrix (viral) transcript copy number by the average Actin (loading control) transcript copy number to obtain an M/A ratio. The M/A ratio for each construct was then divided by the average transcript copy number of the no mimetic control to get fold change increase. Fold change decrease was calculated by taking the reciprocal of fold change increase. Error bars represent two standard deviations of three independent experiments.

2.7.1 Mimetic toxicity – red blood cell lysis assay

Purified RBCs in sterile PBS were counted by a CBC panel (graciously performed by the Hamilton Regional Laboratory in St. Joseph's Hospital) and $5.0x10^8$ cells were added to separate 1.5 mL microcentrifuge tubes. Purified proteins in PBS were added to each tube to a final concentration of 50 µM and were incubated at 37°C and 5%CO_2 for 1-72 hours. As controls, sterile PBS and Lysis buffer (0.1% SDS, 1% Triton X-100) were incubated with the RBCs. Samples were centrifuged at 1,000 x g for 5 minutes and the supernatants (in triplicates) were placed in separate wells of a 96 well clear-bottom plate. The absorbance was read at 420 nm using the Biotek MicroQuant Plate Reader. Percent Lysis (%Lysis) was calculated as follows: $(A_{420}\text{-PBS})/(\text{Lysis-PBS})x100$, where '$A_{420}$' represents the average absorbance of the variable supernatant, 'PBS' represent average absorbance of the PBS buffer supernatant and 'Lysis'

represents the average absorbance of the lysis buffer supernatant. Statistical significance was calculated using Student's t-test.

2.7.2 Mimetic toxicity – MDCK cell growth assay

To access toxicity of the mimetic, MDCK cell growth was measured. MDCK cells were seeded into separate wells of a 24-well plate at a concentration of $5.0x10^5$ cells/well in MEM+10%FBS. Cells were allowed to adhere to the wells for 16-24 hours at 37°C and 5% CO_2. The media was removed and cells were incubated with purified recombinant proteins at 50 µM in MEM+10% FBS, MEM alone or 1% Triton X-100 at 37°C and 5% CO_2 for 0, 4, 8, 24, 48 and 72 hours. The media was removed and the cells were washed twice with sterile PBS. The cells were treated with 5 µg/mL Trypsin-EDTA at 37°C and 5% CO_2 for 10 minutes. The cells were then transferred to a 1 cm cuvette and the absorbance was measured in triplicates at 800 nm (5 µg/mL Trypsin-EDTA was used as the blank).

2.7.3 Mimetic toxicity – ATP bioluminescence assay

To access toxicity of the mimetic on MDCK cells, total ATP was measured as an indicator for cell viability. MDCK cells were seeded into separate wells of a 24-well plate at a concentration of $5.0x10^4$ cells/well in MEM+10%FBS and allowed to adhere to the wells for 16-24 hours at 37°C and 5% CO_2. The media was removed and cells were incubated with purified recombinant proteins at 50 µM in MEM+10% FBS, MEM+10% FBS alone or lysis buffer (0.1% SDS 1% Triton X-100) at 37°C and 5% CO_2 for 0, 4, 8, 24, 48 and 72 hours. After the appropriate time, the media was removed and the cells

were washed twice with sterile PBS. The ViaLight™ Plus kit (Lonza, Mississauga ON) was then used to detect metabolic activity through a bioluminescent measurement of total ATP. Lysis buffer was added to the wells of the cells, which were then scraped with a pipet and transferred to separate eppendorf tubes. The cell lysates were incubated with equal volumes of the AMR Reagent (containing Luciferase and luciferin) according to the manufacturer's guidelines for 10 minutes at room temperature. The tubes were placed in the 20/20n luminometer (Promega, Madison WI) and 1 second integrated luminescence readings were taken in triplicates.

2.8.1 Polyacrylamide gel electrophoresis of proteins

Protein samples were incubated with equal volumes of 2X sample buffer (100 mM Tris pH 7.0, 4% SDS, 2 mM EDTA, 10% (v/v) glycerol, 0.002% (w/v) bromophenol blue, 10% (v/v) β-mercapoethanol) and boiled at 100°C for 10 minutes. Polyacrylamide gels (discontinuous gel system) were cast on the mini-PROTEAN Tetra Cell Casting Module (Bio Rad, Mississauga ON). A 12% resolving gel (375 mM Tris-HCl pH 6.8, 0.1% (v/v) SDS, 12% (v/v) Acryl/Bis-Acryl, 0.4% (v/v) TEMED, 0.1% (v/v) APS) was first poured into the chamber, followed by a stacking gel (5% (v/v) Acryl/Bis-Acryl, 100 mM Tris-HCl pH 8.7, 0.1% (v/v) SDS, 0.1%(v/v) APS, 0.4% (v/v) TEMED). A 10 or 15 well comb was added to the stacking gel and once solidified the gel was assembled in the mini-PROTEAN Tetra Cell (Bio Rad). The cell was filled with SDS running buffer (25 mM Tris pH 9.5, 192 mM glycine, 0.1% SDS) and boiled proteins in sample buffer were added to separate wells of the gel. Proteins were electrophoretically separated by 50 V

through the stacking gel and 150 V through the resolving gel using the PowerPac Universal Power Supply (Bio Rad).

2.8.2 Western blot analysis

Proteins on polyacrylamide gels from **Section 2.7.1** were electrophoretically transferred to a nitrocellulose membrane using the iBlot apparatus (Invitrogen) on the P3 setting for 7 minutes. The membrane was blocked with 5% (w/v) skim milk powder in PBS+0.1% Tween-20 (PBST) for 1 hour and incubated with either anti-GST, anti-β-actin, anti-DnaK, or anti-His_6 primary antibodies (all at a 1:5000 dilution from Sigma) in blocking buffer overnight at 4°C. The membrane was washed three times in PBST for 15 minutes and incubated with 1:5000 goat anti-mouse-HRP (Sigma) secondary antibody in blocking buffer for 1 hour. The membrane was washed three times for 15 minutes in PBST and protein was visualized with enhanced chemiluminescence (Pierce).

2.9 Cellular uptake of peptide mimetics assay

MDCK cells were seeded in 24-well plates at a concentration of $5.0x10^5$ cells/well in MEM+10% FBS and allowed to adhere to the wells for 16-24 hours at 37°C and 5% CO_2. The media was removed and purified recombinant proteins in MEM+10%FBS (at a final concentration of 20 μM) were added to the cells and incubated for 1 hour at 37°C and 5% CO_2. After 1 hour, the cells were washed with sterile PBS and then incubated with 0.5 mg/mL Trypsin-EDTA (Sigma) for 5 minutes at 37°C and 5% CO_2. Trypsin treated cells were harvested at 500 x g for five minutes, the Trypsin was removed and

the cells were resuspended in 2X sample buffer and boiled for 10 minutes. Samples were separated by electrophoresis in a 12% acrylamide gel and analysed by western blot analysis as described above.

2.10 Nuclear isolation method

MDCK cells were seeded into separate 20 cm^2 cell culture dishes and grown at 37°C and 5% CO_2 until confluent. Media was removed and cells were incubated with 5 mg of purified protein in MEM for 1 hour at 37°C/5%CO_2. Plates were washed twice with sterile PBS, treated with 0.5 mg/mL Trypsin, and incubated with ice cold nuclear extraction buffer (10 mM HEPES pH 7.9, 10 mM KCl, 0.1 mM EDTA, 0.4% IGEPAL, 1 mM DTT, 1 cOmplete EDTA-free protease inhibitor table) for 10 minutes. Cells were scraped with a sterile cell scraper, and centrifuged at 16, 000 x g for 3 minutes at 4°C. The pellet was resuspended in 2X sample buffer, boiled for ten minutes and saved at -20°C as the nuclear fraction.

The supernatant was treated with 10% tetrachloroacetic acid (TCA) at 0°C overnight. Samples were centrifuged at 16, 000 x g for 20 minutes at 4°C, the supernatant was discarded and the pellet was incubated with ice cold acetone for 1 hour at -80°C. Samples were centrifuged again at 16, 000 x g for 20 minutes (4°C), the supernatant was discarded and the pellet (cytosolic fraction) was resuspended in 2X sample buffer and boiled for 10 minutes.

Both cytosolic and nuclear fractions were electrophoretically separated and analyzed by western blot as described in **Section 2.8**.

2.11 GST pull down assay

Plasmids containing GST-tagged genes were transformed into *E. coli* BL21 (DE3) or Rosetta (DE3) *pLysS* and cell lysates containing recombinant GST-tagged proteins were obtained as previously described above. Glutathione-agarose beads (Sigma-Aldrich) were swelled in deionized water for two hours at room temperature, harvested at 500 x g for 5 minutes and washed three times with PBS. The glutathione-agarose beads were then incubated with *E. coli* lystates containing either overexpressed GST or GST-$PA_{257-716}$ for two hours at 4°C while shaking. The beads (containing GST-tagged proteins) were washed twice with PBS and incubated with 1 mg of purified recombinant HisMBP-NLS-$PB1_{1-20}$ or HisMBP-NLS-Ctrl at 4°C overnight. A sample of the unbound protein fraction was collected, while the beads were washed 4 times for 15 minutes while nutating at 4°C in a high salt buffer (20 mM Tris pH 7.0, 500 mM NaCl, 0.1% v/v Triton X-100). A sample of the final wash fraction was collected, and the all fractions (including the beads) were then resuspended in 2X sample buffer, boiled, electrophoretically separated on a 12% SDS-PAGE gel and analyzed by western blot as previously described.

2.12.1 HSA construct expression optimization in *E. coli*

Gateway® destination vector containing the His-HSA-NLS-$PB1_{1-20}$ mimetic gene (cloned as described in **Sections 2.1 and 2.5**) was transformed into *E. coli* Rosetta (DE3) *pLysS* or *E. coli* Rosetta-Game (DE3) *pLysS* and a single colony was picked and grown in LB broth overnight at 37°C and 250 RPM. Stationary phase cells were

inoculated at a 1:50 ratio in 50 mL of LB broth supplemented with 100 µg/mL of ampicillin. Cells were incubated at 37°C and 250 RPM until the cultures reached an OD_{600} of 0.55, at which cells were then evenly distributed into sixteen different culture tubes (3 mL) with the following conditions: 1 mM PMSF (added or not added), induction temperature (16°C or 37°C), incubation temperature post induction (21°C, 37°C) and incubation time (2 hours or 3 hours). Cells were induced with the addition of 1 mM IPTG and incubated at the appropriate conditions and times. The OD_{600} of each culture was recorded and cells were harvested at 8,000 x g for 2 minutes. The cell pellets were resuspended in (OD_{600} x 100 µL) of 2X sample buffer, and boiled for 20 minutes. Samples were analysed by western blot analysis as described in Section 2.8.

2.12.2 HSA construct expression in a cell-free expression system

The His-HSA-NLS-$PB1_{1-20}$ construct cloned into the *pDEST17* destination vector was purified from *E. coli* NEB Turbo and 1 µg of DNA was used in the Promega Cell-Free Expression System (Promega, Madison WI) in a half-reaction according to the manufacturer's guidelines. The reaction was incubated at 37°C for 1 hour, and 2X sample buffer was added in a 1:1 ratio. The sample was boiled for 10 minutes and ran twice on a 12% polyacrylamide gel as described in **Section 2.8.1**. One of the gels was analyzed by western blot using an anti-His_6 antibody as described in **Section 2.8.2**, while the other gel was incubated for 1 hour with Coomassie staining solution (0.25% w/v Coomassie R-250, 45% v/v methanol, 10% v/v glacial acetic acid). The gel was destained in destaining solution (45% v/v methanol, 10% v/v glacial acetic acid) for 2 hours and bands were visualized by eye.

2.13.1 Genetic cloning of HisHSA-NLS-PB1$_{1-20}$ into the *pPicz9ssamp* yeast expression vector

The His-HSA-NLS-PB1$_{1-20}$ PCR product was amplified using overlapping PCR as previously described (Heckman and Pease, 2007). The forward primer for the NLS-PB1 PCR product contained the palindromic XhoI nucleotides at the 5' end (as well as the last 18 nucleotides of the *P. pastoris* α secretion factor) while the reverse primer contained the first 18 nucleotides of HSA at the 5' end. The forward primer for the HSA PCR product contained the first 18 nucleotides of NLS-PB1 at the 5' end while the reverse primer contained the palindromic EcoRI nucleotides at the 5' end. The PCR product was purified using the BioBasic PCR Purification kit (BioBasic, Markham ON) according to the manufacturer's guidelines. 5 µg of purified PCR product and *pPicz9ssamp* vector (obtained from Dr. William Sheffield) was digested with 20 units of XhoI and EcoRI (New England Biolabs) in 0.1 µg/mL BSA and 1X NEBuffer 4 (50 mM potassium acetate, 20 mM Tris-acetate, 10 mM magnesium acetate, 1 mM DTT, pH 7.9) for 1 hour at 37ºC. DNA was PCR purified using the BioBasic kit and the cut HisHSA-NLS-PB1$_{1-20}$ PCR product was ligated with the cut *pPicz9ssamp* vector in a 3:1 (insert: vector) molar ratio with 10 units of T4 DNA Ligase (Invitrogen) in 1X Ligase Buffer (66 mM Trish-HCl pH 7.6, 6.6 mM $MgCl_2$, 10 mM DTT, 66 µM ATP, 3.3 µM ^{32}P pyrophosphate) at 16ºC for 16 hours and 1 µL was subsequently electroporated into E. coli NEB Turbo cells as described in **Section 2.2.2**. Colonies were picked and screen vectors with the insert present were sequenced at the MOBIX facility at McMaster University.

2.13.2 Electrocompetent *P. pastoris* preparation and transformation

0.5 mL of an overnight culture of *P. pastoris* (obtained from Dr. William Sheffield) was inoculated into 100 mL of sterile YPD (2% w/v yeast extract, 2% bacto-peptone, 2% dextrose) media and incubated at 30ºC and 250 RPM until OD_{600} reached 1.4. The culture was centrifuged at 1, 500 x g for 5 minutes at 4ºC, the supernatant was discarded and the pellet was resuspended in 100 mL of ice cold sterile deionized water. The culture was harvested twice more and resuspended first in 50 mL of ice cold sterile deionized water and then 5 mL of ice cold sterile deionized water. The cultures were harvested once more and the pellet was resuspended in 1 mL of ice cold 1.0 M sorbitol. The cultures were aliquoted in 80 µL aliquots and stored at -80ºC until needed.

5 µg of linearized vector (digested with 10 units of SacI for 1 hour at 37ºC) from **Section 2.13.1** was incubated with 80 µL of elecrocompetent *P. pastoris* cells on ice for 5 minutes and then transferred to a 0.2 cm electroporation cuvette (BioRad). The cells were electroporated using an electroporation unit with settings of a 1.5 kV charging voltage, 25 µF capacitance and100 Ω resistance. 1 mL of 1 M ice-cold sorbitol was immediately added to each cuvette and the cells were incubated at 30ºC for 1 hour. The transformation reaction was then plated on YPDS+100 µg/mL zeocin and incubated at 30ºC until colonies appeared (3-4 days).

2.13.3 *P. pastoris* miniexpression

A colony from **Section 2.13.2** was inoculated into 2.5 mL of YPD+100 µg/mL zeocin and grown overnight at 30ºC + 250 RPM. The next morning, the culture was centrifuged at 1, 500 x g for 5 minutes and the pellet was resuspended in BMM (100 mM potassium phosphate pH 6.0, 1.34% w/v yeast nitrogen base, $4x10^{-5}$% w/v biotin, 0.5% v/v methanol) to an OD_{600} of 1.0. The culture was incubated for 72 hours at 30ºC and 250 RPM with the addition of 0.5% (v/v) final concentration of methanol every 24 hours. Additionally, after every 24 hours, a 100 µL aliquot would be removed from the culture, centrifuged at 14, 000 x g for 5 minutes and the pellet resuspended in 50 µL of 2X sample buffer. These samples would be analyzed by western blot as described in **Section 2.8.2**.

2.14.1 Genetic cloning of HisMBP-NLS-$PB1_{1-20}$ into *pUB1000*

The HisMBP-NLS-$PB1_{1-20}$ PCR product was amplified from the *pDEST-HisMBP* destination vector created in **Section 2.1** using primers described in the Appendix. The 5' end of the forward primer contained the palindromic SalI nucleotides while the 5' end of the reverse primer contained the palindromic BamHI nucleotides. The PCR product was confirmed by agarose gel electrophoresis and purified using the BioBasic PCR purification kit according to the manufacturer's guidelines. Four micrograms of purified PCR product and *pUB1000* vector (obtained from Dr. Howard Jenkinson) were digested with 20 units of SalI and BamHI (New England Biolabs) in NEBuffer 4 (50 mM potassium acetate, 20 mM Tris-acetate, 10 mM magnesium acetate, 1 mM DTT, pH 7.9) for 1 hour at 37ºC. DNA was purified with the BioBasic kit and the cut HisMBP-

NLS-$PB1_{1-20}$ PCR product was ligated with the cut *pUB1000* vector in a 3:1 (insert: vector) molar ratio with 10 units of T4 DNA Ligase (Invitrogen) in 1X Ligase Buffer (66 mM Trish-HCl pH 7.6, 6.6 mM $MgCl_2$, 10 mM DTT, 66 µM ATP, 3.3 µM ^{32}P pyrophosphate) at 16ºC for 16 hours. The ligation reaction was purified using the BioBasic kit and the DNA was stored at -20°C until needed.

2.14.2 Electrocompetent *L. lactis* MG1363 preparation and transformation

GM17G media (0.5% w/v neopeptone, 0.5% w/v bactosoytone, 0.5% w/v beef extract, 0.25% w/v yeast extract, 0.05% w/v ascorbic acid, 0.1% w/v glycerolphosphate-$5H_2O$, 0.5% w/v glucose, 2.5% w/v glycine) was inoculated with an overnight culture of stationary phase *L. lactis* MG1363 in a 1:50 ratio and incubated at 30°C until the OD_{600} reached 0.5. The cells were incubated on ice for 10 minutes and harvested by centrifugation at 3, 000 x g for 10 minutes at 4°C. The supernatant was discarded and the cell pellet was washed twice in 1/10 initial culture volume of ice cold *L. lactis* electrocompetent wash buffer (0.5M sucrose, 10% v/v glycerol) and resuspended in 1/100 initial culture volume of wash buffer and stored in 50 µL aliquots at -80°C until needed.

One microgram of the ligation reaction from **Section 2.14.1** was incubated with electrocompetent *L. lactis* cells on ice for 15 minutes. The transformation reaction was then transferred to a 0.2 cm electroporation cuvette (BioRad) and electroporated at a 2.5 kV charging voltage, 25 µF capacitance and 200 Ω resistance. One milliliter of recovery media (GM17G, 0.5 M sucrose, 20 mM $MgCl_2$, 2 mM $CaCl_2$) was immediately

added and incubated on ice for 10 minutes. Cells were then incubated at 30°C for an additional 2 hours and the transformation reaction was plated on GM17 agar plates supplemented with 5 µg/mL erythromycin and incubated for 24-48 hours at 30°C. Individual colonies were selected, the plasmids were purified and the insert was confirmed by PCR diagnostics and gel electrophoresis.

2.14.3 *L. lactis* anaerobic secretion assay

Individual colonies selected from **Section 2.14.2** were inoculated in 2 mL of M17G media (GM17G without 2.5% w/v glycine) and incubated overnight at 30°C. The overnight culture was inoculated in a fresh M17G media in a 1:50 ratio and placed in the AnaeroGen™ chamber (Thermo Scientific) at 30°C overnight according to the manufacturer's guidelines. The next day, bacteria were harvested at 1,500 x g for 10 minutes. The pellet was resuspended in 25 µL of 2X sample buffer and was boiled for 10 minutes and stored at -20°C until needed. The supernatant was passed through a 0.2 µm filter (Pall), and TCA was added to 10%. The sample was then incubated on ice for 1 hour and centrifuged at 16, 000 x g for 20 minutes at 4°C. The supernatant was discarded and the precipitated protein pellet was incubated with 1 mL of ice cold acetone at -80°C for 1 hour. The sample was centrifuged at 16, 000 x g for 20 minutes at 4°C, the supernatant was discarded and the pellet was resuspended with 15 µL of 50 mM NaOH and then 25 µL of 2X sample buffer. The sample was boiled for 10 minutes and both the secreted protein fraction and cytosolic protein fraction were analyzed by western blot.

CHAPTER THREE

RESULTS

3.1 – Inhibition of Influenza A replication using a non-toxic cell penetrating $PB1_{1-20}$ mimetic *in vitro*

HEK293T cells transfected with plasmids expressing the N-terminus of the PB1 subunit (first 25 amino acids) were previously shown to decrease Influenza virus titer compared to cells transfected with an empty plasmid (Ghanem et al 2007). A dose-response viral inhibition assay was used to show that the N-terminus of the PB1 subunit was necessary to inhibit viral growth, but only the first 20 amino acids ($PB1_{1-20}$) was sufficient to do so. The $PB1_{1-20}$ peptide mimetic was fused to the HIV-1 Tat NLS (as a cell penetrating protein) and 6xHistidine-tagged Maltose Binding Protein (as a carrier molecule) to create a HisMBP-NLS-$PB1_{1-20}$ chimeric protein (for a complete list of purified proteins used in this study, see **Supplementary Figure S3**).

3.1.1 The HisMBP-NLS-$PB1_{1-20}$ mimetic inhibits Influenza replication and growth

MDCK cells were incubated with recombinant protein for 1 hour and then infected with pandemic 2009 H1N1 Influenza A for 24 hours. The cells were then visualized by fluorescence microscopy and the number of infected cells was quantified (**Fig 3.1.1A**). At a concentration of 50 µM, the PB1 mimetic was able to inhibit viral replication by 96.5±1.3% ($p<0.001$) compared to the no virus control (**Fig 3.1.1B**). The mimetic became less effective at lower concentrations, with a percent inhibition of 15.4±2.7% and 11.9±0.57% at 10 µM and 5 µM, respectively. A control mimetic containing random twenty amino acids of (HisMBP-NLS-Ctrl) but with the same overall charge as $PB1_{1-20}$

was used as a negative control and showed no significant inhibition at any concentration ($p<0.05$).

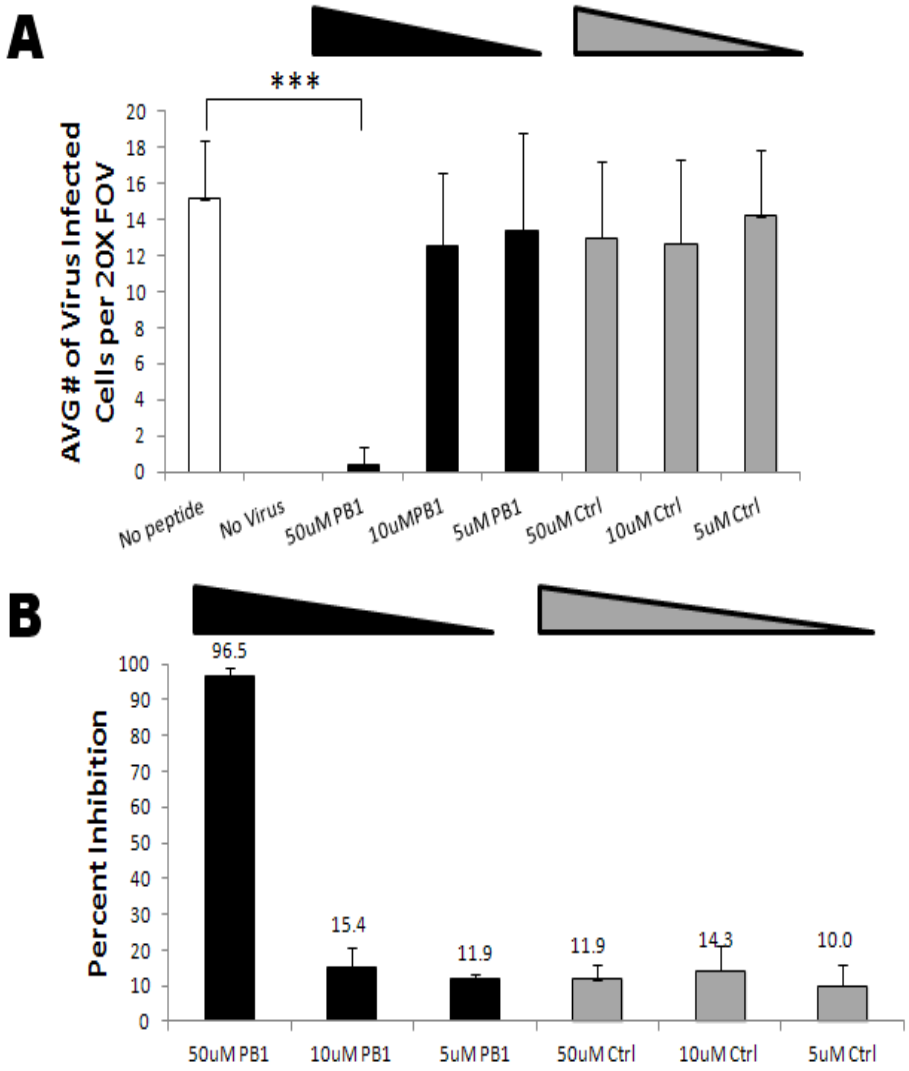

Figure 3.1.1 The HisMBP-NLS-PB1$_{1-20}$ mimetic inhibits Influenza A replication and growth
MDCK cells were incubated with cell culture media containing purified recombinant HisMBP-NLS-PB1$_{1-20}$, HisMBP-NLS-Ctrl (random mimetic control) or no mimetic for 1 hour. The cells were then infected with A/2009/H1N1 for 24 hours and visualized by fluorescence microscopy (**A**) The number of virus-infected cells per 20X Field of View are given. (**B**) Results from Panel A are expressed as Percent Inhibition compared with the no peptide control (white bar) is 100%. Error bars represent 2 standard deviations of three independent experiments. *** $p < 0.001$ calculated using Student's t-test.

3.1.2 The HisMBP-NLS-PB1$_{1-20}$ mimetic is non toxic *in vitro*

To ensure that the anti viral effect from **Figure 3.1.1** was not due to protein toxicity (since Influenza requires live cells to replicate and grow) a red blood cell hemolysis assay was used. Any pathogen or peptide toxic to red blood cells will lyse them, releasing hemoglobin protein in the supernatant (Blocker et al 1999). The hemoglobin can be detected by measuring the absorbance at 420 nm, and this method was used to measure the toxicity of the peptide mimetics. RBCs were incubated with 2-fold dilutions of either HisMBP-NLS-PB1$_{1-20}$ or HisMBP-NLS-Ctrl in PBS for 1 and 24 hours. Cells were harvested, and the supernatant was transferred to a 96-well plate where the absorbance at 420 nm was read by a plate reader. At all dilutions, both the HisMBP-NLS-PB1$_{1-20}$ mimetic (**Fig 3.1.2A**) and the HisMBP-NLS-Ctrl (**Fig 3.1.2B**) control mimetic were non toxic ($p<0.0001$ compared to the lysis buffer) to RBCs.

To show that the proteins do not negatively affect cell replication, MDCK cells were incubated with either HisMBP-NLS-PB1$_{1-20}$ (PB1), HisMBP-NLS-Ctrl (Ctrl), no mimetic (MEM) or 1% Triton X-100 (Triton) for 24 hours. At the indicated time points, the cells were collect by treatment with Trypsin and the absorbance was measured to assay the viability of the cells (Mohler et al 1996). At all time points, there was no difference between either the PB1 or Ctrl treated cells compared to the MEM only (no mimetic) control (**Fig 3.1.2C**). Triton X-100 was used as a negative control to lyse the cells, therefore resulting in little to no absorbance. Data from Panel C is also shown as a bar graph (**Fig 3.1.2D**) to more conveniently compare averages and deviations.

We further investigated toxicity of the mimetic on MDCK cells by measuring metabolic activity via ATP bioluminescence after mimetic treatment (Crouch et al 1993). MDCK cells were incubated with 50 μM of HisMBP-NLS-PB1$_{1\text{-}20}$, HisMBP-NLS-Ctrl, MEM alone (no mimetic positive control) or lysis buffer (negative control) over 72 hours. At each time point, the cells were washed and lysed open with lysis buffer, and total ATP was measured with the Lonza ViaLight Plus kit (see Materials and Methods) by reading the bioluminescence (in relative luminescence units) produced by Luciferase, which catalyzes the production of light from ATP and luciferin. At all time points, no appreciable difference in ATP levels was observed between cells treated with either the PB1 or Ctrl mimetics compared to the MEM control, suggesting that the proteins do not affect metabolic activity (**Fig 3.1.2E**). Lysis buffer was used as a negative control and very little luminescence was detected. Results from Panel E are shown in bar graph format to compare means (**Fig 3.1.2F**).

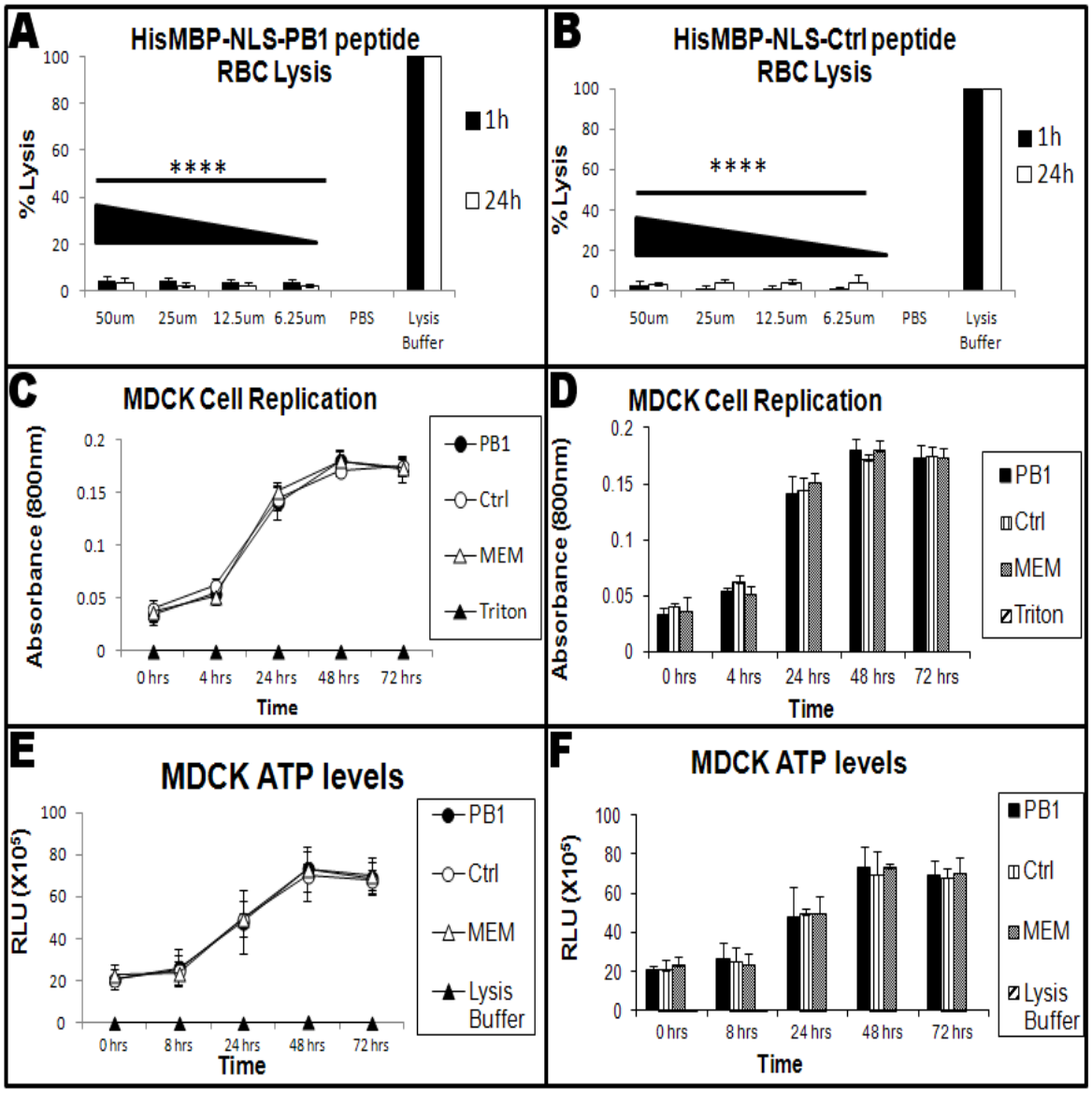

Figure 3.1.2 The PB1 mimetic is non toxic *in vitro*

Toxicity of the HisMBP-NLS-PB1$_{1\text{-}20}$ mimetic was investigated *in vitro*. **(A)** Diminutive toxicity was observed by measuring the absorbance at 420 nm of RBC supernatants over 72 hours after treatment with PB1, a non specific control mimetic (Ctrl), PBS (negative control) or lysis buffer (positive control) **(B)** Results from (A) are shown as percent lysis (see materials and methods for calculations). *** $p < 0.001$ compared to the lysis control. **(C)** MDCK cell replication was measured in the presence of either mimetics, MEM (no mimetic), or Triton X-100 (negative control) over 72 hours. **(D)** Results from (C) are shown as bar graphs to more conveniently compare means. Error bars represent two standard deviations of triplicate readings. **(E)** Total MDCK ATP was determined by the bioluminescent measurement of total ATP after treatment with PB1, Ctrl, MEM (no peptide) or lysis buffer. **(F)** Data from Panel (E) is represented as a bar graph. Error bars represent 2 standard deviations of three independent experiments.

3.2 – Molecular Modeling of the PB1-PA Interaction Increases the Anti-Viral Activity of the PB1 Mimetic

ZMM *in silico* molecular modeling hypothesized that mutating threonine at position six to glutamate (T6E) or arginine (T6R) would decrease the free energy of binding (see **Supplementary Figure S1**), therefore stabilizing the PB1/PA interaction and increasing the anti-viral activity of the mimetic. A dose-response viral inhibition assay was performed to investigate if the T6E and T6R mutations would increase anti-Influenza activity of the PB1 mimetic.

3.2.1 The T6E and T6R mutations increase the anti-Influenza potency of the PB1 mimetic

MDCK cells were incubated with purified proteins for 1 hour and then challenged with pandemic H1N1 Influenza A for 24 hours. The cells were visualized by fluorescence microscopy showing virus infected cells in green and non-infected cells in red (**Fig 3.2.1A**). The native PB1 mimetic showed 98% viral inhibition at 50 µM, with decreasing potency at 25 (36% inhibition) and 12.5 µM (16% inhibition), respectively (panels a-c). The T6E (panels d-f) and T6R (panels g-i) mutants displayed similar dose-response relationships, with 98% inihibition at 50 µM and decreasing potency at 25 and 12.5 µM, respectively. Cells were treated with media without any purified protein (panel j), a non-specific 50 µM HisMBP-NLS control mimetic (panel k) and media without virus (panel l) as controls. Compared to the native mimetic however, both the T6E and T6R mutants displayed statistically higher viral inhibition at 25 and 12.5 µM (**Fig 3.2.1B**). at 25 µM, the native mimetic displayed only 36% viral inhibition, while the T6E and T6R

constructs displayed 71% and 77% inhibition, respectively. At 12.5 µM, the native mimetic displayed only 16% viral inhibition, while the T6E and T6R constructs displayed 27% and 70% inhibition, respectively.

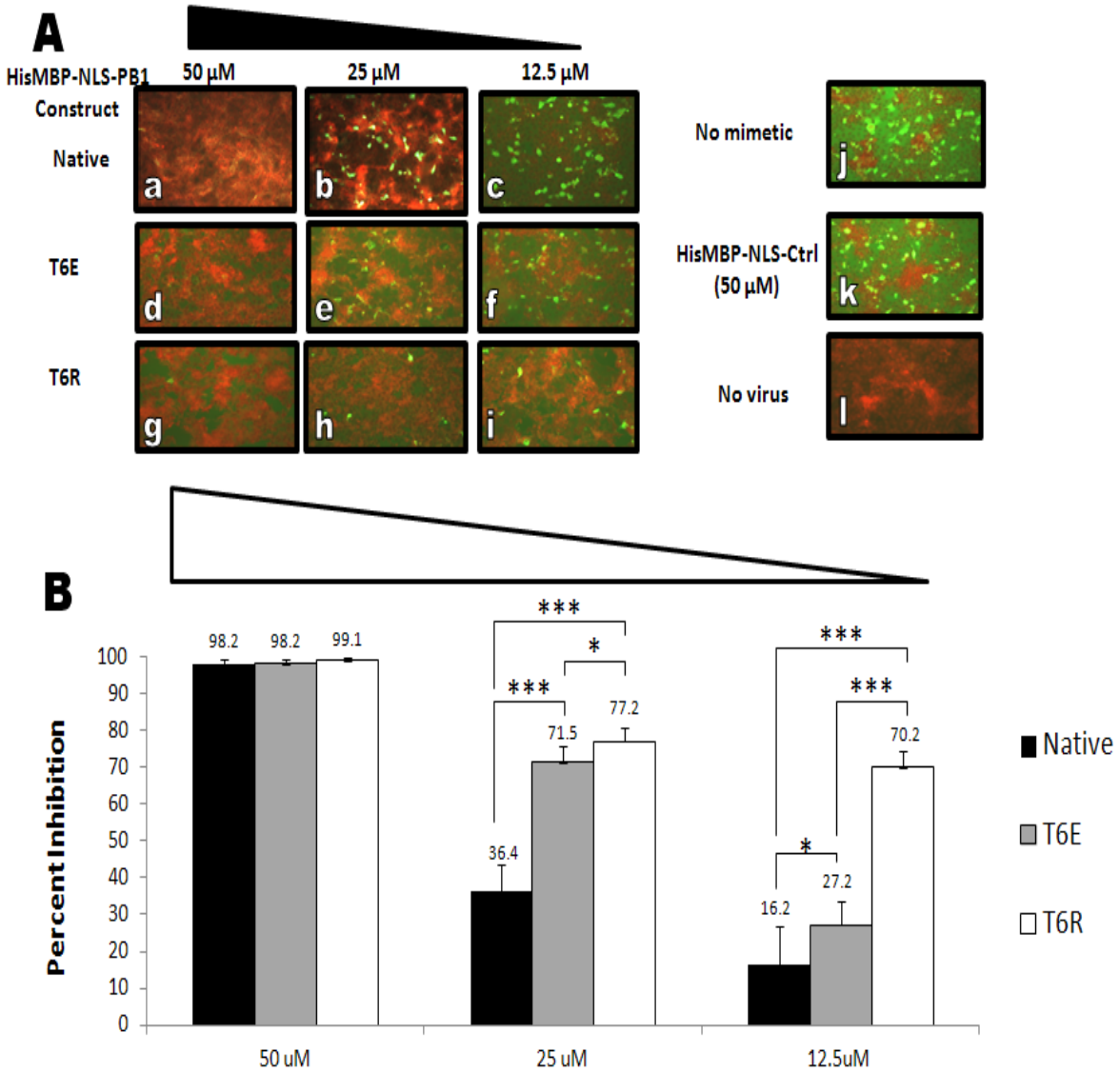

Figure 3.2.1 The T6E and T6R mutations increase the *in vitro* anti-Influenza potency of the PB1 mimetic

MDCK cells were incubated in media with and without purified recombinant proteins. The cells were then challenged with pandemic H1N1 Influenza A and the number of virus infected cells were visualized by fluorescence microscopy with a DFA. **(A)** Microscopy fields show Influenza infected cells in greenand non infected MDCK cells in red. **(B)** Results from (A) are expressed as percent inhibition normalized to the no mimetic control (0%). Error bars represent two standard deviations of three independent experiments. * $p < 0.05$, *** $p < 0.001$

3.2.2 The T6E and T6R mimetics increase anti-viral potency of the PB1 mimetic by decreasing total *in vitro* viral transcript

We hypothesize that the PB1 mimetics are binding to viral PA, thereby preventing assembly of the polymerase and thus inhibiting transcription and replication of the viral genome. To investigate if the T6E and T6R mutations increase the potency of the PB1 mimetic, a qPCR assay was performed to quantify the number of viral transcript present in Influenza-infected MDCK cells after treatment with each mimetic. MDCK cells were treated with the native PB1, T6E, T6R or Ctrl mimetics and infected with Influenza A. After 24 hours, total nucleic acid was extracted from virus infected cells and used in a qPCR assay to quantify the total viral transcript copy number. Viral fold change decrease (**Fig 3.2.2A**) compared to the no mimetic control was calculated by normalizing the viral transcript copy number (**Fig 3.2.2B**) to the Actin control copy number (**Fig 3.2.2C**). While the native PB1 mimetic yielded an average fold change decrease of 43.4 at 25 μM compared to the no mimetic control, the T6E and T6R mutants (at the same concentration) yielded an average fold change decrease of 70.1 and 136.3, respectively. Similar to the viral inhibition result in Fig 3.2.1, the T6E and T6R mutations appear to increase the potency of the PB1 mimetic, with the T6R appearing to be the most potent mimetic.

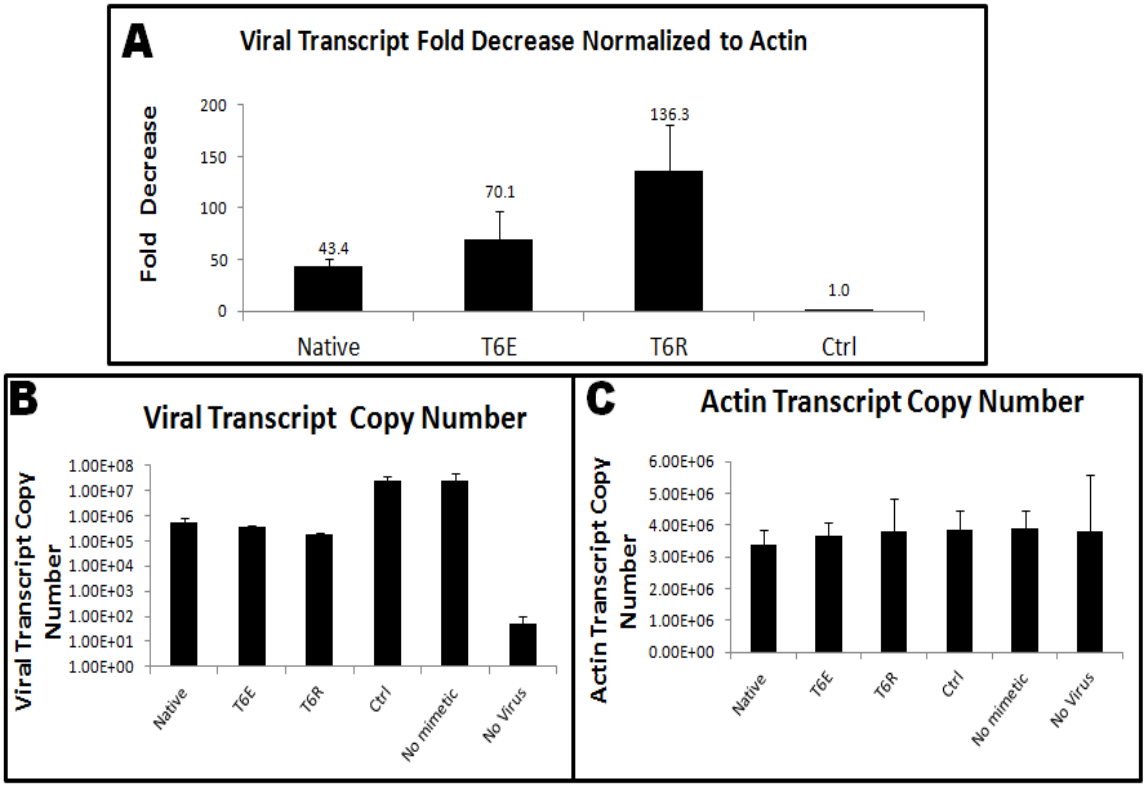

Figure 3.2.2 The T6R and T6E mutations increase the anti-viral potency of the PB1 mimetic by decreasing viral transcript levels

MDCK cells were treated with 25 µM of mimetic and then challenged with Influenza A for 24 hours. The cells were lysed and total RNA (viral and host) was extracted and quantified using a qPCR assay. **(A)** Viral transcript (M2 gene) fold decrease is shown for each construct by normalizing the total viral transcript from (B) with the Actin transcript from (C) and comparing each ratio with the no mimetic control as described in the methods section. **(B)** Viral transcript for each construct is shown as copy number. **(C)** Total Actin transcript (used as a normalization control) for each construct is shown as copy number.

3.2.3 The native PB1, T6E, and T6R mimetics are non toxic *in vitro*

To ensure that the previous Figure 3.2 results were not due to toxicity, MDCK cell toxicity of the three mimetics was investigated with an *in vitro* RBC lysis assay and an MDCK cell replication assay. RBCs were treated with 50 µM of each mimetic and were incubated for 0, 4, 24, 48 and 72 hours. The cells were harvested, and the supernatant was transferred to a 96 well plate, where the absorbance at 420 nm was read in triplicates by a plate reader. At all time points, the mimetics and the PBS negative

control displayed statistically lower absorbance compared to the lysis buffer (positive control), indicating diminutive toxicity (**Fig. 3.2.3A**). When normalized to the PBS and lysis buffer controls (see materials and methods for calculations), all mimetics exhibited less than 7% lysis at all time points, indicating a lack of hemolysis and thus a lack of toxicity (**Fig. 3.2.3B**).

To show that the mimetics do not negatively affect MDCK cell replication, MDCK cells were incubated with native, T6E, and T6R mimetics, as well as media alone (MEM, positive control) and Triton X-100 (negative control) over 72 hours. Cells were treated with Trypsin, and the optical density at 800 nm (OD_{800}) was measured as a direct quantification of total cell number. At each time point, there was no appreciable difference between cells treated with either mimetic or media alone, indicating no effect on cell replication (**Fig. 3.2.3C**). Data from panel C is shown as a bar graph to compare means (**Fig. 3.2.3D**). Taken together, results from the RBC lysis and MDCK growth assays indicate that the PB1 mimetics appear to be non toxic *in vitro*.

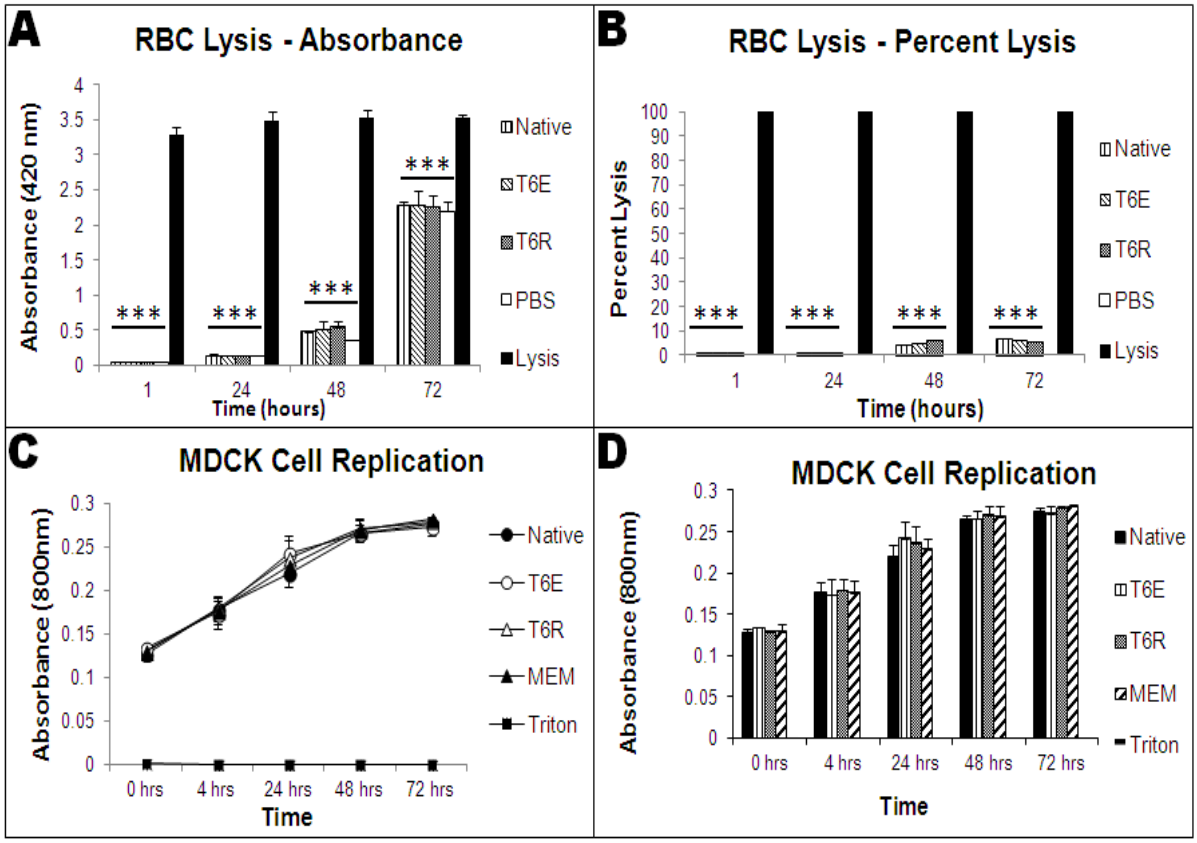

Figure 3.2.3 The native, T6E, and T6R PB1 mimetics are non toxic *in vitro*

Toxicity of the HisMBP-NLS-PB1$_{1\text{-}20}$ Native, T6E and T6R mimetics were investigated *in vitro*. **(A)** Diminutive toxicity was observed by measuring the absorbance at 420 nm of RBC supernatants over 72 hours after treatment with each PB1 mimetic, PBS (negative control) or lysis buffer (positive control) **(B)** Results from (A) are shown as percent lysis (see materials and methods for calculations). *** $p < 0.001$ compared to the lysis control. **(C)** MDCK cell replication was measured in the presence of either PB1 mimetics, MEM (no mimetic), or Triton X-100 (negative control) over 72 hours. **(D)** Results from (C) are shown as bar graphs to more conveniently compare means. Error bars represent two standard deviations of triplicate readings.

3.3 – Mimetic mechanism of action

In order to bind the C-terminus of PA and prevent assembly of the Influenza polymerase, the mimetic must enter the cell and get targeted to the nucleus. We hypothesize that the NLS on the mimetic acts as a cell-penetrating protein, which escorts recombinant proteins across the cell plasma membrane and targets it to the host nucleus.

3.3.1 – The NLS is sufficient for recombinant protein mimetic entry into the cell

We hypothesize that the HIV-1 Tat NLS is a sufficient component to promote recombinant protein entry into cells. To show this, MDCK cells were seeded into separate wells of a 24-well plate and incubated with media containing different HisMBP fusion proteins for 1 hour: NLS-$PB1_{1-20}$, NLS-$PB1_{1-20}$ T6E, NLS-$PB1_{1-20}$ T6R, $PB1_{1-20}$ (no NLS) and HisMBP alone (see **Supplementary Figure S3**). The cells were then washed, treated with Trypsin, harvested and resuspended in 2X sample buffer. Samples were separated by SDS-PAGE and analyzed by western blot analysis with antibodies against 6xHis and β-actin (cell loading control). The input control was blotted to demonstrate that the stated proteins were in fact incubated with the cells. Only proteins containing the NLS were detected in MDCK lysates (**Fig 3.3.1**). Treating the cells with Trypsin ensured that any protein stuck to the outside of the cell membrane (and not necessarily inside the cell) that was not removed by washing was degraded and not detected by western blot.

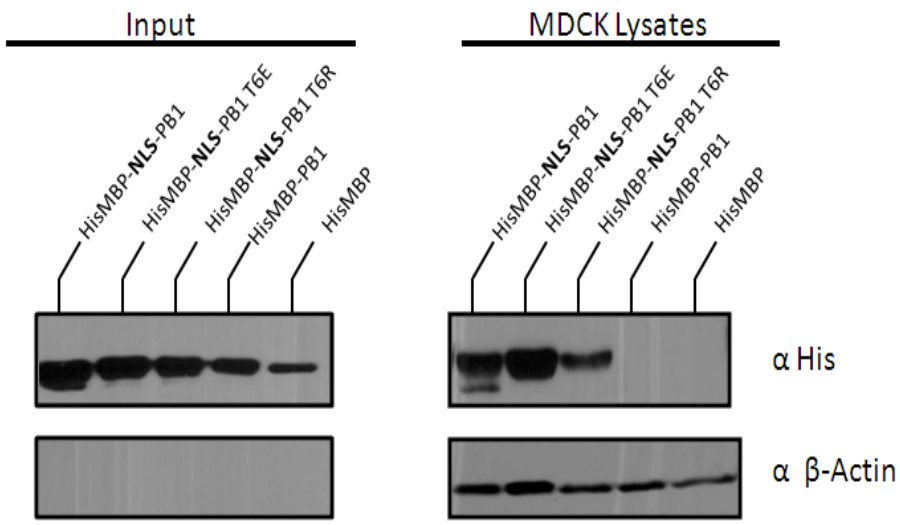

Figure 3.3.1 The NLS is necessary and sufficient for recombinant protein cell entry
MDCK cells were incubated with media containing purified 6xHis-tagged proteins for 1 hour. Cells were washed, treated with Trypsin, harvested and electropheresed by SDS-PAGE. Samples were blotted with antibodies against 6xHis and β-actin (loading control). Only proteins containing a nuclear localization signal were detected in MDCK lysates.

3.3.2 – The NLS transports mimetics to the cell nucleus

To show that the mimetics are targeted to the cell nucleus (where polymerase-dependent transcription and replication of viral material occurs), cells were fractionated and nuclei were examined for the presence of mimetics by western blot. MDCK cells were incubated with PB1 mimetics (containing an NLS) and HisMBP-$PB1_{1-20}$ (no NLS control). Cells were then treated with a buffer containing IGEPAL/NP-40, a detergent that solubilizes the plasma membrane but keeps the nuclear membrane intact (Dyer et al 1995). Both the cytosolic and nuclear fractions were electrophoresed and blotted with antibodies against His_6, Actin (cytosolic protein), and Lamin A (inner nucleus protein). Only proteins containing an NLS were detected in the nucleus (**Fig 3.3.2**). The NLS-tagged proteins were not detected in the cytoplasm, suggesting that the proteins that

cross the plasma membrane are targeted to the nucleus entirely. The HisMBP-PB1$_{1-20}$ mimetic without the NLS was not detected in the nuclear fraction.

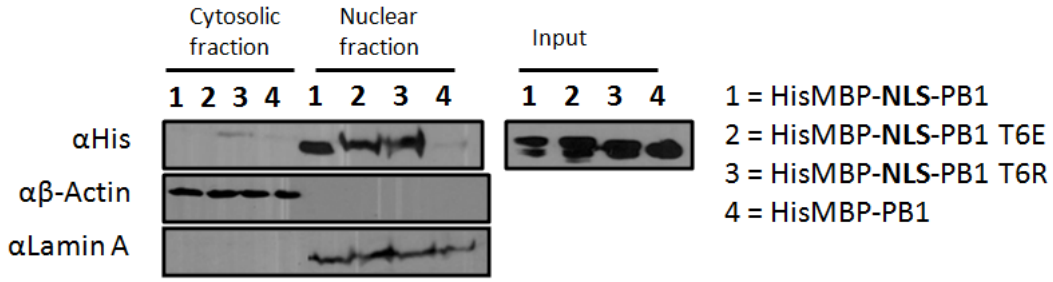

Figure 3.3.2 The NLS is sufficient to transport recombinant proteins to the nucleus
MDCK cells were incubated with purified recombinant proteins and lysed with a nuclear extraction buffer containing 0.4% IGEPAL. After centrifugation, the supernatant was TCA precipitated and resuspended in sample buffer as the cytosolic fraction and the pellet was resuspended in sample buffer as the nuclear fraction. Samples were electrophoresed by SDS-PAGE, transferred to a nitrocellulose membrane and blotted with antibodies against 6xHis, β-actin (cytosolic protein) or Lamin A (nuclear protein). Only proteins with an NLS were detected in the nucleus.

3.3.3 The HisMBP-NLS-PB1$_{1-20}$ mimetic binds to GST-PA$_{257-716}$ *in vitro*

The published partial crystal structure of the Influenza polymerase reported that the N-terminus of PB1 (first 25 amino acids) interacts with the C-terminus of PA (amino acids 257-716) during assembly of the heterotrimeric polymerase (He et al 2008). We hypothesize that our PB1 peptide mimetic would similarly bind the C-terminus of PA, preventing Influenza PB1 from binding and therefore inhibiting the critical assembly of the polymerase. We used a GST pull down assay to show the HisMBP-NLS-PB1$_{1-20}$ interaction with the C-terminus of PA (PA$_{257-716}$). *E. coli* cells overexpressing recombinant GST or GST-PA$_{257-716}$ (bait) were lysed and the cell lysate was incubated with Glutathione-Agarose beads for two hours. The beads (now bound to GST-tagged proteins) were washed, and incubated with purified recombinant HisMBP-NLS-PB1$_{1-20}$ or HisMBP-NLS-Ctrl2 (prey) overnight. The beads were washed with a high salt buffer and proteins were eluted from the beads with the addition of 2X sample buffer and

boiled for 10 minutes. Samples were analyzed by PAGE on a 12% acrylamide gel and analyzed by western Blot. The HisMBP-NLS-PB1$_{1-20}$ protein was pulled down from GST-PA$_{257-716}$, but not GST alone suggesting an interaction between PB1$_{1-20}$ and PA$_{257-716}$ (**Fig 3.3.3**). As a control, HisMBP-NLS-Ctrl2 did not elute from beads bound to GST-PA$_{257-716}$, suggesting that PA$_{257-716}$ does not interact with the control peptide, the HisMBP carrier protein or the nuclear localization signal.

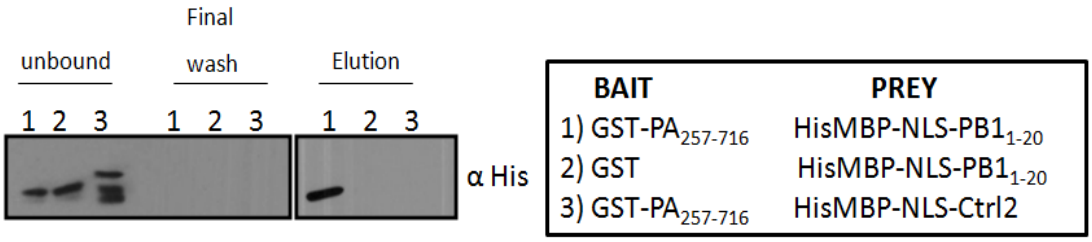

Figure 3.3.3 The HisMBP-NLS-PB1$_{1-20}$ mimetic binds to GST-PA$_{257-716}$ *in vitro*
E. coli cell lysates containing overexpressed recombinant GST-PA$_{257-716}$ or GST (bait) were incubated with glutathione-agarose beads overnight at 4°C. The beads (now bound to GST-tagged proteins) were then incubated with HisMBP-NLS-PB1$_{1-20}$ or a control mimetic HisMBP-NLS-Ctrl2 (prey), washed, resuspended with 2X sample buffer and electrophoresed by SDS-PAGE. Unbound 6xHis-tagged proteins, final wash and elution fractions off the beads are shown. C-terminal GST tagged PA (and not GST alone) is able to pull down the HisMBP-NLS-PB1$_{1-20}$ mimetic, but cannot pull down the control mimetic as displayed in the elution fraction.

3.4 – Evaluating efficacy of the 7mer mimetic

The HisMBP-NLS-PB1$_{1-20}$ mimetic inhibits Influenza replication and growth more effectively than the 7mer constructs

Previously unpublished work in our laboratory showed that the first seven amino acids of the PB1 peptide (PB1$_{1-7}$) are sufficient to inhibit Influenza viral growth (see **Supplementary Figure S2**). A dose dependent viral inhibition assay was performed to access the efficacy of the 7-mer mimetics (including T6E and T6R mutations) compared

to the original HisMBP-NLS-$PB1_{1-20}$ mimetic. MDCK cells were incubated with purified proteins for 1 hour and then infected with pandemic H1N1 Influenza A for 24 hours. Influenza virus was detected by DFA staining showing virus infected cells in green and non-infected cells in red (**Fig 3.4A**). The PB1 20-mer mimetic showed 98% viral inhibition activity at 50 µM (panel a), with decreasing efficacy at 25 µM (64%) and 12.5 µM (7%) (panels b and c, respectively). The $PB1_{1-7}$ construct showed a much lower viral inhibition activity compared to the 20-mer mimetic: 25% at 50 µM (panel d), 16% at 25 µM (panel e) and 4% at 12.5 µM (panel f). Similarly, both the T6E and T6R 7-mer mimetics showed very weak viral inhibition even at 50 µM (panels g-l). A random peptide control (Ctrl) showed no significant decrease in virus-infected cells at any concentration (panels m, n, o). Overall, the 50 µM 20-mer peptide had the greatest percent inhibition at 98.0%, followed by the same peptide at 25 µM with a percent inhibition of 64.0% (**Fig 3.4B**). All other 7mer constructs (at any concentration) had a percent inhibition of 25% or lower, suggesting that the 20mer mimetic inhibits viral growth more effectively than the 7mer mimetics.

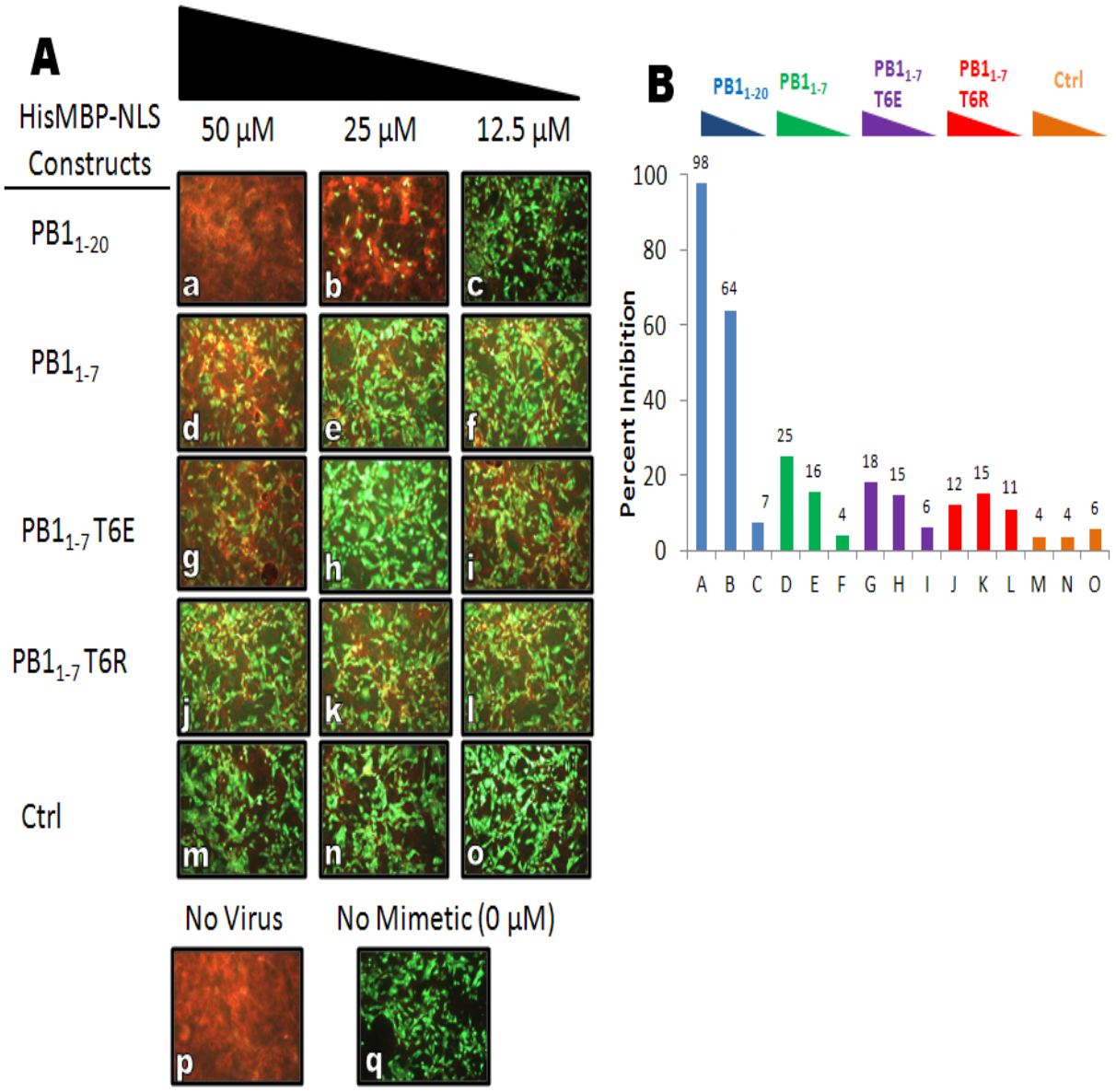

Figure 3.4 The HisMBP-NLS-PB1$_{1-20}$ mimetic inhibits Influenza A replication more effectively than the 7mer constructs

MDCK cells were incubated with cell culture media containing purified recombinant proteins or no peptide for 1 hour. The cells were then challenged with A/2009/H1N1 for 24 hours and visualized by Direct Fluorescent Antibody (DFA) staining **(A)** Microscopy fields representing Influenza-infected cells (green) and non-infected MDCK cells (red) are shown for each peptide **(B)** Results from (A) are expressed as percent inhibition normalized to the no mimetic control (0%)

CHAPTER FOUR

DISCUSSION

Ghanem et al have shown that a plasmid expressing a peptide mimetic consisting of the first 25 amino acids of the PB1 subunit can inhibit viral replication when transfected into human embryonic kidney cells (Ghanem et al 2007). The results presented in this thesis continue this area of work by designing a smaller mimetic (20 amino acids instead of 25), attaching it to the *E. coli* maltose binding protein and HIV-1 Tat nuclear localization signal and showing that it inhibits Influenza replication and growth in a dose dependent manner.

4.1 Inhibition of Influenza replication using a non-toxic 20-mer PB1 mimetic

Results in **Section 3.1** demonstrate that when attached to a soluble cell-penetrating protein, the first 20 amino acids of PB1 can inhibit viral replication in a dose dependent manner. Furthermore, the mimetic is non-toxic *in vitro*, implying that the antiviral phenotype observed is not due to cell toxicity. A random peptide of 20 amino acids containing the same total charge as $PB1_{1\text{-}20}$ was used as a negative control (Ctrl) and showed no antiviral activity at any concentration. Although the negative control here was a random sequence with the same charge as the $PB1_{1\text{-}20}$ mimetic, the peptide sequence is a critical component of the mimetic. Our laboratory has evidence showing that a PB2 mimetic that disrupts the interaction between $PB1_C$ and $PB2_N$ cannot inhibit Influenza replication when the mimetic sequence is scrambled (**Supplementary Figure S4**). This observation reiterates the fact that peptide mimetics rely on the primary amino acid structure for specificity and not just total charge alone. Furthermore, our laboratory

has evidence that this mimetic does not activate any pathogen-associated molecular patterns in LLC-MK2 cells, has it was unable to inhibit Respiratory Syncytial Virus replication in vitro, while an RSV-specific mimetic was (data not shown).

The mimetic is also shown to be non toxic *in vitro*, and does not cause hemolysis of red blood cells nor does it negatively affect MDCK cell replication even in prolonged exposure up to 72 hours. To ensure that the mimetic does not affect metabolic activity, total ATP was measured through the well established Luciferase bioluminescence assay (which uses ATP to produce light), and no significant difference was observed between the mimetic and no mimetic treated cells control. ATP was used as a marker for metabolically active cells since it serves as the principle donor of free energy and is involved in most catabolic and anabolic processes (Crouch et al 1993).

Maltose binding protein was chosen as a suitable proof of principle carrier protein for the mimetic since it is very soluble and can force non-soluble fusion partners into solution (Nallamsetty et al 2005). HIV-1 Tat NLS was chosen as a cell-penetrating peptide since it was previously used by our group to facilitate the efficient import of GST-tagged proteins (>26 kDa) into *C. pneumoniae* (Stone et al 2011).

4.2 Using molecular modeling to increase potency of the PB1 mimetic

ZMM molecular modeling predicted two significant amino acid substitutions at PB1 position 6 that would hypothetically improve interaction with PA: T6E and T6R. The program employs the two-step Monte Carlo minimization method to search for

energetically favourable conformations of proteins and their ligands (Garden and Zhorov 2010). In the first step, several random starting protein conformations are generated, and the flawed conformations where the two proteins overlap in three dimensional space are omitted. In the second step, the best conformations generated from the first step are repeated several hundred times in order to obtain the best energy profile. The T6E and T6R mutations were investigated for their anti viral potency compared to the native T6 mimetic. Both T6E and T6R mutants contained higher anti viral activity compared to the native PB1 mimetic as they exhibited higher percent inhibition at the same concentration. The T6R construct appeared to be the more effective of the two, as it exhibited a minimum of 70% viral inhibition even at a low concentration of 12.5 μM, whereas the native mimetic and T6E exhibited a 16.2% and 27.2% inhibition at this concentration (respectively). Furthermore, a qPCR assay measuring M2 gene transcript normalized to actin (loading control to ensure the same number of cells was recovered after 24 hours) also suggests an increase in potency with the T6R and T6E mutations. The native PB1 mimetic contained 43 times less viral transcript compared to the no mimetic control at 25 μM, while the T6E and T6R constructs contained 70 and 136 times less, respectively. Taken together, the *in vitro* Influenza inhibition data here is consistent with the ZMM molecular modeling prediction that the T6R mutation in PB1 has a higher affinity for PA compared to T6E, which has a higher affinity compared to the native mimetic.

Interestingly, Obayashi et al suggested in their PB1-PA crystal structure paper that a lack of contact between Thr 6 and PA could be exploited by amino acid

substitution to interact with the nearby Leu 666 and/or Phe 710 residues of PA (Obayashi et al 2008; **Figure 4.1**). Hypothetically, the relatively bulky and charged glutamic acid and arginine amino acids most likely fit inside the binding pocket of PA much better than the endogenous threonine residue and make contact with one or both of these amino acids, most likely through hydrogen bonding with the either the amine or carbonyl group of the polypeptide backbone. One would also expect hydrophobic interactions between side chain groups of Leu 666/Phe 710 with a hydrophobic amino acid such as phenylalanine, which ZMM also predicts to have a lower energy binding profile compared to the native threonine residue.

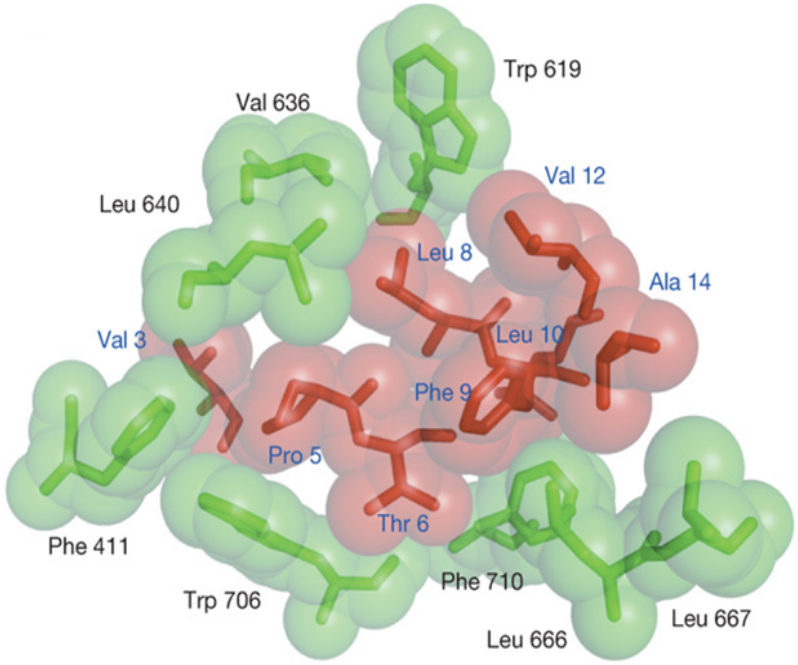

Figure 4.1 Space-filling representation of $PB1_N$ in complex with PA_C (Obayashi et al 2008)
A space-filling representation diagram based on the crystal structure of $PB1_N$ (red) in complex with PA_C (green) is shown. The Thr 6 residue does not make physical contact with another PA_C residue, suggesting that an amino acid substitution at this position could potentially exploit interaction with the nearby Leu 666 and/or Phe 710.

4.3 Mimetic mechanism of action

We hypothesize that the PB1 mimetics are entering the cell by means of the NLS, and are being targeted to the nucleus where they interact with the C-terminus of PA, thereby preventing assembly of the polymerase complex. Results presented in Section 3.3.1 show that the NLS is sufficient to transport large proteins through the plasma membrane and into the cytoplasm. Molecules over 900 Daltons cannot passively diffuse through the plasma membrane, and therefore require modification or a cell-penetrating peptide (CPP) to transport them through the membrane (Mason 2010). Although controversial, there are two main theories regarding the specific mechanism by which NLS containing proteins translocate through membranes: absorptive endocytosis and lipid bilayer interaction. Drin et al have shown that cationic CPPs similar to the HIV-1 Tat NLS incorporate into endocytotic vesicles in a temperature and energy dependent manner when internalized into cells, suggesting that the peptides penetrate the cell membranes by an absorptive endocytosis process (Drin et al 2003). Cells treated with molecular inhibitors of endocytosis were nearly depleted of cationic CPPs, further supporting the endocytosis mechanism. The second lipid bilayer theory suggests that the positively charged NLS (YGRKKRRQRRR) interacts with the negatively charged phosphate groups on the plasma membrane. As the NLS saturates the proximal phosphate groups on the first side of the bilayer, they begin to attract the distal phosphate groups on the cytoplasmic side, thereby thinning the membrane and allowing the NLS to begin translocation. As the NLS enters the hydrophobic interface, it gets saturated by water molecules which solvate the charged residues. This creates a transient (less than a microsecond) water pore that provides the physical passage of the

peptide into the cell (Herce and Garcia 2007). Although data here do not confirm either theory, they reiterate that a cationic CPP such as the NLS is sufficient to translocate large proteins past the plasma membrane (Milletti 2012; Vives et al 1997).

Using a nuclear extraction assay in **Section 3.3.2**, NLS-tagged constructs were shown to be localized in the nucleus, and that the NLS was sufficient for this to occur. Nuclei were extracted using an IGEPAL/NP-40 buffer which solubilizes the sphingomyelin-rich plasma membrane but keeps the sphingomyelin-deficient nuclear membrane intact (van Meer et al 2008). To ensure that the nuclei were properly extracted, an anti-lamin A antibody was used as a nuclear extract control, since lamin A is a well known inner nuclear protein not present in the cytoplasm (Dechat et al 2008). Targeting of NLS-containing proteins to the nucleus is mediated by the well established Ran GTP/GDP gradient through the nuclear pore complex (Rout and Aitchinson 2001).

Using an *in vitro* GST pull down assay, the HisMBP-NLS-$PB1_{1-20}$ mimetic was shown to interact with the C-terminus of GST-tagged PA (GST-$PA_{257-716}$). The mimetic did not interact with GST alone, nor did GST-$PA_{257-716}$ interact with a non specific control protein (HisMBP-NLS-Ctrl2), suggesting that the $PB1_{1-20}$ mimetic specifically interacted with $PA_{257-716}$ despite the addition of large tags and carrier proteins.

Given the above data, we propose a mechanism of virulence inhibition: the HisMBP-NLS-$PB1_{1-20}$ mimetic traverses the cell plasma membrane by means of the NLS which acts as a cell-penetrating protein. It is then targeted to the nucleus through

the well established Ran GTP/GDP gradient and binds the C-terminus of PA, possibly preventing binding of full length viral PB1 and ultimately assembly of the polymerase. Without the assembly of the functional polymerase, both transcription and replication of viral RNA is inhibited, thereby preventing the production of progeny virus (Cheng et al 2012).

Despite showing interaction between the mimetic and $PA_{257-716}$, prevention of polymerase assembly cannot be concluded from the results in **Section 3.3**. Nevertheless, co-immunoprecipitation studies were attempted to show this (data not shown). MDCK cells were incubated with mimetics and subsequently infected with Influenza: the cells were lysed and the His-tagged PB1 mimetics were immunoprecipitated using Nickel NTA beads and probed with a PA antibody to show that the mimetics bound to PA. The unbound fraction was then probed with a PB1 antibody (which only recognizes the C-terminus) to show that the mimetic prevented viral PB1 from interacting with PA, thus preventing assembly of the polymerase. Data from these experiments were inconclusive, possibly due to the lack of efficiency of the antibodies for immunoprecipitation studies.

4.4 Evaluating the efficacy of the 7-mer mimetic

While previous work in our laboratory has shown that the first seven amino acids of the PB1 protein is sufficient to inhibit Influenza replication and growth at 0.2-1.0 mM, results here show that at 50 µM, the 7-mer (when attached to HisMBP-NLS) is less effective (18% inhibition compared to 98%) and loses its activity at lower concentrations in a

dose dependent manner. It is important to note however that the NLS-$PB1_{1-7}$ peptide used in **Supplementary Figure S2** was not attached to a carrier molecule and was not a recombinant protein purified by affinity chromatography. Instead it was a synthetic peptide made by a commercial company (Peptide 2.0) by solid-phase peptide synthesis. It is possible that the first seven amino acids may be sufficient to inhibit Influenza growth and replication at lower concentrations, but the addition of a large carrier molecule such as Maltose Binding Protein distorts the interaction (through steric hindrance) between $PB1_N$ and PA_C as suggested by lock and key induced fit crystal structure model (He et al 2008). The thirteen other amino acids in the $PB1_{1-20}$ peptide may provide a long enough linker between HisMBP-NLS and the peptide for the first seven amino acids to interact with PA, although much more biochemical analysis must be performed to confirm this.

A more likely hypothesis (given the published crystal structure of $PB1_N$ in complex with PA_C) is that the first seven amino acids only provide minimal polypeptide interactions with PA, therefore require a higher concentration to reach 100% viral inhibition in order for the peptide to outcompete viral PB1. Met 1, Asp 2 and Val 3 of PB1 all form anti-parallel beta-sheet like interactions with Ile 621, Gly 622 and Glu 623 of PA, respectively. The polar side chain group of Asn 4 hydrogen bonds with the carbonyl backbone of Trp 706, while its own amine backbone hydrogen bonds with the carbonyl of Ile 621. The PB1 Pro 5 residue forms hydrophobic interactions with Phe 411 and Trp 706 of PA. While these polypeptide interactions are probably sufficient for the 7-mer peptide to bind with PA, it still lacks the numerous possible interactions from the other

13 amino acids (**Figure 4.2**). For instance, the carbonyl backbones of Phe 9, Leu 10 and Val 11 all form hydrogen bonds with the side chain groups of Gln 670 and Arg 673 of PA, while the charged Lys 11 of PB1 forms hydrogen bonds with the carbonyl backbone of Thr 618 and the Glu 617 R group (Obayashi et al 2008). These additional interactions likely strengthen the PB1 interaction with PA, contributing to the increased potency of the 20-mer compared to the 7-mer.

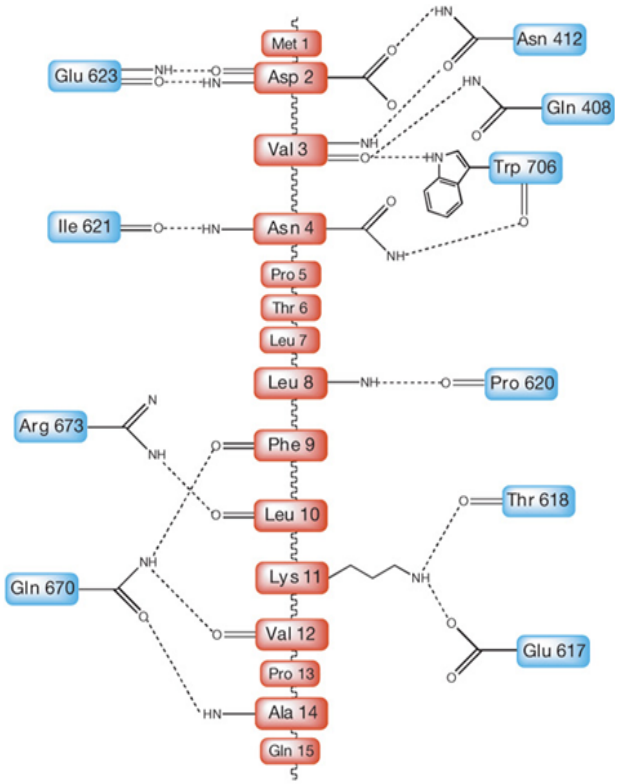

Figure 4.2 Schematic diagram of hydrogen bonding between $PB1_{1-15}$ and PA_C (Obayashi et al 2008)
A schematic diagram based on the crystal structure of PB1-PA complex shows the hydrogen bonds (dashed lines) between $PB1_{1-25}$ (red) and PA_C (blue). Hydrophobic interactions are not shown although some residues (such as Pro 5) participate in them.

4.5 The global burden of Influenza and need for effective therapies

Influenza remains a major global burden today, with infection leading to increased hospitalizations and loss of economic efficiency due to illness and death (Molinari et al 2007). Although seasonal vaccines exist and are used to reasonable success, the high rate of mutation in the Influenza genome (1 mutation per replication cycle per genome) leads to the evolutionary resistance to host neutralizing antibodies and anti-virals (Drake 1993; Cheng et al 2012). Influenza vaccines are also strain-specific and are generally ineffective against a virus that has undergone antigenic drift or shift. This poses a significant issue should another pandemic virus enter the population, as current seasonal vaccines would be ineffective and creation of a specific vaccine might take several months to develop (Cheng et al 2012).

The subunits of the Influenza polymerase remain intriguing therapeutic targets since i) the virus keeps their RNA levels at a much lower amount compared to the other Influenza proteins thus decreasing the likelihood of a mutation per replication cycle ii) the polymerase is absolutely necessary for full virulence and iii) the termini of the polymerase subunits (PB1, PB2 and PA) are very well conserved among Influenza strains (**Fig 1.4**), indicating that a mutation in these domains would likely decrease viral fitness (von Itzstein 2007; Guu et al 2008; Tsai et al 2006). Results here show that a PB1 mimetic attached to a soluble cell-penetrating protein can effectively bind to PA and prevent replication of Influenza *in vitro*. The polymerase is an especially good target since it involves the interaction of viral proteins, therefore making it unlikely that the mimetic would be toxic to the host. Previous work in our laboratory have attempted to

design p85β SH3 and TRIM25 CCD mimetics that target the Influenza NS1 effector protein, since NS1 is known to bind these domains (Hale et al 2008). However, these mimetics displayed significant *in vitro* toxicity above 10 μM (data not shown), which is not surprising considering that other critical cellular proteins need to bind these domains as well, and the mimetics would inhibit those interactions in addition to NS1. Therefore, anti viral mimetics should ideally be viral peptides that bind specifically to other viral proteins in order to minimize any interaction with critical host proteins. Current work in our laboratory investigates the use of a PB2 mimetic to disrupt the interaction between $PB1_C$ and $PB2_N$ which, unlike the NS1 mimetics, is effective and non toxic (**Supplementary Figure S4**). Hypothetically, other Influenza protein-protein interactions that occur in the host nucleus can be targeted with mimetics such as NP and M1 or M1 and NS2 (Cheng et al 2012; Das et al 2010).

Vaccine development against the polymerase subunits is highly unlikely since they are localized in the nucleus and not surface exposed, however research into small molecule therapeutics that inhibit the polymerase is well underway: viramidine (nucleoside inhibitor) and favipiravir (nucleotide analogue) are both in clinical trials, although not yet FDA or Health Canada approved for clinical use (Cheng et al 2012). A 2012 study also identified three small molecule compounds that inhibit Influenza A and B replication by preventing the interaction between PB1 and PA (Muratore et al 2012). Although small molecules have been used extensively as therapeutics because of their small size and ability to passively diffuse across membranes (therefore allowing them to reach their target in any organelle without any major modifications), the issue with their use as

effective anti virals reside within their specificity. Usually, the molecule binds to a certain site on the protein with such high specificity that a single amino acid mutation in the protein can demolish the interaction. The advantage of using peptide mimetics is that binding between the peptide and the protein target involve multiple amino acid interactions, where a single point mutation is unlikely to completely abrogate binding (Loregian and Palu 2005). Nevertheless, in order for peptide mimetics to be an effective clinical therapeutic there are several challenges that must be addressed (discussed below).

4.6.1 Future directions – carrier molecule

For peptide mimetics to be a viable therapeutic, their propensity for degradation by proteases must be addressed (Mason 2010). Human Serum Albumin (HSA) has previously been used as a carrier protein to increase plasma half-life of IFN-β from 8 hours to 36-40 hours, suggesting that it may be an effective carrier molecule for peptide mimetics as both amino and carboxy termini are also exposed (Sung et al 2003). Using HSA as a carrier molecule was previously attempted by designing a His-HSA-NLS-$PB1_{1\text{-}20}$ chimeric construct and expressing it in *E. coli* Rosetta *pLysS* (to account for the rare codon bias in *E. coli*). However, significant protein degradation was observed despite investigating several expression conditions (**Supplementary Figure S5**). HSA has seventeen disulfide bridges in its structure (Sugio et al 1999); therefore we attempted to express the construct in *E. coli* Rosetta-Gami, which accounts for the rare codon bias in *E. coli* and has mutations in thioredoxin reductase and glutathione reductase that make the reducing cytoplasm a more oxidizing environment conducive

for disulfide bonds (de Marco 2009). After getting no expression, we attempted to move to the eukaryotic *Pichia pastoric* (PichiaPink™ by Invitrogen) yeast system, but also could not successfully express the construct (data not shown). Expression of the HSA construct was even attempted in a cell-free expression system without success. Current work in the laboratory involves the use of the soluble monomeric IgG1 Fc region as a carrier molecule, which has been successfully expressed in *E. coli* (Ying et al 2012).

4.6.2 Future directions – delivery of therapeutic mimetics

Because of their propensity for proteolytic degradation, peptide mimetics require an effective delivery method in order to be a viable therapeutic (Mason 2010). Probiotics are harmless, non-pathogenic bacteria commonly used in the food and milk industry. They have been used to administer therapeutic treatments for Crohn's disease, colon cancer and other diseases (Bahey-El-Din et al 2010; Jakubovics et al 2005). Our laboratory initially attempted the use of the Gram positive *Lactococcus lactis* probiotic bacteria as a delivery vehicle for the secretion of the HisMBP-NLS-PB1$_{1\text{-}20}$ mimetic. We attempted to use *L. lactis* as proof of principle that a probiotic bacterium could express and secrete our peptide mimetic in an *in vitro* transwell system and inhibit the replication of Influenza A when MDCK cells are infected with the virus. We genetically engineered the gene into a *Lactococcus* expression and secretion plasmid (in frame with a Sec-dependent *usp45* leader sequence) and transformed this into *L. lactis* (Borrero et al 2011). Despite detecting minimal cytosolic expression, we could not detect secreted protein (data not shown). Our laboratory is currently investigating the use of other Gram positive secretion systems as delivery vehicles, which is quite possibly the biggest

challenge peptide mimetics face as a therapeutic. Whichever probiotic strain is used as a delivery vehicle, the bacteria must be able to express and secrete enough peptide mimetic to clinically inhibit Influenza replication *in vivo* (initially in mouse models and eventually in clinical trials). Experiments conducted in this thesis were all performed *in vitro*, and percent inhibition was based on statistical significance compared to controls, not clinical significance. It is quite conceivable that a higher protein concentration might be needed *in vivo*, and the delivery vehicle (which surely will not be under control of the T7 promoter and will not express recombinant proteins at *E. coli* levels) must be able to successfully secrete enough protein to reach clinical significance.

4.6.3 Future directions – biochemical investigation of the binding relationship between native/T6E/T6R $PB1_{1-20}$ and PA

Although the data here suggest that the T6R mutation inhibits viral replication *in vitro* better than the T6E and native PB1 peptide, we cannot conclude that the interaction with PA is improved. Isothermal titration calorimetry (ITC) is currently being used to investigate the binding relationship (specifically the dissociation constant, K_D) between PA and the PB1 peptides. ITC is commonly used to determine the thermodynamic relationship between two interacting molecules, even those as large as proteins (Jelesaroy and Bosshard 1999). We hypothesize that the T6R mutant will have the lowest dissociation constant with PA, indicating a stronger thermodynamic relationship as predicted by ZMM. Alternatively, surface plasmon resonance (SPR) is another technique that can be used to determine the dissociation constant between two proteins by immobilizing one of them on a sensor chip (Pattnaik 2005).

4.7 Closing Remarks

Despite the existence of seasonal vaccines, Influenza remains a major global burden today, and is responsible for abrupt and sporadic global pandemics. Due to antigenic drift and shift, vaccines lose efficacy against new strains, and the virus develops resistance to current small molecule anti virals. The polymerase is an ideal drug target since its components are very well conserved among different Influenza strains and it is necessary for full virulence. This thesis provides evidence that a dominant negative cell penetrating peptide mimetic can inhibit *in vitro* Influenza replication. Peptide mimetics are novel anti-Influenza strategies and are less susceptible to antigenic drift and shift mediated resistance since they involve multiple amino acid interactions. Nevertheless, before peptide mimetics can become viable *in vivo* therapeutics, there are a number of obstacles to address. Research and optimization of peptide mimetics is not for the faint of heart, but presents a novel and exciting strategy to combat a persistent problem.

References

Air GM. (2012) Influenza neuraminidase. *Influenza Other Respir Viruses* **4**, 245-256.

Alexander DJ. (2007) An overview of the epidemiology of avian influenza. *Vaccine* **25**:5637–5644.

Amorim MJ, Kao RY, Digard P. (2013) Nucleozin targets cytoplasmic trafficking of viral ribonucleoprotein-Rab11 complexes in influenza A virus infection. *J Virol* **8**, 4694-4703.

Bahey-El-Din M, Gahan CG, Griffin BT. (2010) *Lactococcus lactis* as a cell factory for delivery of therapeutic proteins. *Curr Gene Ther* **10**, 34-45.

Barman S, Adhikary L, Chakrabarti AK, Bernas C, Kawaoka Y, Nayak DP. (2004) Role of transmembrane domain and cytoplasmic tail amino acid sequences of influenza a virus neuraminidase in raft association and virus budding*. J Virol* **78**, 5258–5269.

Binh NT, Wakai C, Kawaguchi A, Nagata K. (2013) The N-terminal region of influenza virus polymerase PB1 adjacent to the PA binding site is involved in replication but not transcription of the viral genome. *Front Microbiol* **4**, 1-5.

Blocker A, Gounon P, Larquet E, Niebuhr K, Cabiaux V, Parsot C, Sansonetti P. (1999) The tripartite type III secreton of Shigella flexneri inserts IpaB and IpaC into host membranes. *J Cell Biol* **147**, 683-693.

Boivin S, Cusack S, Ruigrok RW, Hart DJ. (2010) Influenza A virus polymerase: structural insights into replication and host adaptation mechanisms. *J Biol Chem* **37**, 28411-28417.

Blok J, Air GM. (1982) Block deletions in the neuraminidase genes from some influenza A viruses of the N1 subtype. *Virology* **118**, 229-234.

Borrero J, Jiménez JJ, Gútiez L, Herranz C, Cintas LM, Hernández PE. (2011) se of the usp45 lactococcal secretion signal sequence to drive the secretion and functional expression of enterococcal bacteriocins in Lactococcus lactis. *Appl Microbiol Biotechnol* **89**, 131-143.

Bucher DJ, Kilbourne ED. (1972) A2 (N2) neuraminidase of the X-7 Influenza virus recombinant: determination of molecular size and subunit composition of the active unit. *J Virol* **10**, 60–66.

Burmeister WP, Ruigrok RW, Cusack S. (1992) The 2.2 A resolution crystal structure of influenza B neuraminidase and its complex with sialic acid. *EMBO J* **11**, 49-56.

Bossart-Whitaker P, Carson M, Babu YS, Smith CD, Laver Wg, Air GM. (1993) Three-dimensional structure of influenza A N9 neuraminidase and its complex with the inhibitor 2-deoxy 2,3-dehydro-N-acetyl neuraminic acid. *J Mol Biol* **232**, 1069–1083.

Brankston G, Gitterman L, Hirji Z, Lemieux C, Gardam M. (2007) Transmission of influenza A in human beings. *Lancet Infect Dis* **7**, 257-265.

Bridges CB, Kuehnert MJ, Hall CB. (2003) Transmission of influenza: implications for control in health care settings. *Clin Infect Dis* **37**, 1094-10101.

Carrat F, Flauhault A. (2007) Influenza vaccine: The challenge of antigenic drift. *Vaccine* **25**, 6852-6862.

Chandrasekaran A, Srinivasan A, Raman R, Viswanathan K, Raguram S, Tumpey TM, Sasisekharan V, Sasisekharan R. (2008) Glycan topology determines human adaptation of avian H5N1 virus hemagglutinin. *Nat Biotechnol* **26**, 107-113.

Chen J, Lee KH, Steinhauer DA, Stevens DJ, Skehel JJ, Wiley DC. (1998) Structure of the hemagglutinin precursor cleavage site, a determinant of influenza pathogenicity and the origin of the labile conformation. *Cell* **95**, 409-417.

Chen W, Calvo PA, Malide D, Gibbs J, Schubert U, Bacik I, Basta S, O'Neill R, Schickli J, Palese P, Henklein P, Bennink JR, Yewdell JW. (2001) A novel influenza A virus mitochondrial protein that induces cell death. *Nat Med* **12**, 1306-1312

Cheng VC, To KK, Tse H, Hung IF, Yuen KY. (2012). Two Years after Pandemic Influenza A/2009/H1N1: What Have We Learned? *Clin Microbiol Rev* **25**, 223-263.

Cox NJ, Subbarao K. (2000) Global epidemiology of influenza: past and present. *Annu Rev Med* **51**, 407-421.

Crouch SP, Kozlowski R, Slater KJ, Fletcher J. (1993). The use of ATP bioluminescence as a measure of cell proliferation and cytotoxicity. *J Immunol Methods*. **160**, 81-88.

Das K, Aramini JM, Ma LC, Krug RM, Arnold E. (2010) Structures of influenza A proteins and insights into antiviral drug targets. *Nat Struct Mol Biol* **17**, 530-538.

Dawood FS, Jain S, Finelli L, Shaw MW, Lindstrom S, Garten RJ, Gubareva LV, Xu X, Bridges CB, Uyeki TM. (2009) Emergence of a novel swine-origin influenza A (H1N1) virus in humans. *N Engl J Med* **360**, 2605-2615.

de Marco A. (2009) Strategies for successful recombinant expression of disulfide bond-dependent proteins in Escherichia coli. *Microb Cell Fact* **8**, 1-18.

Dechat T, Pfleghaar K, Sengupta K, Shimi T, Shumaker DK, Solimando L, Goldman RD. (2008) Nuclear lamins: major factors in the structural organization and function of the nucleus and chromatin. *Genes Dev* **22**, 832-853.

Dias A, Bouvier D, Crepin T, McCarthy AA, Hart DJ, Baudin F, Cusack S, Ruigrok RW. (2009) The cap-snatching endonuclease of influenza virus polymerase resides in the PA subunit. *Nature* **458**, 914-918.

Drake JW. (1993) Rates of spontaneous mutation among RNA viruses. *Proc Natl Acad Sci U S A* **90**, 4171-4175.

Drin G, Cottin S, Blanc E, Rees AR, Temsamani J. (2003) Studies on the internalization mechanism of cationic cell-penetrating peptides. *J Biol Chem* **33**, 31192-31201.

Dyer RB, Herzog NK. (1995) Isolation of intact nuclei for nuclear extract preparation from a fragile B-lymphocyte cell line. *Biotechniques* **19**, 192-195.

Edinger TO, Pohl MO, Stertz S. (2014) Entry of influenza A virus: host factors and antiviral targets. *J Gen Virol* **95**, 263-277.

Efthymiadis A, Briggs LJ, Jans DA. (1998) The HIV-1 Tat nuclear localization sequence confers novel nuclear import properties. *J Biol Chem* 273, 1623-1628

Els MC, Air GM, Murti KG, Webster RG, Laver WG. (1985) An 18-amino acid deletion in an influenza neuraminidase. *Virology* **142**, 241-247.

Fiore AE, Uyeki TM, Broder K, Finelli L, Euler GL, Singleton JA, Iskander JK, Wortley PM, Shay DK, Bresee JS, Cox NJ; Centers for Disease Control and Prevention (CDC). (2010) *MMWR Recomm Rep* **59**, 1-62

Fitch WM, Bush RM, Bender CA, Cox NJ. (1997) Long term trends in the evolution of H(3) HA1 human influenza type A. *Proc Natl Acad Sci U S A* **94**, 7712-7718.

Fleming DM, van der Velden J, Paget WJ. (2003) The evolution of influenza surveillance in Europe and prospects for the next 10 years. *Vaccine* **16**, 1749-1753.

Fouchier RA, Munster V, Wallensten A, Bestebroer TM, Herfst S, Smith D, Rimmelzwaan GF, Olsen B, Osterhaus AD. (2005) Characterization of a novel influenza A virus hemagglutinin subtype (H16) obtained from black-headed gulls. *J Viro*l **79**, 2814-2822.

Foy HM, Cooney MK, Allan ID, Albrecht JK. (1987) Influenza B in households: virus shedding without symptoms or antibody response. *Am J Epidemol* **126**, 506-515.

Frost WH (2006) The epidemiology of influenza. 1919. *Public Health Rep* **121**(Suppl 1), 149–159.

Fujimura T, Esteban R. (2011) Cap-snatching mechanism in yeast L-A double-stranded RNA virus. *Proc Natl Acad Sci U S A* **43**, 17667-17671.

Fujioka Y, Tsuda M, Hattori T, Sasaki J, Sasaki T, Miyazaki T, Ohba Y. (2011) The Ras-PI3K signaling pathway is involved in clathrin-independent endocytosis and the internalization of influenza viruses. *PLoS One* **6**, 1-9.

Fujioka Y, Tsuda M, Nanbo A, Hattori T, Sasaki J, Sasaki T, Miyazaki T, Ohba Y. (2013) A Ca(2+)-dependent signalling circuit regulates influenza A virus internalization and infection. *Nat Commun* **14**, 2763.

Gack MU, Albrecht RA, Urano T, Inn KS, Huang IC, Carnero E, Farzan M, Inoue S, Jung JU, García-Sastre A. (2009) Influenza A virus NS1 targets the ubiquitin ligase TRIM25 to evade recognition by the host viral RNA sensor RIG-I. *Cell Host Microbe* **5**, 439-449.

Garden DP, Zhorov BS. (2010) Docking flexible ligands in proteins with a solvent exposure- and distance-dependent dielectric function. *J comput Aided Mol Des* **24**, 91-105.

Ghanem A, Mayer D, Chase G, Tegge W, Frank R, Kochs G, García-Sastre A, Schwemmle M. (2007) Peptide-mediated interference with influenza A virus polymerase. *J virol* **14**, 7801-7804.

Glaser L, Stevens J, Zamarin D, Wilson IA, García-Sastre A, Tumpey TM, Basler CF, Taubenberger JK, Palese P. (2005) A single amino acid substitution in 1918 influenza virus hemagglutinin changes receptor binding specificity. *J Virol* **79**, 11533-11536

Gonzalez S, Zurcher T, Ortín J. (1996) Identification of two separate domains in the influenza virus PB1 protein involved in the interaction with the PB2 and PA subunits: a model for the viral RNA polymerase structure. *Nucleic Acids Res* **15**, 4456-4463.

Guu TS, Dong L, Wittung-Stafshede P, Tao YJ. (2008) Mapping the domain structure of the influenza A virus polymerase acidic protein (PA) and its interaction with the basic protein 1 (PB1) subunit. *Virology* **379**, 135-142.

Hale BG, Randall RE, Ortín J, Jackson D. (2008) The multifunctional NS1 protein of

influenza A viruses. *J Gen Virol* **89**, 2359-2376.

Hara K, Nakazono Y, Kashiwagi T, Hamada N, Watanabe H. (2013) Co-incorporation of the PB2 and PA polymerase subunits from human H3N2 influenza virus is a critical determinant of the replication of reassortant ribonucleoprotein complexes. *J Gen Virol* **94**, 2406-2416.

Hardelid P, Fleming DM, McMenamin J, Andrews N, Robertson C, SebastianPillai P, Ellis J, Carman W, Wreghitt T, Watson JM, Pebody RG. (2011) *Euro Surveill* **16**, 19763.

Harrison SC. (2008) Viral membrane fusion. *Nat Struct Mol Biol* **7**, 690-698.

Hay AJ, Zambon MC, Wolstenholme AJ, Skehel JJ, Smith MH. (1988) Molecular basis of resistance of influenza A viruses to amantadine. *J Antimicrob Chemother* **18**, 19-29.

Hayden FG, Pavia AT. (2006) Antiviral management of seasonal and pandemic influenza. *J Infect Dis* **194**, 119-126

He X, Zhou J, Bartlam M, Zhang R, Ma J, Lou Z, Li X, Li J, Joachimiak A, Zeng Z, Ge R, Rao Z, Liu Y. (2008) Crystal structure of the polymerase PA(C)-PB1(N) complex from an avian influenza H5N1 virus. *Nature* **454**, 1123-1126.

Heckman KL, Pease LR. (2007) Gene splicing and mutagenesis by PCR-driven overlap extension. *Nat Protoc* **4**, 924-932.

Henle W, Lief F, Fabiyi A. (1958) STRAIN-SPECIFIC COMPLEMENT-FIXATION TEST IN ANTIGENIC ANALYSIS AND SERODIAGNOSIS OF INFLUENZA. *Lancet* **271**, 818-820.

Helenius A. (1992) Unpacking the incoming influenza virus. *Cell* 69, 577-578

Herce HD, Garcia AE. (2007) Molecular dynamics simulations suggest a mechanism for translocation of the HIV-1 TAT peptide across lipid membranes. *Proc Natl Acad U S A* **104**, 20805–20810.

Hurt AC. (2014) The epidemiology and spread of drug resistant human influenza viruses. *Curr Opin Virol* **8**, 22-29.

Jakubovics NS, Strömberg N, van Dolleweerd CJ, Kelly CG, Jenkinson HF. (2005) Differential binding specificities of oral streptococcal antigen I/II family adhesins for human or bacterial ligands. *Mol Microbiol* **55**, 1591-1605.

Jelesarov I, Bosshard HR. (1999) Isothermal titration calorimetry and differential

scanning calorimetry as complementary tools to investigate the energetics of biomolecular recognition. *J Mol Recognit* **12**, 3-18.

Jin H, Leser GP, Zhang J, Lamb RA. (1997) Influenza virus hemagglutinin and neuraminidase cytoplasmic tails control particle shape. *EMBO J* **16**, 1236-1247.

Kawaoka Y, Krauss S, Webster RG. (1989) Avian-to-human transmission of the PB1 gene of influenza A viruses in the 1957 and 1968 pandemics. *J Virol* **63**, 4603-4608.

Kim TH, Johnstone J, Loeb M. (2011) Vaccine herd effect. *Scand J Infect Dis* **9**, 683-689.

Kiso M, Takahashi K, Sakai-Tagawa Y, Shinya K, Sakabe S, Le QM, Ozawa M, Furuta Y, Kawaoka Y. (2010) T-705 (favipiravir) activity against lethal H5N1 influenza A viruses. *Proc Nat Acad Sci U S A* **107**, 882-887.

Kwong JA, Dorfman T, Quinlan BD, Chiang JJ, Ahmed AA, Choe H, Farzan M. (2011) A tyrosine-sulfated CCR5-mimetic peptide promotes conformational transitions in the HIV-1 envelope glycoprotein. *J Virol* **15**, 7563-7571.

Laemmli UK. (1970) Cleavage of structural proteins during the assembly of the head of bacteriophage T4. *Nature* **227**, 680-685.

LaForce FM, Nichol KL, Cox NJ. (1994) Influenza: virology, epidemiology, disease, and prevention. *Am J Prev Med* **10**, 31-44.

Layne SP, Monto AS, Taubenberger JK. (2009) Pandemic influenza: an inconvenient mutation. *Science* **5921**, 1560-1561.

Lagacé-Wiens PR, Rubinstein E, Gumel A (2010) Influenza epidemiology--past, present, and future. *Crti Care Med* **38**, e1-e9.

Li Q, Qi J, Zhang W, Vavricka CJ, Shi Y, Wei J, Feng E, Shen J, Chen J, Liu D, He J, Yan J, Liu H, Jiang H, Teng M, Li X, Gao GF. (2010) The 2009 pandemic H1N1 neuraminidase N1 lacks the 150-cavity in its active site. *Nat Struct Mol Biol* **10**, 1266-1268.

Lidwell OM. (1974) Aerial dispersal of micro-organisms from the human respiratory tract. *Soc Appl Bacteriol Symp Ser* **3**, 135-154.

Lindstrom SE, Hiromoto Y, Nishimura H, Saito T, Nerome R, Nerome K. (1999) Comparative analysis of evolutionary mechanisms of the hemagglutinin and three internal protein genes of influenza B virus: multiple cocirculating lineages and frequent reassortment of the NP, M, and NS genes. *J virol* **73**, 4413-4426.

Liu T, Muller J, Ye Z. (2002) Association of influenza virus matrix protein with

ribonucleoproteins may control viral growth and morphology. *Virology* **304**, 89-96.

Loregian A, Palu G. (2005) Disruption of protein-protein interactions: towards new targets for chemotherapy. *J Cell Physiol* **3**, 750-762.

Mason JM. (2010) Design and development of peptides and peptide mimetics as antagonists for therapeutic intervention. *Future Med Chem* **12**, 1813-1822.

Milletti F. (2012) Cell-penetrating peptides: classes, origin, and current landscape. *Drug Discov Today* **17**, 15-16.

Mohler WA, Charlton CA, Blau HM. (1996) Spectrophotometric quantitation of tissue culture cell number in any medium. *Biotechniques* **21**, 264-266.

Molinari NA, Ortega-Sanchez IR, Messonnier ML, Thompson WW, Wortley PM, Weintraub E, Bridges CB. (2007) The annual impact of seasonal influenza in the US: measuring disease burden and costs. *Vaccine* **27**, 5086-5096.

Monto AS. (2008) Epidemiology of influenza. *Vaccine* **26**, 45-48.

Monto AS, Gravenstein S, Elliott M, Colopy M, Schweinle J. (2000) Clinical signs and symptoms predicting influenza infection. *Arch Intern Med* **160**, 3243-3247.

Moscona A. (2009) Global transmission of oseltamivir-resistant influenza. *N Engl J Med* **360**, 953-956.

Muratore G, Goracci L, Mercorelli B, Foeglein Á, Digard P, Cruciani G, Palù G, Loregian A. (2012) Small molecule inhibitors of influenza A and B viruses that act by disrupting subunit interactions of the viral polymerase. *Proc Natl Acad U S A* **109**, 6247-6252.

Nachman MW, Crowell SL. (2000) Estimate of the mutation rate per nucleotide in humans. *Genetics* **156**, 297-304.

Nallamsetty S, Austin BP, Penrose KJ, Waugh DS. (2005) Gateway vectors for the production of combinatorially-tagged His6-MBP fusion proteins in the cytoplasm and periplasm of Escherichia coli. *Protein Sci* **12**, 2964-2971.

Nemeroff ME, Barabino SM, Li Y, Keller W, Krug RM. (1998). Influenza virus NS1 protein interacts with the cellular 30 kDa subunit of CPSF and inhibits 3'end formation of cellular pre-mRNAs. *Mol Cell*, **7**. 991-1000.

Newcomb LL, Kuo RL, Ye Q, Jiang Y, Tao YJ, Krug RM. (2009) Interaction of the influenza a virus nucleocapsid protein with the viral RNA polymerase potentiates unprimed viral RNA replication. *J Virol*. **83**, 29-36.

Obayashi E, Yoshida H, Kawai F, Shibayama N, Kawaguchi A, Nagata K, Tame JR, Park SY. (2008) The structural basis for an essential subunit interaction in influenza virus RNA polymerase. *Nature* **454**, 1127-1131.

Olitsky PK, Gates FL. (1922) EXPERIMENTAL STUDIES OF THE NASO PHARYNGEAL SECRETIONS FROM INFLUENZA PATIENTS. *J Exp Med* **35**, 553-559.

Osterholm MT, Kelley NS, Sommer A, Belongia EA. (2012) Efficacy and effectiveness of influenza vaccines: a systematic review and meta-analysis. *Lancet Infect Dis* **12**, 36-44.

Osterhaus AD, Rimmelzwaan GF, Martina BE, Bestebroer TM, Fouchier RA.(2000) Influenza B virus in seals. *Science,* **288**. 1051-1053.

Paterson RG, Lamb RA. (1990) Conversion of a class II integral membrane protein into a soluble and efficiently secreted protein: multiple intracellular and extracellular oligomeric and conformational forms. *J Cell Biol* **110**, 999–1011.

Pattnaik P. (2005) Surface plasmon resonance: applications in understanding receptor-ligand interaction. *Appl Biochem Biotechnol* **126**, 79-92.

Pappas C, Aguilar PV, Basler CF, Solórzano A, Zeng H, Perrone LA, Palese P, García-Sastre A, Katz JM, Tumpey TM. (2008) Single gene reassortants identify a critical role for PB1, HA, and NA in the high virulence of the 1918 pandemic influenza virus. *Proc Natl Acad Sci U S A* **105**, 3064-3069.

Presti RM, Zhao G, Beatty WL, Mihindukulasuriya KA, da Rosa AP, Popov VL, Tesh RB, Virgin HW, Wang D. (2009) Quaranfil, Johnston Atoll, and Lake Chad viruses are novel members of the family Orthomyxoviridae. *J Virol* **83**, 11599-11606.

Potter Cw. (2001) A history of influenza. *J Appl Microbiol* **4**, 572-579.

Resa-Infante P, Jorba N, Coloma R, Ortin J. (2011) The influenza virus RNA synthesis machine: advances in its structure and function. *RNA Biol* **8**, 207-215.

Robb NC, Smith M, Vreede FT, Fodor E. (2009) NS2/NEP protein regulates transcription and replication of the influenza virus RNA genome. *J Gen virol* **90**, 1398-1407.

Rout MP, Aitchison JD. (2001) The nuclear pore complex as a transport machine. *J Biol Chem* **276**, 16593-16596.

Schnell JR, Chou JJ. (2008) Structure and mechanism of the M2 proton channel of influenza A virus. *Nature* **451**, 591-595.

Sidwell RW, Bailey KW, Wong MH, Barnard DL, Smee DF. (2005) In vitro and in vivo influenza virus-inhibitory effects of viramidine. *Antiviral Res* **68**, 10-17.

Shahab, Shamsa Z., and W. Paul Glezen. "Influenza virus." Viral diseases in pregnancy. Springer New York, 1994. 215-223.

Shimizu T, Takizawa N, Watanabe K, Nagata K, Kobayashi N. (2011) Crucial role of the influenza virus NS2 (NEP) C-terminal domain in M1 binding and nuclear export of vRNP. *FEBS Lett*. **585**, 41-46.

Shinde V, et al (2009). Triple-reassortant swine influenza A (H1) in humans in the United States, 2005-2009*. N. Engl. J. Med*. **360**:2616– 2625

Shinya K, Ebina M, Yamada S, Ono M, Kasai N, Kawaoka Y. (2006) Avian flu: influenza virus receptors in the human airway. *Nature* **44**, 435-436.

Sidwell RW, Bailey KW, Wong MH, Barnard DL, Smee DF. (2005) In vitro and in vivo influenza virus-inhibitory effects of viramidine. *Antiviral Red* **68**, 10-17.

Skehel JJ, Wiley DC. (2000) Receptor binding and membrane fusion in virus entry: the influenza hemagglutinin. *Annu Rev Biochem* **69**, 531-569.

Smith GJ, Vijaykrishna D, Bahl J, Lycett SJ, Worobey M, Pybus OG, Ma SK, Cheung CL, Raghwani J, Bhatt S, Peiris JS, Guan Y, Rambaut A. (2009) Origins and evolutionary genomics of the 2009 swine-origin H1N1 influenza A epidemic. *Nature* **459**, 1122-1125.

Smith W, Andrews C, Laidlaw P. (1933) A virus obtained from influenza patients. *Lancet* **222**, 66-68.

Stohr K, Kieny MP, Wood D. (2006) Influenza pandemic vaccines: how to ensure a low-cost, low-dose option. *Nat Rev Microbiol* **8**, 565-566.

Stone CB, Bulir DC, Emdin CA, Pirie RM, Porfilio EA, Slootstra JW, Mahony JB. (2011) Chlamydia Pneumoniae CdsL Regulates CdsN ATPase Activity, and Disruption with a Peptide Mimetic Prevents Bacterial Invasion. *Front Microbiol* **2**, 21.

Subbarao K, Joseph T. (2007) Scientific barriers to developing vaccines against avian influenza viruses. *Nat Rev Immunol* **4**, 267-278.

Sugio S, Kashima A, Mochizuki S, Noda M, Kobayashi K. (1999) Crystal structure of human serum albumin at 2.5 A resolution. *Protein Eng* **6**, 439-446.

Sugiyama K, Obayashi E, Kawaguchi A, Suzuki Y, Tame JR, Nagata K, Park SY.

(2009) Structural insight into the essential PB1-PB2 subunit contact of the influenza virus RNA polymerase*. EMBO J* **12**, 1803-1811.

Sung C, Nardelli B, LaFleur DW, Blatter E, Corcoran M, Olsen HS, Birse CE, Pickeral OK, Zhang J, Shah D, Moody G, Gentz S, Beebe L, Moore PA. (2003) An IFN-beta-albumin fusion protein that displays improved pharmacokinetic and pharmacodynamic properties in nonhuman primates. *J Interferon cytokin Res* **23**, 25-36.

Taubenberger JK. (2006) The origin and virulence of the 1918 "Spanish" influenza virus. *Proc Am Philos Soc* **150**, 86-112.

Taubenberger JK, Hultin JV, Morens DM. (2007) Discovery and characterization of the 1918 pandemic influenza virus in historical context. *Antivir Ther* **12**, 581-591

Takeda M, Leser GP, Russell CJ, Lamb RA. Influenza virus hemagglutinin concentrates in lipid raft microdomains for efficient viral fusion. (2003) *Proc Natl Acad Sci U S A* **25**, 14610-14617.

Thompson JD, Higgins DG, Gibson TJ. (1994) Improved sensitivity of profile searches through the use of sequence weights and gap excision. *Comput Appl Biosci* **10**, 19-29.

Treanor J. (2004) Influenza vaccine--outmaneuvering antigenic shift and drift. *N Engl J Med* **350**, 218-220.

Tulip WR, Varghese JN, Baker AT, van Donkelaar A, Laver WG, Webster RG, Colman PM. (1991) Refined atomic structures of N9 subtype influenza virus neuraminidase and escape mutants. *J Mol Biol* **221**, 487-497.

Toyoda T, Adyshev DM, Kobayashi M, Iwata A, Ishihama A. (1996) Molecular assembly of the influenza virus RNA polymerase: determination of the subunit-subunit contact sites. *J Gen Virol* **77**, 2149-2157.

Tsai CH, Lee PY, Stollar V, Li ML. (2006) Antiviral therapy targeting viral polymerase. *Curr Pharm Des* **11**, 1339-1355

Vives E, Brodin P, Lebleu B. (1997) A truncated HIV-1 Tat protein basic domain rapidly translocates through the plasma membrane and accumulates in the cell nucleus. *J Biol Chem* **272**, 16010-16017.

van Meer G, Voelker DR, Feigenson GW. (2008) Membrane lipids: where they are and how they behave. *Nat Rev Mol Cell Biol* **2**, 112-124.

von Itzstein M. (2007) The war against influenza: discovery and development of

sialidase inhibitors. *Nat Rev Drug Discov* **12**, 967-974.

Webby RJ, Webster RG. (2001) Emergence of influenza A viruses. *Philos Trans R Soc Lond B Biol Sci* **356**, 1817-1828.

Wilks S, de Graaf M, Smith DJ, Burke DF. (2012) A review of influenza haemagglutinin receptor binding as it relates to pandemic properties. *Vaccine* **29**, 4369-4376.

Ying T, Chen W, Gong R, Feng Y, Dimitrov DS. (2012) Soluble monomeric IgG1 Fc. *J Biol Chem* **23**, 19399-19408.

Zambon MC. (2001) The pathogenesis of influenza in humans. *Rev Med Virol*. **11**, 227-241.

APPENDIX

5.1 Supplementary Figures

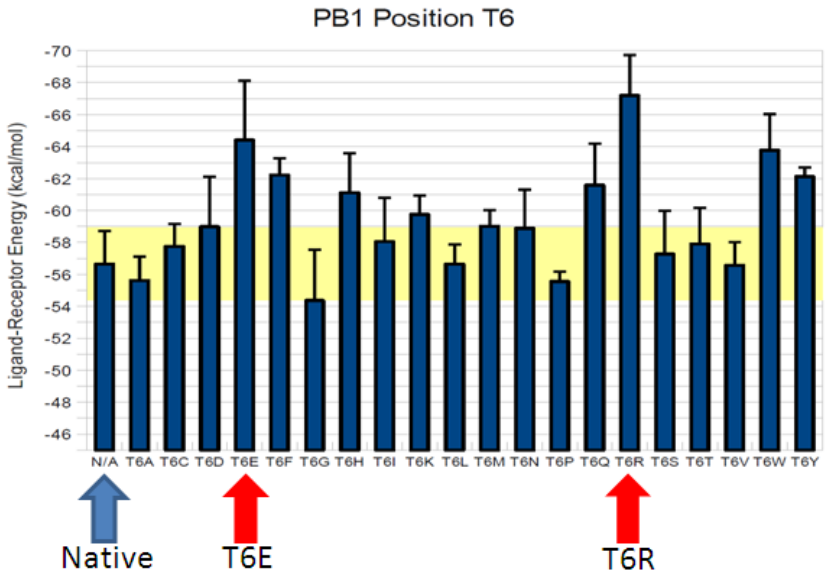

Supplementary Figure S1 ***In silico*** **ZMM molecular modeling predicts low energy mutants at the PB1 position 6**

The crystal structure of C-terminal PA in complex with N-terminal PB1 was used to model different amino acid substitutions at various positions in the PB1 protein and calculate the hypothetical free energy of binding (only results from position 6 are shown here). The simulation yielded several lower energy state amino acid substitutions compared to the parent protein (blue arrow), with glutamic acid (E) and arginine (R) being highlighted (red arrow). The molecular modeling shown here was performed by Seiji Sugiman-Marangos on the McMaster SHARCNET computers in 2011 before the start of my Masters.

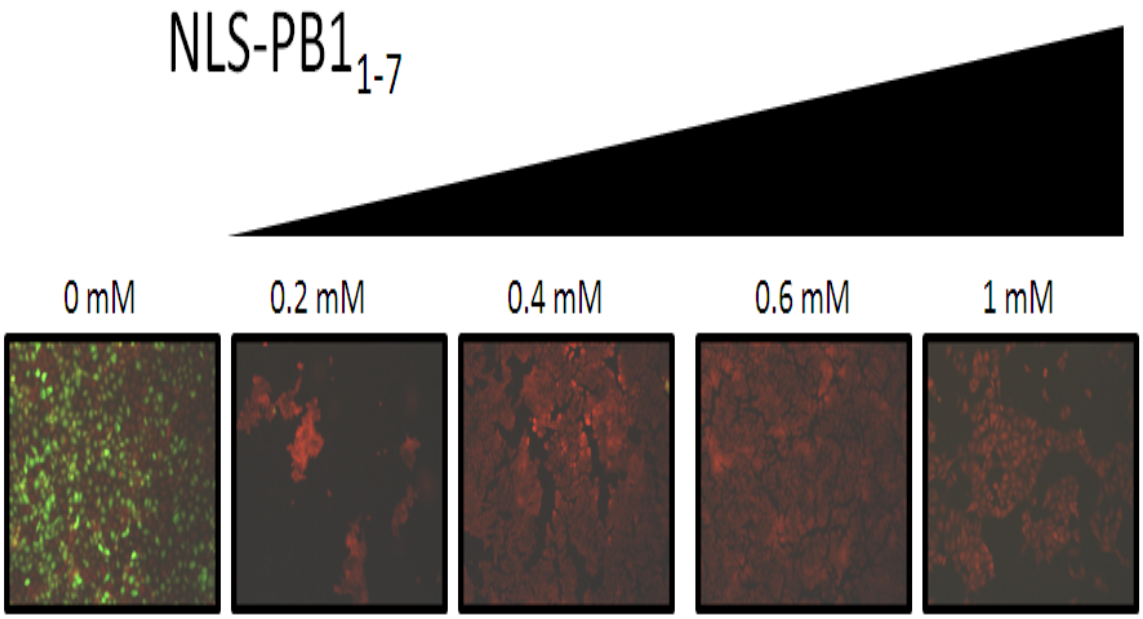

Supplementary Figure S2. NLS-PB1$_{1-7}$ inhibits Influenza A replication and growth

MDCK cells were treated with purified NLS-PB1$_{1-7}$ at the given concentrations and subsequently challenged with Influenza A . Cells were incubated at 37°C+5%CO_2 for 24 hours and visualized by Direct Fluorescent Antibody (DFA) Microscopy. Virus infected cells are shown in green and non-infected MDCK cells are shown in red. This experiment was performed by Lieqi Liu in 2010 before the start of my Masters.

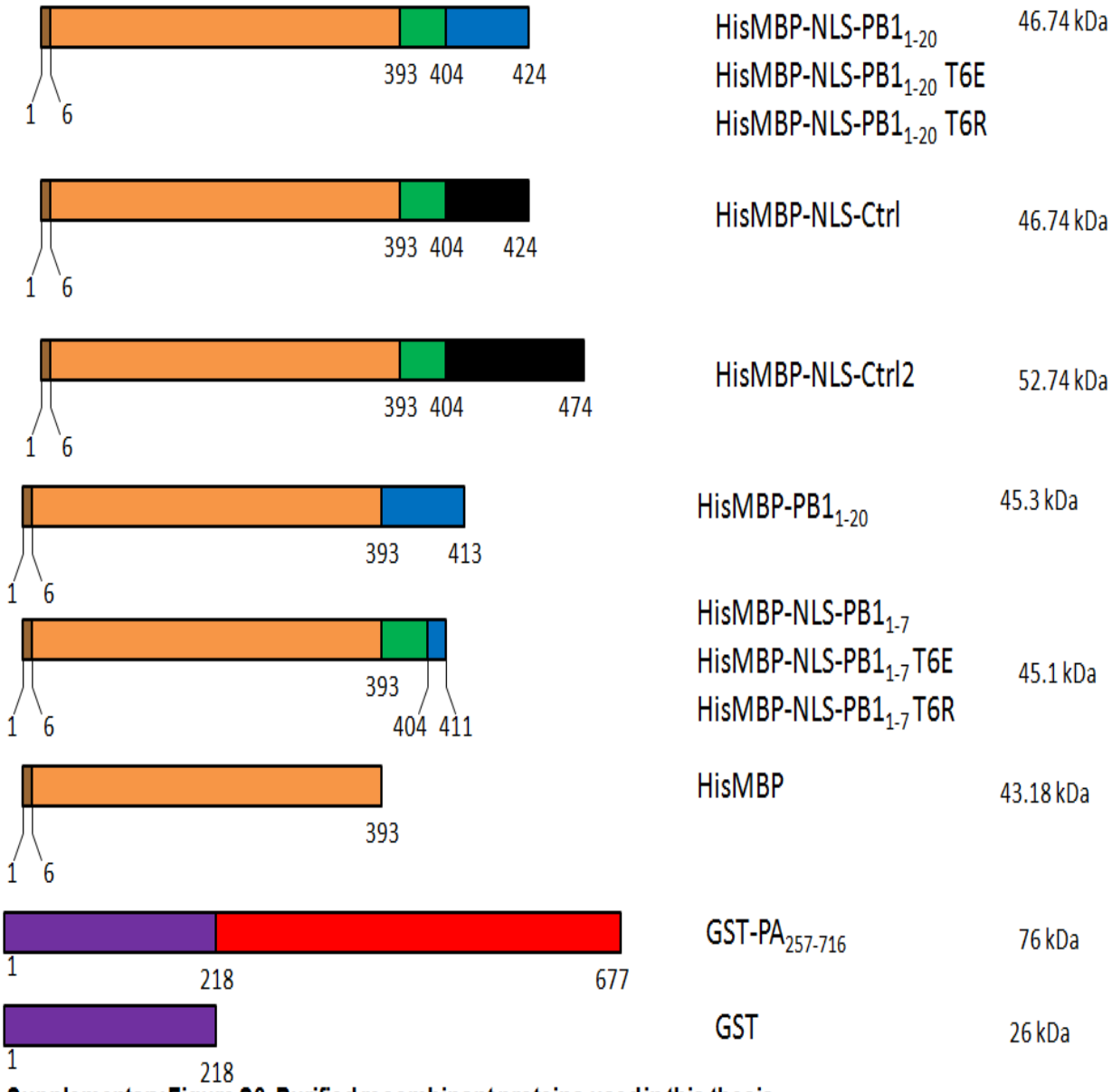

Supplementary Figure S3. Purified recombinant proteins used in this thesis

Constructs were designed by overlapping PCR as stated in the methods section and are shown from amino to carboxy terminus (left to right). Proteins were expressed in *E. coli* and affinity purified by FPLC. 6x Histidine tag is brown, MBP orange, NLS green, $PB1_N$ blue, and non specific random control peptides (Ctrl/Ctrl2) black, GST purple and PA_C red. Numbers beneath each construct represent amino acid number. Constructs here are not to scale and kDa sizes are approximate.

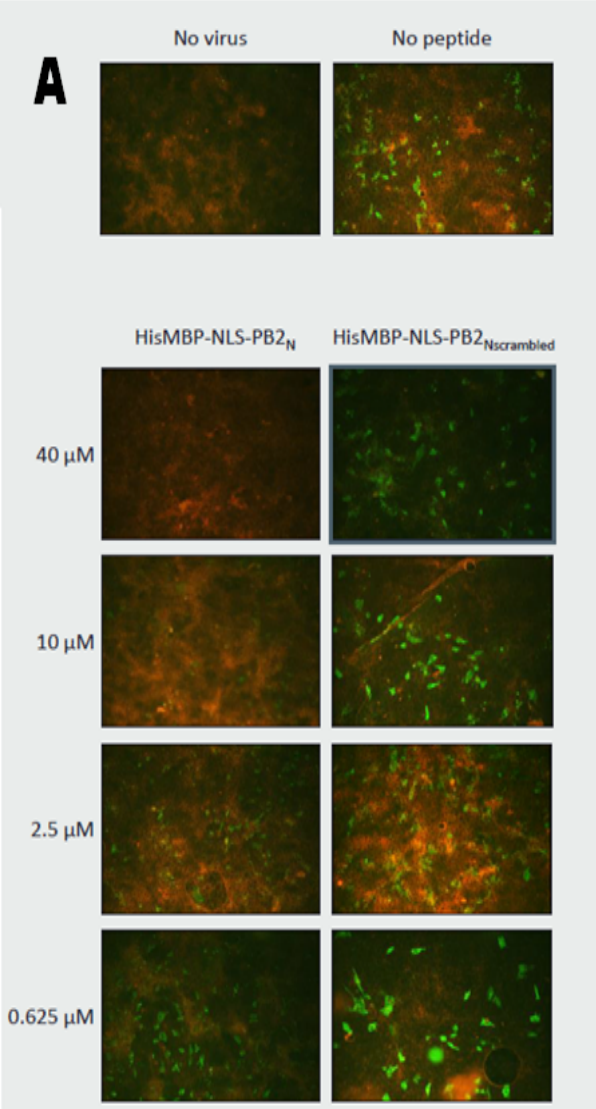

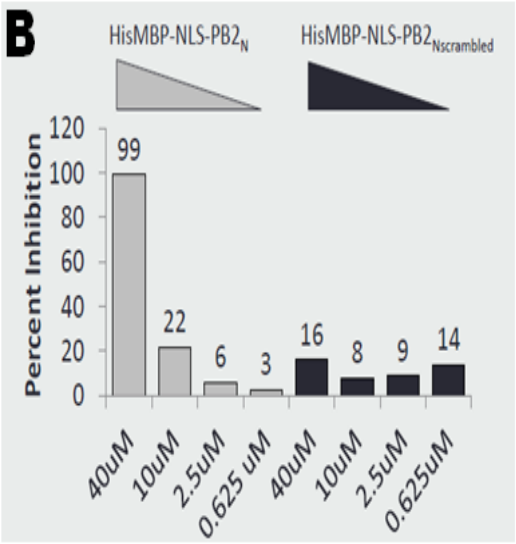

Supplementary Figure S4. A $PB2_N$ mimetic inhibits Influenza A replication

MDCK cells were incubated with HisMBP-NLS-$PB2_N$, HisMBP-NLS-$PB2_{Nscrambled}$, or no mimetic and challenged with A/2009/H1N1 for 24 hours and visualized by DFA Microscopy. **(A)** Microscopy fields representing Influenza-infected cells (green) and non-infected MDCK cells (red) are shown for each mimetic. **(B)** Results from (A) are expressed as percent inhibition, normalized to the no mimetic control. Experiment performed by Steven Liang.

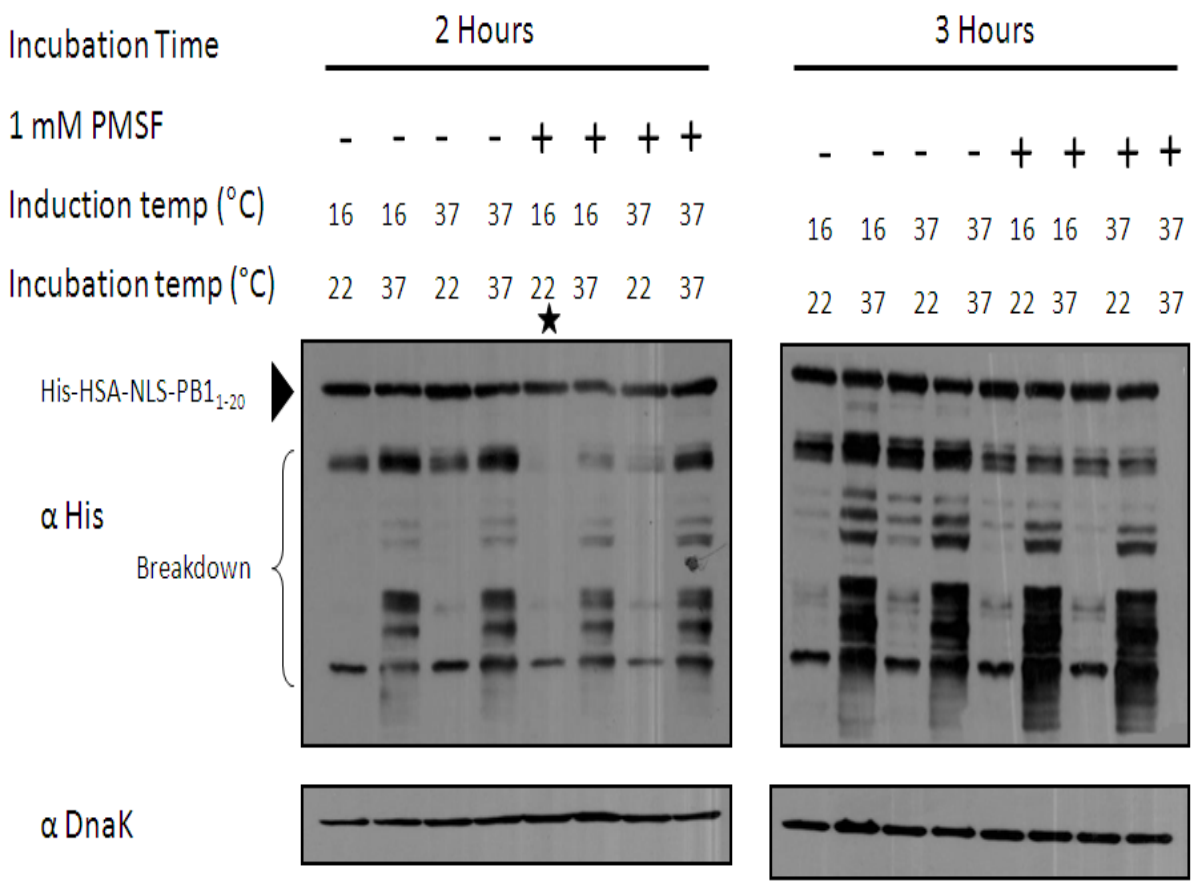

Supplementary Figure S5. Overexpression of His-HSA-NLS-PB1$_{1-20}$ in *E. coli* leads to C-terminal degradation

An expression plasmid expressing His-HSA-NLS-PB1$_{1-20}$ was transformed in *E. coli* Rosetta *pLysS*, cells were grown until an OD_{600} of 0.55 and subsequently cultured at the stated conditions (all cultures induced with 0.5 mM IPTG). Cells were then harvested, the pellet was resuspended in sample buffer and the samples were electrophoresed and blotted with antibodies against 6xHistidine or DnaK (loading control). Degradation is present in nearly all conditions; the one condition with the least degradation (marked with a star) was not reproducible when cultures were scaled up to 6 L.

5.2 – Supplementary Tables

Strain	Plasmid backbone	Plasmid Gene	Antibiotic resistance	Recombinant protein
E. coli BL21 (DE3)	*pDESTHisMBP*	PB1 20-mer peptide	Amp	HisMBP-NLS-$PB1_{1-20}$ 20-mer
E. coli BL21 (DE3)	*pDESTHisMBP*	T6E PB1 20-mer peptide	Amp	HisMBP-NLS-$PB1_{1-20}$ 20-mer T6E
E. coli BL21 (DE3)	*pDESTHisMBP*	T6R PB1 20-mer peptide	Amp	HisMBP-NLS-$PB1_{1-20}$ 20-mer T6R
E. coli Rosetta *pLysS*	*pDEST15*	PA (257-716)	Amp	GST-$PA_{257-716}$
P. pastoris X-33	*pPicz9ssamp*	PB1 20-mer peptide	Amp, Zeo	His-HSA-NLS-$PB1_{1-20}$ 20-mer (yeast)
P. pastoris X-33	*pPicz9ssamp*	HSA	Amp, Zeo	HSA
E. coli BL21 (DE3)	*pDEST HisMBP*	T6E PB1 7-mer peptide	Amp	HisMBP-NLS-PB_{1-20} 7-mer T6E
E. coli BL21 (DE3)	*pDEST HisMBP*	T6R PB1 7-mer peptide	Amp	HisMBP-NLS-PB_{1-20} 7-mer T6R
E. coli BL21 (DE3)	*pDEST HisMBP*	PB1 7-mer peptide	Amp	HisMBP-NLS-$PB1_{1-20}$ 7-mer
E. coli Rosetta *pLysS*	*pDEST17*	HSA PB1 20-mer peptide	Amp	His-HSA-NLS-$PB1_{1-20}$ 20-mer
E. coli BL21 (DE3)	*pDEST15*	GST	Amp	GST
E. coli BL21 (DE3)	*pDESTHisMBP*	Ctrl peptide	Amp	His-MBP-NLS-Ctrl
E. coli BL21(DE3)	*pDESTHisMBP*	PB1 20-mer peptide (NO NLS)	Amp	HisMBP-$PB1_{1-20}$ 20mer
E. coli BL21(DE3)	*pDEST17*	HisMBP	Amp	His-MBP
E. coli Rosetta-Gama pLysS	*pDEST17*	HSA PB1 20-mer peptide	Amp	His-HSA-NLS-$PB1_{1-20}$ 20-mer
L. lactis MG1363	*pUB1000*	PB1 20-mer peptide	Ery	His-MBP-NLS-$PB1_{1-20}$ 20-mer

Table 5.1 – List of expression strains

Note: All PB1 and Ctrl genes contain an NLS unless otherwise stated

Amp = 100 µg/mL ampicillin
Ery = 5 µg/mL erythromycin
Zeo = 100 µg/mL zeocin

PCR product	Forward Primer (5'-3')	Reverse Primer (5'-3')
NLS-PB1	GGGGACAAGTTTGTACAAAAAAGCAGGCTTA GATTACGATATCCCAACGACCGAAAACCTGTA TTTTCAGGGCGCTTATGGCCGTAAAAAACGCC GTC	GGGGACCACTTTGTACAAGAAAGCTGGG TCTTACATATCTACATTTGGTGTCAGCAG GAACAGACGACGTCGTTGACGGCGTTTT TTACGGCCATAAGC
NLS-PB1 T6E	GGGGACAAGTTTGTACAAAAAAGCAGGCTTA GATTACGATATCCCAACGACCGAAAACCTGTA TTTTCAGGGCGCTTATGGCCGTAAAAAACGCC GTC	GGGGACCACTTTGTACAAGAAAGCTGGG TCTTACATATCTACATTTGGTTCCAGCAG GAACAGTTTAACTGGTGCTTGATTGGCAA TAGAGGTAGTACGACGTCGTTGACGGCG TTTTTTACGGCCATA
NLS-PB1 T6R	GGGGACAAGTTTGTACAAAAAAGCAGGCTTA GATTACGATATCCCAACGACCGAAAACCTGTA TTTTCAGGGCGCTTATGGCCGTAAAAAACGCC GTC	GGGGACCACTTTGTACAAGAAAGCTGGG TCTTACATATCTACATTTGGCCTCAGCAG GAACAGTTTAACTGGTGCTTGATTGGCAA TAGAGGTAGTACGACGTCGTTGACGGCG TTTTTTACGGCCATA
$PA_{257-716}$	GGGGACAAGTTTGTACAAAAAAGCAGGCTTA GATTACGATATCCCAACGACCGAAAACCTGTA TTTTCAGGGCATGATTGAACCATTCTTGAGGA CG	GGGGACCACTTTGTACAAGAAAGCTGGG TCTTACATATCTACATTTGG TTGGCAAAGAATTCGAGCTCAT
NLS-PB1 7-mer	GGGGACAAGTTTGTACAAAAAAGCAGGC TTAGATTACGATATCCCAACGACCGAAA ACCTGTATTTTCAGGGCGCTTATGGCCGTAAA AAACGCCGTC	GGGGACCACTTTGTACAAGAAAGCTGGG TCTTACATATCTACATTTGGTGTCAGACG ACGTCGTTGACGGCGTTTTTTACGGCCAT AAGC
NLS-PB1 T6E 7-mer	GGGGACAAGTTTGTACAAAAAAGCAGGC TTAGATTACGATATCCCAACGACCGAAA ACCTGTATTTTCAGGGCGCTTATGGCCGTAAA AAACGCCGTC	GGGGACCACTTTGTACAAGAAAGCTGGG TCTTACATATCTACATTTGGTGTCAGACG ACGTCGTTGACGGCGTTTTTTACGGCCAT AAGC
NLS-PB1 T6R 7-mer	GGGGACAAGTTTGTACAAAAAAGCAGGC TTAGATTACGATATCCCAACGACCGAAA ACCTGTATTTTCAGGGCGCTTATGGCCGTAAA AAACGCCGTC	GGGGACCACTTTGTACAAGAAAGCTGGG TCTTACATATCTACATTTGGTGTCAGACG ACGTCGTTGACGGCGTTTTTTACGGCCAT AAGC
PB1 (NO NLS)	GGGGACAAGTTTGTACAAAAAAGCAGGCTTA GATTACGATATCCCAACGACCGAAAACCTGTA TTTTCAGGGCAGTACTACCTCTATTGCCAATC AAGC	GGGGACCACTTTGTACAAGAAAGCTGGG TCTTACATATCTACATTTGGTGTCAGCAG GAACAGTTTAACTGGTGCTTGATTGGCAA TAGAGGTAGTACT
PB1 pPic	GGGATCCTCGAGAAAAGAGAGGCTGAAGCTA TGGATGTAAATCCAACACTGCTGTTCCTGAAA GTTCCAGCACAAAATGCCATTTCTACCACTTA TGGCCGTAAAAAACGCCGTCAACGA	CTCACTCTTGTGTGCGTCACGACGTCGTT GACGGCGTTTTTTACGGCCATAAGTGGT AGAAATGGCATTTTGTGCTGGAACTTTCA GGAACAGCAGTGTTGGATTTACATCCAT
HSA pPic	CGCCGTCAACGACGTCGTGACGCACACAAGA GTGAGG	GGGATCGAATTCTTAATGGTGATGGTGAT GGTG
NLS-PB1 pUB	GGGATCGTCGACATGATCCATCACCATCACCA TCA	GGGATCGGATCCTTACATATCTACATTTG GTGTC

Table 5.2 – List of cloning primers used in this thesis

Note: All PCR products except for the $PA_{257-716}$, HSA pPic and NLS-PB1 pUB constructs were designed using overlapping PCR with no template